A Study of Synchronization Issues of Wavelet Packet based Multicarrier Modulation

D.Karamehmedović

Supervisor:
Dr.ir. H.Nikookar

Mentor:
ir. M.K.Lakshmanan

January, 2009

IRCTR-A-033-08

International Research Center for Telecommunications and Radar
Department of Electrical Engineering, Mathematics and Computer Science
Delft University of Technology
Mekelweg 4, 2628 CD Delft, The Netherlands

A Study of Synchronization Issues of Wavelet Packet based Multicarrier Modulation

by

D.Karamehmedović

A Thesis

Presented to the Faculty of the Graduate School of
Technische Universiteit Delft
In Partial Fulfillment of the Requirements
for the Degree of

Master of Science in Telecommunication

Technische Universiteit Delft
January 2009

Abstract

Wavelet Packet based Multi-Carrier Modulation (WPMCM) offers an alternative to the well-established OFDM as an efficient multicarrier modulation technique. It has strong advantage of being generic transmission scheme whose actual characteristics can be widely customized to fulfill several requirements and constraints of advanced communication systems.

In the last decades wavelets have been favorably applied in signal and image processing fields but they just recently attracted attention of the telecommunication community. Therefore, some research questions remain to be addressed before novel WPMCM can be used in practice. One of the major concerns involves the performance of WPMCM transceivers under various synchronization errors.

In this thesis we analyze the interference in WPMCM transmission caused by the carrier frequency offset, phase noise and time synchronization errors. Using standard wavelets the sensitivity of WPMCM transceivers to these errors is evaluated through simulation studies and their performances are compared and contrasted to OFDM.

New wavelets are designed to alleviate the WPMCM's vulnerability to synchronization errors. Consequently, a filter design framework is built that facilitates the development of new wavelet bases according to the specific demands. In this regard the expressions for Inter Carrier Interference (ICI) and Inter Symbol Interference (ISI) in WPMCM transmission are first derived and stated as a convex optimization problem. Then an optimal filter that best handles these deleterious effects is designed and developed by means of Semi Definite Programming (SDP). Through computer simulations the performance advantage of the newly designed filter over standard wavelet filters is proven and further its performance is compared to the conventional OFDM.

Acknowledgement

First, I would like to express my gratitude to my supervisor dr.ir.H.Nikookar for offering invaluable assistance, expertise and guidance. I would also like to thank my mentor M.Sc.M.K.Lakshmanan whose friendship, continued assistance, stimulating suggestions and encouragement helped me throughout the course of this work.

I'm also grateful to dr.J.Löfberg from Linköpings University for offering technical assistance.

Further, I thank my fellow students at IRCTR department (Haval, Berna, Danielle, …) for creating an enjoyable and encouraging atmosphere in the office. Thanks go also to all my friends for their valuable help and support.

Finally, I want to thank my family for their constant encouragement and love on which I have relied throughout my time at TU Delft.

Contents

List of figures

List of tables

Acronyms

AWGN	Additive White Gaussian Noise
BER	Bit Error Rate
CPE	Common Phase Error
CWT	Continuous Wavelet Transform
dBc	Decibel relative to the Carrier
DAB	Digital Audio Broadcasting
DFT	Discrete Fourier Transform
DVB	Digital Video Broadcasting
DPSK	Differential Phase Shift Keying
DWT	Discrete Wavelet Transform
DWPT	Discrete Wavelet Packet Transform
FDM	Frequency Division Multiplexing
FFT	Fast Fourier Transform
FIR	Finite Impulse Response
GUI	Graphical User Interface
HPF	High Pass Filter
IDFT	Inverse Discrete Fourier Transform
IDWT	Inverse Discrete Wavelet Transform
IDWPT	Inverse Discrete Wavelet Packet Transform
IFFT	Inverse Fast Fourier Transform
ICI	Inter Carrier Interference
ISI	Inter Symbol Interference
LMI	Linear Matrix Inequality
LP	Linear Programming
LPF	Low Pass Filter
MBWA	Mobile Broadband Wireless Access
MCM	Multi-Carrier Modulation
MIMO	Multiple-Input Multiple-Output

MSE	Mean Square Error
OFDM	Orthogonal Frequency Division Multiplexing
PAN	Personal Area Network
PAPR	Peak-to-Average Power Ratio
PSD	Power Spectral Density
QPSK	Quadrature Phase Shift Keying
SDP	Semi Definite Programming
SIR	Signal to Interference Ratio
SNR	Signal to Noise Ratio
UMTS	Universal Mobile Telecommunications System
UWB	Ultra Wide Band
WPT	Wavelet Packet Transform
WPMCM	Wavelet Packed based Multi Carrier Modulation

Notations

$\sum_{n=0}^{N} y[n]$	Summation of y over $n \in 0,\ldots,N$
$\int_{a}^{b} y(x)dx$	Integration of Function y with Respect to x over Interval [a, b]
$\prod_{n=0}^{N} y[n]$	Product of y over $n \in 0,\ldots,N$
$\langle A, B \rangle$	The Inner Product of A and B
$\|x\| = \sqrt{\|\langle x, x \rangle\|}$	Norm of a Vector $\boldsymbol{x}$
δ	Kronecker Delta Function
A^*	Conjugate of A
$\tilde{A}$	Paraconjugate of A
L	Lebesque Integral
$\overline{\underset{k}{Span}\{\varphi_k(t)\}}$	Over-bar denotes Closure
$\bigcap_{k\in\mathbb{Z}} X_k$	Intersection of Spaces X_k for all $k \in \mathbb{Z}$
$\bigcup_{k\in\mathbb{Z}} X_k$	Union of Spaces X_k for all $k \in \mathbb{Z}$
$j = \sqrt{(-1)}$	Imaginary Number
$\mathbb{Z} = \{\ldots,-1,0,1,\ldots\}$	Integer Numbers
$\forall$	For All

List of Symbols

N	-	Number of Subcarriers
T	-	Symbol Duration of Symbols in Single Carrier Transmission
T_{MC}	-	Symbol Duration of Symbols in Multicarrier Transmission
R_s	-	Data Rate
S	-	Transmitted Signal
R	-	Received Signal
a_k	-	Constellation Symbols
N_{CP}	-	Length of the Cyclic Prefix
φ	-	Scaling Function
ψ	-	Wavelet Function
h	-	Scaling Filter Coefficients (LPF)
g	-	Wavelet Filter Coefficients (HPF)
H	-	Scaling Filter (Analysis)
G	-	Wavelet Filter (Analysis)
$\hat{H}$	-	Scaling Filter (Synthesis)
$\hat{G}$	-	Wavelet Filter (Synthesis)
$\tilde{H}$	-	DFT of Scaling Filter
$\tilde{G}$	-	DFT of Wavelet Filter
λ, γ	-	DWT Coefficients
κ	-	Continuous Scale
χ	-	Continuous Translation

α	-	Discrete Scale Index
β	-	Discrete Translation Index
ζ	-	DWPT Coefficients
ξ	-	WPMCM Subcarriers
l	-	Level in the Wavelet Packet Tree (binary tree)
p, k	-	Subcarrier Index
u	-	Multicarrier Symbol Index
t	-	Time Instance
f	-	Frequency
f_ε	-	Relative Frequency Offset
$\phi(n)$	-	Phase Noise
ϕ_0	-	Initial Phase
w	-	Additive White Gaussian Noise
σ_w^2	-	Phase Noise Variance
σ_{wn}	-	Phase Noise Floor Variance
S_ϕ	-	Power Spectral Density of the Phase Noise
$f_{c\phi}$	-	Corner Frequency of the Phase Noise Filter
Φ	-	Phase Rotation Angle
t_ε	-	Time Offset
L	-	Length of a Filter
K	-	Regularity Order
r_h	-	Autocorrelation Sequence of Filter H
r_g	-	Autocorrelation Sequence of Filter G

r_{hg} - Cross-correlation Sequence of Filters H and G

R_h - Fourier Transform of r_h

We should be taught not to wait for inspiration to start a thing. Action always generates inspiration. Inspiration seldom generates action.
— Frank Tibolt

1

Introduction

During the last decades many digital communications services were deployed with constantly growing data rates like digital radio and television, Internet, mobile telephony, video conferencing, etc. This rapid progress of telecommunication market has created a need for new techniques that can accommodate high data rates. In conventional single-carrier communication systems the data is transmitted sequentially and therefore duration of each symbol is inversely proportional to the data rate R_s. Higher data rates result in shorter symbol duration. The problem however arises in dispersive channels when the duration of transmitted symbols becomes shorter than the delay introduced by the channel. As a result the received symbols are widely spread in time causing Inter Symbol Interference (ISI). The amount of ISI in a given channel increases for growing data rate R_s limiting the connection speed. Today, UMTS is one of the fastest single carrier solutions on the market that can operate in dispersive environments at a rate of 3.84×10^6 chips/s.

1.1 Multicarrier Modulation

ISI can be significantly reduced by employment of Multi-Carrier Modulation (MCM) technique. MCM subdivides the total bandwidth in N narrow channels, which are transmitted in parallel. The original data stream at rate R_s is divided into N streams each having data rate of R_s/N and therefore N times longer symbol duration, i.e. $T_{MC} = NT$. The figure 1.1 illustrates the composed signals for single-carrier and multicarrier modulation.

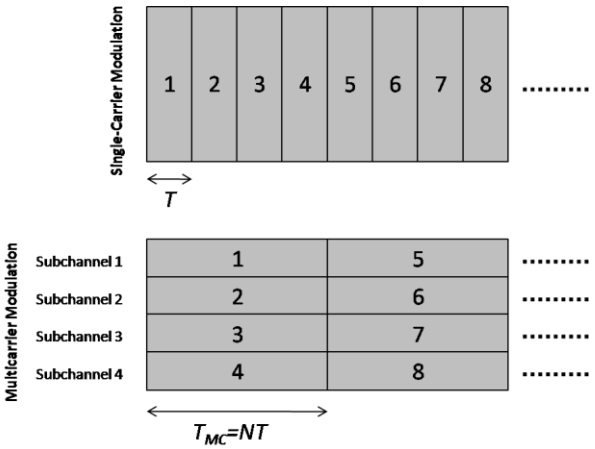

Figure 1.1: Single-carrier and Multicarrier Modulation

Each data symbol in single-carrier systems occupies the entire available bandwidth while an individual data symbol in multicarrier system only occupies a fraction of the total bandwidth. Therefore, narrow band interference or strong frequency band attenuation can cause single-carrier transmission to completely fail but in MCM they only affect subcarriers located at particular frequencies;

MCM can be implemented using several techniques. The first multicarrier systems realized was Frequency Division Multiplexing (FDM). In FDM the composite multicarrier signal is obtained by shifting baseband parallel data streams upwards in frequency by modulating them on different sinusoidal carriers. The FDM signal must consist of subcarriers that don't have overlapping spectra otherwise crosstalk would occur between different subchannels. In practical systems the guard bands are inserted between subcarriers in order to accommodate for local oscillators imperfections and/or channel effects like Doppler spread. Figure 1.2 shows the spectrum of composite FDM signal with guard bands.

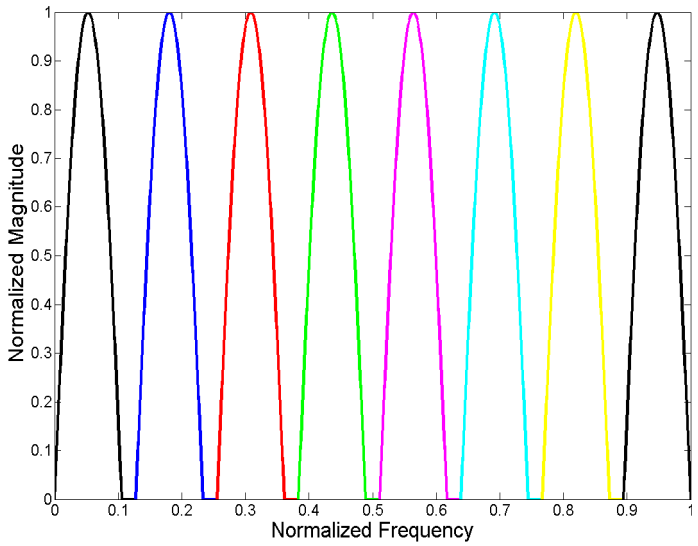

Figure 1.2: FDM Spectrum (8 Subcarriers with Guard Bands)

The growth of high data rate applications has caused spectrum to become scarce. Therefore systems that make use of available bandwidth more efficiently received a lot attention. One of the spectrally efficient multicarrier methods is Orthogonal Frequency Division Multiplexing (OFDM). Although the principle of OFDM existed since early sixties the first real life systems appeared only in the past decade. Today OFDM is the most commonly used multicarrier modulation technique and is widely adopted across the world. One of the first systems to use OFDM was European Digital Audio Broadcasting (DAB) back in 1995 and in short time other standards such as Digital Video Broadcasting (DVB), WiFi (IEEE 802.11a/g/j/n), WiMAX (IEEE 802.16), UWB Wireless PAN (IEEE 802.15.3a) and MBWA (IEEE 802.20) followed.
The high spectral efficiency of OFDM is due to its orthogonal subcarriers which allow their spectrums to overlap. Adjacent subcarriers do not interfere with each other as long as they preserve their orthogonality. Furthermore the guard bands like those used in FDM are no longer necessary, figure 1.3 illustrates this with the spectrum of OFDM for 8 subcarriers.

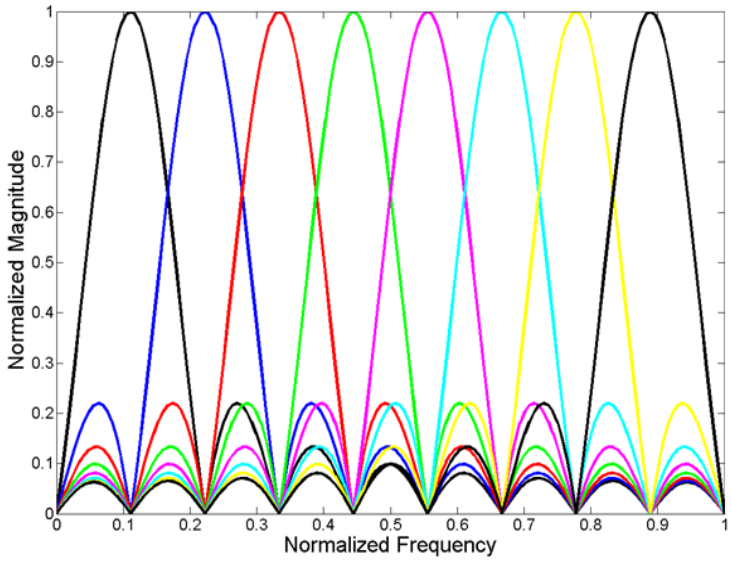

Figure 1.3: OFDM Spectrum (8 subcarriers)

1.2 OFDM

OFDM transmission system can be efficiently implemented using Inverse Fast Fourier Transform (IFFT) at the transmitter side and Fast Fourier Transformation (FFT) at the receiver side. The Fourier transformation allows us to describe a signal as a linear combination of sinusoids which form an orthogonal basis. These sinusoids in OFDM are referred as subcarriers and their number is determined by the length of the FFT vector.
The orthogonality of subcarriers over an OFDM symbol period T_{MC} is achieved by setting inter-carrier spacing to $^{1}/_{T_{MC}}$ Hz. Therefore, the frequency of the k^{th} subcarrier in so-called T-spaced OFDM is given by:

$$f_k = \frac{k}{T_{MC}} \qquad k = 0,1,\ldots,N-1 \tag{1.1}$$

The corresponding k^{th} subcarrier at frequency f_k can therefore be written as:

$$\vartheta_k(t) = e^{j2\pi f_k t} \tag{1.2}$$

An OFDM symbol consists of N subcarriers and after being modulated by the OFDM transmitter can be expressed as:

$$S(n) = \sum_{k=0}^{N-1} a_k e^{j2\pi \frac{kn}{N}}, \qquad 0 \le n \le N-1 \tag{1.3}$$

In equation (1.3) a_k represents mapped complex data symbols.

If we assume ideal channel and perfect synchronization between OFDM transmitter and receiver, the received sequence $R(n)$ is identical to the transmitted signal, i.e. $R(n) = S(n)$. Under these conditions the demodulated data after FFT for the k^{th} subcarrier can be expressed as:

$$\begin{aligned}
\hat{a}_{k'} &= \frac{1}{N}\sum_{n=0}^{N-1} R(n) e^{-j2\pi \frac{k'n}{N}} \\
&= \frac{1}{N}\sum_{n=0}^{N-1}\sum_{k=0}^{N-1} a_k e^{j2\pi \frac{kn}{N}} e^{-j2\pi \frac{k'n}{N}} \\
&= \sum_{k=0}^{N-1} a_k \left(\frac{1}{N}\sum_{n=0}^{N-1} e^{j2\pi \frac{n(k-k')}{N}} \right) \\
&= \sum_{k=0}^{N-1} a_k \delta(k-k') \\
&= a_k
\end{aligned} \tag{1.4}$$

Unfortunately the above scenario describes an utopian situation that does not occur often in reality and therefore the channel effects and oscillators' imperfections should be taken into consideration during system design. Due to delay spread of the channel, OFDM symbols could overlap one another and perfect reconstruction as described in (1.4) may not be possible. In order to decrease amount of ISI in dispersive channels we can insert guard intervals between OFDM symbols. Usually in OFDM the cyclic prefix is used as it makes the OFDM signal appear periodic and therefore avoid the discrete time property of the convolution.
The cyclic prefix is a copy of last N_{CP} samples of OFDM symbols which is appended to the front of each symbol. The effect of the dispersive channels can be efficiently mitigated if the length of

a cyclic prefix is set longer than the span of the channel. Figure 1.4 illustrates an OFDM symbol with cyclic prefix.

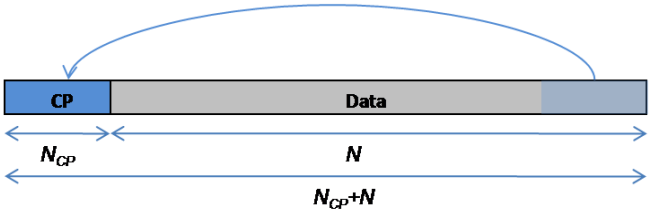

Figure 1.4: OFDM Symbol with Cyclic Prefix

Because cyclic prefix doesn't contain any useable data it decreases the spectral efficiency and therefore it should be kept as short as possible. At the receiver side the cyclic prefix is no longer needed and hence discarded before the demodulation process.
The OFDM transmitter and receiver block diagrams are illustrated in figures 1.5 and 1.6 respectively.

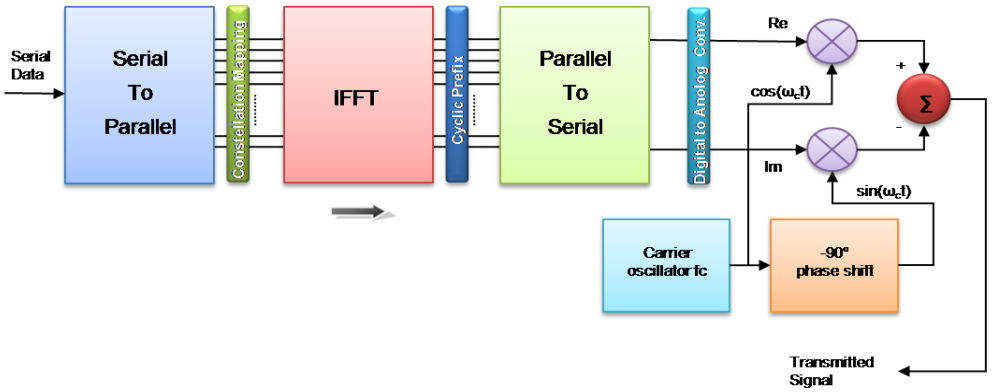

Figure 1.5: OFDM Transmitter

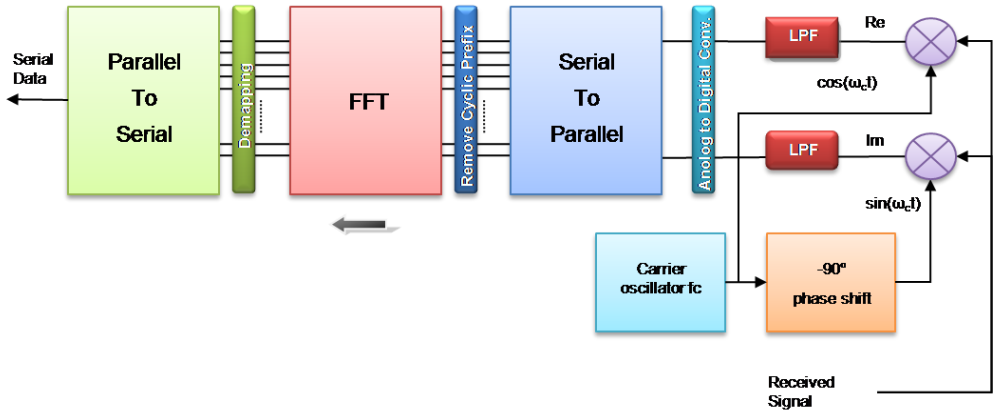

Figure 1.6: OFDM Receiver

1.3 Beyond OFDM (WPMCM)

With each passing day newer and newer telecommunication services are being launched even while existing services continue to flourish. Demand for wireless services is therefore likely to continue so for the foreseeable future. However, with increasing popularity of the wireless services the demands on prime resources like battery power and radio spectrum are put to great test. For example, currently most spectrum has been allocated, and it is becoming increasingly difficult to find frequency bands that can be made available either for new services or to expand existing ones. Even while available frequency bands appear to be fully occupied, a FCC study conducted in 2002 revealed that much of the available spectrum lies fallow most of the time (20 % or less of the spectrum is used) and that spectrum congestions are more due to the sub-optimal use of spectrum than to the lack of free spectrum [1].

Thus in a wireless environment the system requirements, network capabilities, and device capabilities have enormous variations giving rise to significant network design challenges. The design of an intelligent communication system that estimates the channel and adaptively reconfigures to maximize resource utilization is therefore highly desirable. Current developments in wireless communications are therefore towards developing novel signal transmission techniques that allow for significant increases in wireless capacity by operating in licensed spectrum without harmless interference with legitimate users. This idea is introduced in the late 90's by [2] and since then it has been known as cognitive radio.

Multicarrier modulation is recognized as a good platform for cognitive radio as the subcarriers located in the frequency bands occupied by legitimate users can be easily cancelled. OFDM with desirable properties like spectral efficiency and robustness against channel fading and dispersion is one of the possible MCM solutions. However, OFDM employ static subcarriers offering little flexibility and moreover each subcarrier has large side-lobes requiring meticulous filtering and sufficient guard bands.

Recently Wavelet Packet based Multi-Carrier Modulation (WPMCM) has been propounded as an alternative to the OFDM [3] – [6]. WPMCM employs orthogonal subcarriers and similarly to OFDM high spectral efficiency is achieved by the overlapping subcarriers spectra. The greatest motivation for pursuing WPMCM system lies in the flexibility they offer and excellent frequency selectivity. Because WPMCM can be efficiently implemented by an iterative method the number of subcarriers and their bandwidth can be easily changed. Furthermore the specifications of WPMCM can be tailored according to the engineering requirement by just altering the filter coefficients. Using frequency selective filters subcarriers with much lower side-lobes than those of OFDM can be obtained allowing better mitigation of interference [7].

The future transceivers demand great deal of flexibility and adaptability in order to operate in the crowded spectrum. These requirements correspond to the nature of WPMCM making it strong candidate for the upcoming intelligent communication systems. However, few key research questions remain to be addressed before WPMCM can become practically viable. One of the major concerns involves sensitivity and vulnerability of WPMCM transceivers to the synchronization errors, since it is known that those types of errors can destroy orthogonality in

spectral efficient multicarrier systems and cause interference. Because wavelets have just recently emerged as a multicarrier modulation technique there is little known about their sensitivity to synchronization errors and local oscillators' imperfections. This has motivated us to investigate the effect of carrier frequency offset, phase noise and time synchronization errors on WPMCM transmission.

1.4 Objectives and Novelty of the Thesis Work

The primary objectives of the project work are:

- To analyze the interference in WPMCM and OFDM transmissions under influences of carrier frequency offset, phase noise and time synchronization error.
- To establish a simulation setup in MATLAB® for WPMCM and OFDM transceivers, incorporating introduction of relative frequency offset, phase noise and symbol synchronization error.
- To evaluate the performance degradation of WPMCM transceiver in the presence of carrier frequency offset, phase noise and time synchronization error.
- To build a novel framework that facilitates development of new wavelet bases according to the specific demands.
- To design and develop new wavelet filter, which reduces the deleterious effects caused by the time synchronization errors.
- To evaluate the performance of the designed optimal filter.

The objectives of the thesis work are illustrated in the figure 1.7.

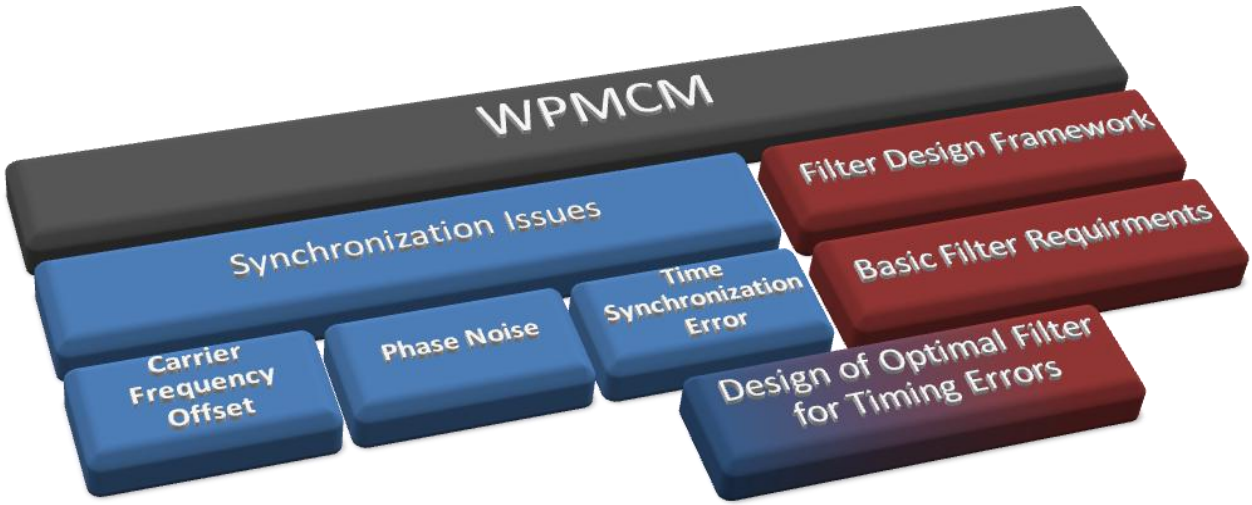

Figure 1.7: Objectives of the Thesis Work

1.5 Outline of the Thesis

In chapter 0 a theoretical foundation is laid for wavelet transformation. The first section of 0nd chapter discusses the basic idea of continuous wavelet transform. In order to work in finite time domain we switch to discrete wavelet transform. Using the underlying principle of multi resolution analysis the discrete wavelet transform is practically realized by the filter banks. At this stage the wavelet packed are introduced and their composition and decomposition is discussed using analysis and synthesis filter banks, respectively. After discussing all theoretical elements, the block diagram of WPMCM is illustrated for the transmitter and receiver. Furthermore, in this chapter we show some standard wavelets that can be used in WPMCM transceivers and give their specifications.

The synchronization errors like: time offset, frequency offset and phase noise, are discussed in chapter 3. For each of these synchronization errors a model is presented and theoretical analysis is given for both WPMCM and OFDM. The Bit Error Rate (BER) performance under time offset, frequency offset and phase noise is investigated by means of simulations studies. The simulations are performed for WPMCM with different types of standard wavelets and compared to OFDM. A part of the results reported in this chapter is published in [8], [9].

The design of wavelets is treated in chapter 4, where the accent is on wavelet design for time synchronization errors. With a little modification the same principle can be applied to other design criteria. The necessary conditions that have to be fulfilled in order to obtain orthogonal wavelets are discussed at the beginning of this chapter. Fusing the time offset analysis from chapter 3 and the wavelet constraints together, allow us to describe the whole design process as an optimization problem. The Semi Definite Programming (SDP) is used to solve the problem and generate optimal filter coefficients. The performance of WPMCM with utilization of optimal filter is examined by simulations and is compared to the results from previous chapter where standard wavelets and OFDM were tested.

Finally, chapter 5 gives a short summary of the work done and concludes the thesis. Furthermore, the recommendations for the further work on WPMCM can be found at the end of chapter 5.

The reasonable man adapts himself to the world.
The unreasonable one persists in trying to adapt the world to himself.
Therefore all progress depends on the unreasonable man.
— George Bernard Shaw, 1903

2

Wavelet Theory

The wavelets theory can be viewed as an extension of Fourier analysis. The basic idea of both transformations is the same: representing a function by a set of other functions. It all started in 1800s when Joseph Fourier discovered that he could superpose cosines and sines to represent other functions. Since then Fourier analysis has been used extensively by scientists and engineers for all kind of problems and applications. However, Fourier analysis does not work equally well for each problem. Linear problems and stationary signals are well suited for Fourier analysis but representation of brief, unpredictable and non-stationary signals on the other hand is much more difficult. The engineers sought for a solution and found it in Wavelet Transform.
The wavelets are a relatively new concept that has been introduced in the 1980s although some pioneering work had been done earlier. Since the 1980s wavelets have attracted considerable interest from the theoreticians and engineers where wavelets have promising applications. Because of the large interest, the wavelet theory has been well developed over the past years and several books on this subject have appeared as a large volume of research articles.
Chronology of developments in the wavelets theory:

- 1805 Fourier analysis developed.
- 1965 Fast Fourier Transform (FFT) algorithm appeared.
- 1980s Beginnings of wavelet theory, modest understanding why/when do wavelets work.

- 1985 Morlet & Grossman work on continuous wavelet transform trying to get perfect reconstruction without redundancy.
- 1987 Mallat unified the work done individually by different researchers.
- 1987 Mallat developed multi-resolution theory, discrete wavelet transform, wavelet construction techniques, but there was still lack of compact support wavelets.
- 1988 Daubechies found compact, orthogonal wavelets with arbitrary number of vanishing moments.
- 1990s Wavelets took off, attracting both mathematicians and engineers.

After the completion of basic theory for wavelet transform, diverse fields have recognized the potential of wavelets. In figure 2.1 few applied fields of wavelets are illustrated but this enumeration is far from complete. It has been also foreseen that wavelets are going to play an important role in many areas of future telecommunication systems [5].

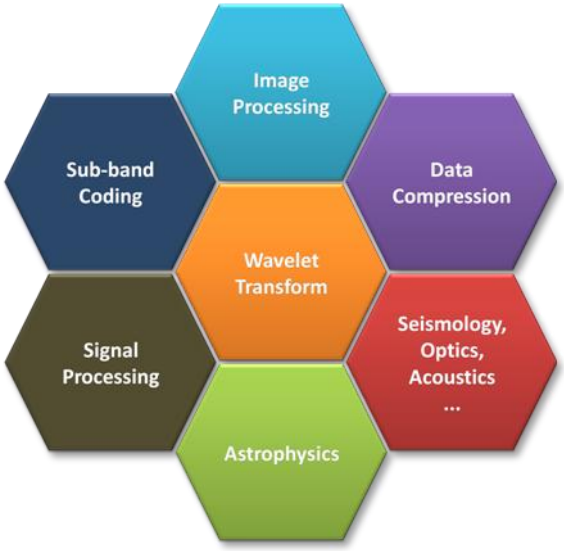

Figure 2.1: Applied Fields that make use of Wavelets

In this chapter we give an overview of fundamental wavelet theory, starting with continuous wavelet transform and going step by step towards discrete wavelet transforms and the use of filter banks in wavelet analysis. We finish this chapter by presenting the novel wavelet packet based multicarrier modulation scheme.
More information about wavelets can be found in [10] – [18].

2.1 Continuous Wavelet Transform

The Continuous Wavelet Transform (CWT) is defined as a sum of a signal multiplied by scaled and shifted version of wavelet basis function. Using different scaling factors the wavelet is stretched or compressed accordingly, while translation parameter cause delay or hastening of the wavelet's onset. The value of translation parameter affects only the location of the wavelet and

has no influence on wavelet duration or bandwidth. For increasing scale, wavelet becomes more dilated and considers the long time/low frequency behavior of the input signal while for the decreasing scale wavelet becomes more compressed and considers short time/high frequency behavior of the input signal. Therefore the scale parameter is inversely proportional to frequency, i.e. low scales correspond to high frequencies and high scales correspond to low frequencies.
The CWT encodes a given time signal in terms of wavelet coefficients that are function of two variables. As a result of wavelet transformation we get a collection of two-dimensional time-scale representation, similar to one illustrated in figure 2.2. The large amplitude in the figure 2.2 corresponds to high frequency-correlation of the signal with wavelet function at certain scale and time instance.

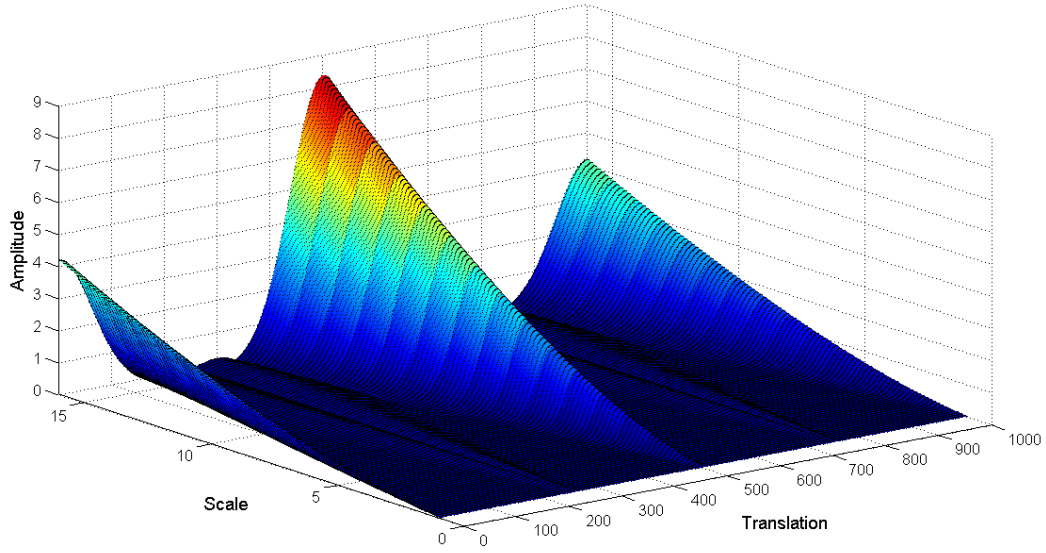

Figure 2.2: Translation-Scale Representation of a Signal

The equation of CWT is given in (2.1), where an input function $f(t)$ is decomposed into a set of wavelet coefficients $\gamma(\kappa,\chi)$. The complex conjugate of the wavelet is given by ψ^*. The parameters κ and χ denote scale and translation respectively, and they represent new dimensions of the wavelet transform.

$$\gamma(\kappa,\chi) = \int_{-\infty}^{\infty} f(t)\psi^*_{\kappa,\chi}(t)dt \qquad (2.1)$$

The wavelets functions used in (2.1) are generated using single mother wavelet by changing the scaling parameter and translating the wavelet along the time axes by amount χ:

$$\psi_{\kappa,\chi}(t) = \frac{1}{\sqrt{\kappa}}\psi\left(\frac{t-\chi}{\kappa}\right) \tag{2.2}$$

An example of scaled and translated wavelet is illustrated in figure 2.3, where Mexican Hat wavelet is shown with three different translation and scale factors. The wavelet shown at the origin represents the mother wavelet, which is neither shifted nor scaled.

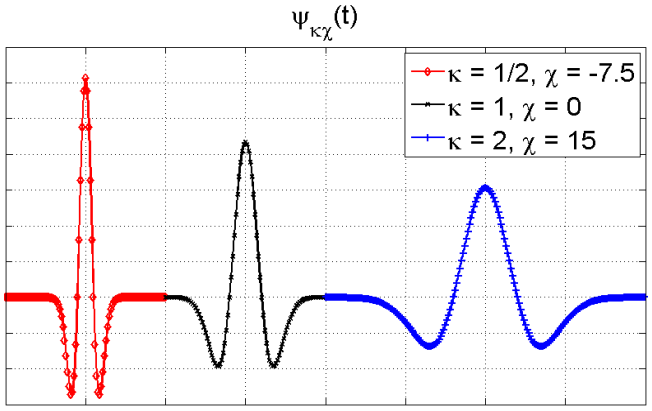

Figure 2.3: Mexican Hat Wavelet at different translations and scales

As majority of the transforms also CWT is reversible. Under suitable assumptions about $f(t)$ and Ψ, the original signal can be reconstructed from wavelet coefficients by applying the formulae for inverse wavelet transform:

$$f(t) = \frac{1}{c_\psi}\int_\kappa\int_\chi \gamma(\kappa,\chi)\frac{1}{\kappa^2}\psi\left(\frac{t-\chi}{\kappa}\right)d\chi d\kappa \tag{2.3}$$

where

$$c_\psi = \int_{\mathbb{R}} \frac{|\hat{\psi}(\omega)|^2}{|\omega|}d\omega \tag{2.4}$$

$\hat{\psi}(\omega)$ in equation (2.4) denotes the Fourier transform of $\psi(t)$.

2.2 Discrete Wavelets Transform

2.2.1 Discrete Variables

For practical problems the wavelet transform as discussed in previous paragraph is not always useful because obtained wavelet coefficients are highly redundant and they have to be calculated analytically. In this form the calculation of the wavelet transform would take a lot of time and computational power, depending on the input signals. Therefore the discrete wavelets are more suited for practical problems.

As the name already indicates the discrete wavelets does not use continuously scalable and translatable wavelets but ones that are scaled and translated in discrete steps. The equation for mother wavelet (2.2) can be rewritten for discrete scale and translation as:

$$\psi_{\alpha,\beta}(t) = \sqrt{\kappa_0^{\alpha}}\,\psi\left(\kappa_0^{\alpha} t - \beta\chi_0\right) \tag{2.5}$$

In equation (2.5) κ_0 stands for fixed dilation step and χ_0 is translation factor. The integers α and β denote scale and translation indices respectively. The most natural choice for dilation step is 2 as this result in octave bands, also known as dyadic scales. In this case for each subsequent value of scale index, wavelet is compressed in frequency domain by a factor 2 and consequently stretched in time domain by the same factor. The translation factor is usually set to 1 in order to get dyadic sampling of the time axes as well.

The output of wavelet transform when discrete wavelets are utilized would be series of wavelet coefficients:

$$\gamma(\alpha,\beta) = \int_{-\infty}^{\infty} f(t)\psi^{*}_{\alpha,\beta}(t)dt \tag{2.6}$$

In order to reconstruct the original signal from wavelet coefficients following condition should be satisfied [10].

$$A\|f\|^2 \le \sum_{\alpha}\sum_{\beta}\left|\langle f,\psi_{\alpha,\beta}\rangle\right|^2 \le B\|f\|^2 \tag{2.7}$$

Equation (2.7) indicates that the energy of the wavelet coefficients should be bounded by two positive bounds ($A > 0$) and ($B < \infty$) where $\|f\|^2$ denotes the energy of input signal $f(t)$.

The wavelets functions $\psi_{\alpha,\beta}(t)$ with $\alpha,\beta \in \mathbb{Z}$ should form a frame bounded by A and B. If the bound A is not equal to the bound B the decomposition wavelet differs from the reconstruction wavelet and we speak of a dual frame. More favorable situation is obtained for so-called tight frame where two bounds are equal to each other. Furthermore if $A = B = 1$ the tight frame becomes an orthogonal basis.
The basis function of a wavelet is called orthogonal if the wavelets generated by dilations and translations are orthogonal to each other, i.e.:

$$\int \psi_{\alpha,\beta}(t)\psi^{*}_{p,r}(t)dt = \begin{cases} 1 & if\ \ \alpha = p\ \ and\ \ \beta = r \\ 0 & otherwise \end{cases} \tag{2.8}$$

In the rest of this chapter we will consider in general orthonormal wavelets. The reconstruction of original signal for orthonormal wavelet basis function can be simply obtained by:

$$f(t) = \sum_{\alpha}\sum_{\beta}\gamma(\alpha,\beta)\psi_{\alpha,\beta}(t) \tag{2.9}$$

2.2.2 Multiresolution Analysis

The complete representation of a signal $f(t)$ requires an infinite number of wavelet functions $\psi_{\alpha,\beta}(t)$, as each following wavelet at increased scale covers only a part of the remaining spectrum. This can be overcome by introducing a low-pass complementary function $\varphi(t)$, called scaling function. The extended scaling functions are generated by time shifted version of a single basis scaling function, i.e.:

$$\varphi_{\alpha,\beta}(t) = 2^{\alpha/2}\varphi(2^{\alpha}t-\beta) \qquad \beta\in\mathbb{Z} \quad \varphi\in L^2 \tag{2.10}$$

L^2 in equation (2.10) implies that the integral of the square of the modulus is well defined.

The Multi-Resolution Analysis (MRA) describes the construction of orthonormal wavelets using family of subspaces that has to satisfy certain properties. The closed subspaces spanned by the scaling functions over integers $-\infty<\beta<\infty$ are defined by:

$$V_{\alpha} = \overline{\underset{\beta}{Span}\left\{\varphi_{\beta}(2^{\alpha}t)\right\}} = \overline{\underset{\beta}{Span}\left\{\varphi_{\alpha,\beta}(t)\right\}} \tag{2.11}$$

The low values of α represent coarse detail of a signal while higher values of α represent the finer detail. MRA requires the spanned spaces by scaling functions V_{α} to have finite energy and that they are ordered by inclusion as $0\cdots\subset V_{-2}\subset V_{-1}\subset V_0\subset V_1\subset V_2\cdots L^2$ [20], i.e.:

$$V_{\alpha}\subset V_{\alpha+1} \quad for\ all \quad \alpha\in\mathbb{Z}$$

$$\bigcap_{\alpha\in\mathbb{Z}} V_{\alpha} = \{0\} \tag{2.12}$$
$$\bigcup_{\alpha\in\mathbb{Z}} V_{\alpha} = L^2(\mathbb{R})$$

According to equation (2.12) the space that contains high resolution signal will also contain information about lower resolution of the signal, for example V_2 contains V_1 which contains V_0 et cetera. The nested vector spaces spanned by the scaling functions are illustrated in figure 2.4.

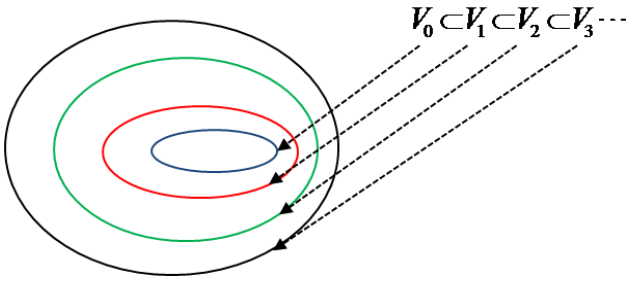

Figure 2.4: Spaces Spanned by the Scaling Functions

We can express scaling function $\varphi(t)$ which span V_0 as a weighted sum of shifted $\varphi(2t)$ which span V_1 using refinement equation:

$$\varphi(t) = \sum_n h(n)\sqrt{2}\varphi(2t-n), \qquad n \in \mathbb{Z} \tag{2.13}$$

In (2.13) $h(n)$ denotes the scaling function coefficients. This equation shows that scaling function can be constructed by the sum of its half-length translations.

The wavelets in MRA are defined as orthogonal bases that span the differences between the spaces spanned by the scaling functions at various scales. Let the subspace spanned by the wavelet be W_{j-1} then spans V_1 and V_2 can be written as:

$$\begin{aligned} &V_1 = V_0 \oplus W_0 \\ &V_2 = V_1 \oplus W_1 = (V_0 \oplus W_0) \oplus W_1 \\ &\vdots \\ &V_{\alpha+1} = V_\alpha \oplus W_\alpha = \bigoplus_{l=0}^{\alpha} W_l \qquad \text{for all } \alpha \in \mathbb{Z} \end{aligned} \tag{2.14}$$

Nested vector spaces spanned by the scaling function and wavelet vector spaces are illustrated in figure 2.5.

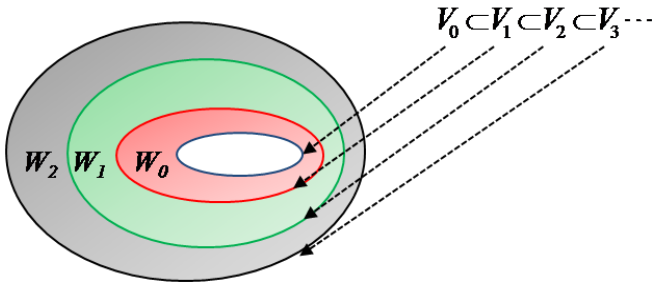

Figure 2.5: Spaces Spanned by the Scaling Functions and Wavelets

The space W_0 spanned by a wavelet is actually a subspace of V_1 $(W_0 \subset V_1)$, and therefore similarly to equation (2.13) also the wavelet functions can be represented by a weighted sum of shifted scaling function $\varphi(2t)$.

$$\psi(t) = \sum_n g(n)\sqrt{2}\varphi(2t-n), \quad n \in \mathbb{Z} \tag{2.15}$$

In (2.15) $g(n)$ denotes the wavelet function coefficients. Because of the orthogonality condition $V_0 \perp W_0 \perp W_1 \perp \cdots \perp W_\alpha$ the scaling and wavelet coefficients are related to each other by:

$$g(n) = (-1)^n h(L-1-n) \quad \textit{for } h(n) \textit{ of length } L \tag{2.16}$$

The reconstruction formulae for DWT using finite resolution of wavelet and scaling function can now be expressed as [19]:

$$f(t) = \underbrace{\sum_{\beta=-\infty}^{\infty} \lambda(\alpha_0,\beta)2^{\alpha_0/2}\varphi(2^{\alpha_0}t-\beta)}_{V_{\alpha_0}} + \underbrace{\sum_{\alpha=\alpha_0}^{\infty}\sum_{\beta=-\infty}^{\infty} \gamma(\alpha,\beta)2^{\alpha/2}\psi(2^{\alpha}t-\beta)}_{\subset W_\alpha} \tag{2.17}$$

The parameter α_0 in (2.17) sets the coarsest scale which is spanned by the scaling function. The rest is spanned by the wavelets which provide the higher resolution details of the signal. Provided that a wavelet system is orthogonal, the discrete wavelet transform (DWT) coefficients $(\lambda(\alpha,\beta) \textit{ and } \gamma(\alpha,\beta))$ can now be defined as (2.18) and (2.19) respectively:

$$\begin{aligned}\lambda(\alpha,\beta) &= \langle f(t), \varphi_{\alpha,\beta}(t)\rangle \\ &= \int f(t)2^{\alpha/2}\varphi(2^{\alpha}t-\beta)dt\end{aligned} \tag{2.18}$$

$$\begin{aligned}\gamma(\alpha,\beta) &= \langle f(t), \psi_{\alpha,\beta}(t)\rangle \\ &= \int f(t)2^{\alpha/2}\psi(2^{\alpha}t-\beta)dt\end{aligned} \tag{2.19}$$

Figure 2.6 illustrates the decomposition of the noisy Doppler function in DWT coefficients at different scales. In this figure we can see how time-varying frequency signal is described by wavelet transform as a function of scale and translation index. More common and compact figure of DWT performed on the same signal is shown in figure 2.7; here depicted colors contain the scale information.

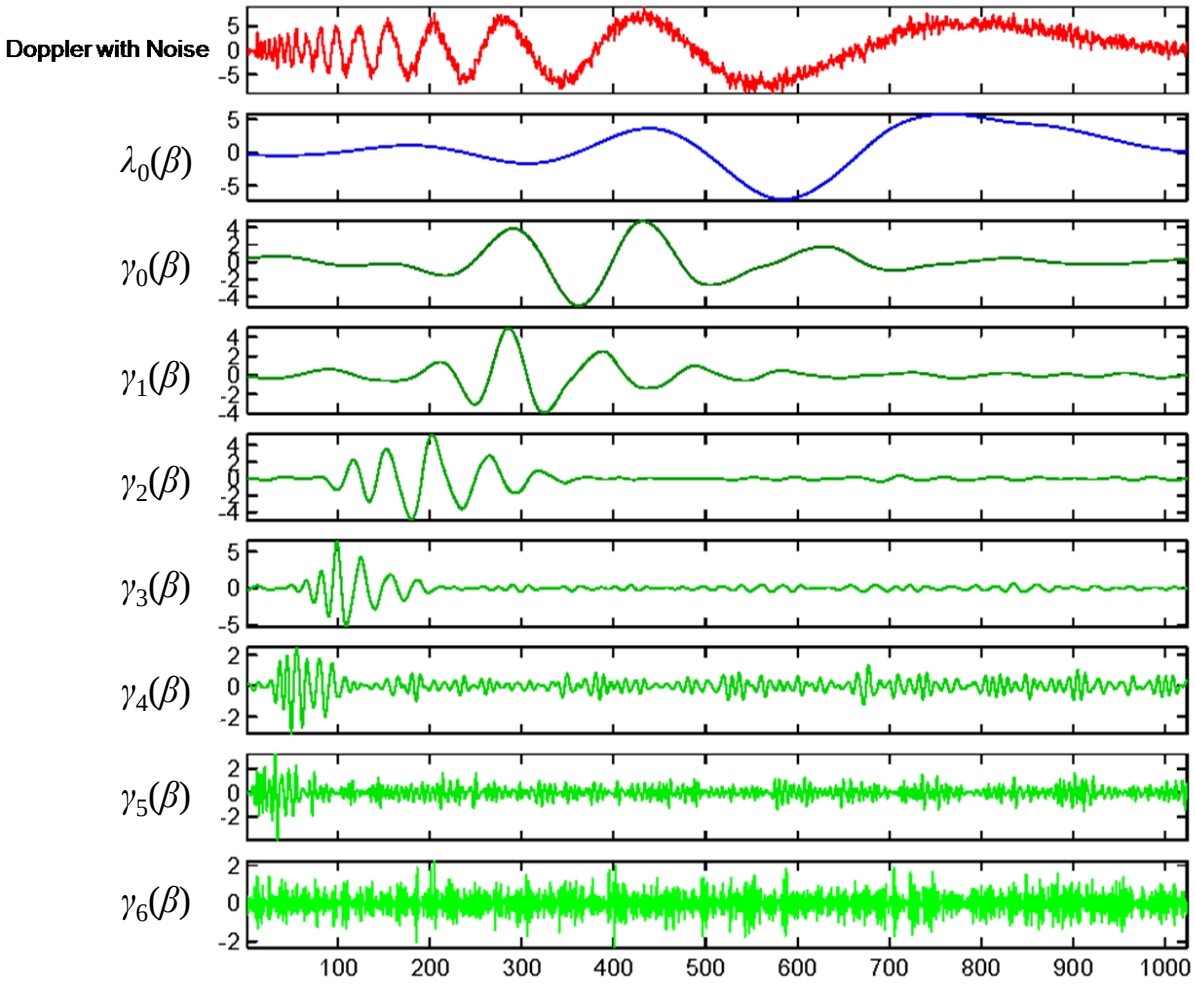

Figure 2.6: Discrete Wavelet Transform of the Noisy Doppler

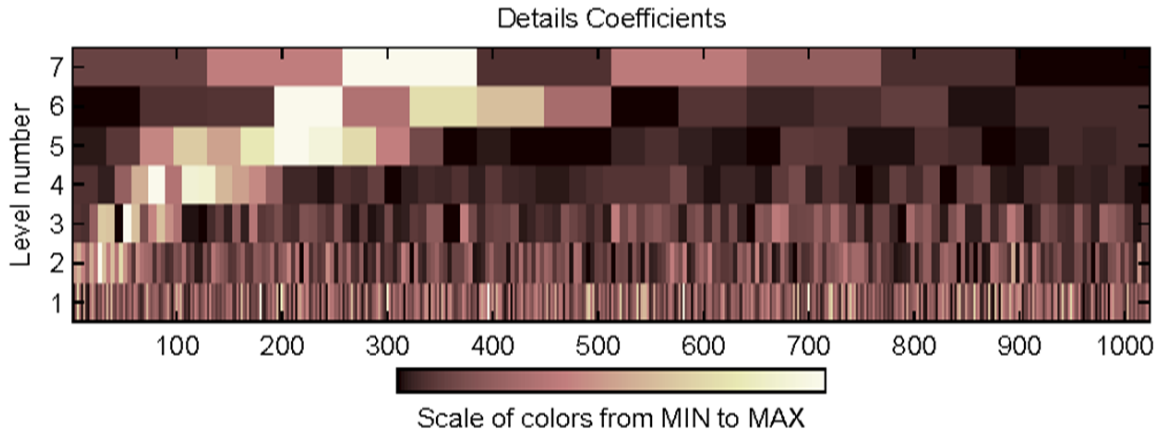

Figure 2.7: Discrete Wavelet Transform of the Noisy Doppler

2.3 Filter Banks

2.3.1 Multirate Systems

The discrete wavelet transform can be efficiently represented by filtering operations. The weights $h(n)$ given by scaling function coefficients in (2.13) can be represented by low-pass filter H. Similarly the weights of wavelet function $g(n)$ corresponds to high-pass filter G. Therefore the equations (2.13) and (2.15) can be viewed as discrete time filtering with filters H and G respectively [20], [21]. In the rest of this thesis we will refer to filter H as scaling filter and to filter G as wavelet filter.

Filtering a signal can be viewed as the convolution of signal with filter's coefficients. For a Finite Impulse Response (FIR) filter H of length L and an input signal $x(n)$ the filtering operation is given by:

$$x(n) * h(n) = \sum_{k=0}^{L-1} x(k)h(n-k) \tag{2.20}$$

Due to orthogonality condition wavelet and scaling filter are related to each other according to equation (2.16). In frequency domain the spectrum of wavelet filter can be seen as the mirror image at frequency of ½ π of scaling filter's spectrum. The scaling filter is actually half band Low-Pass Filter (LPF) and complementary wavelet filter is half band High-Pass Filter (HPF). The frequency responses of both filters are illustrated in figure 2.8.

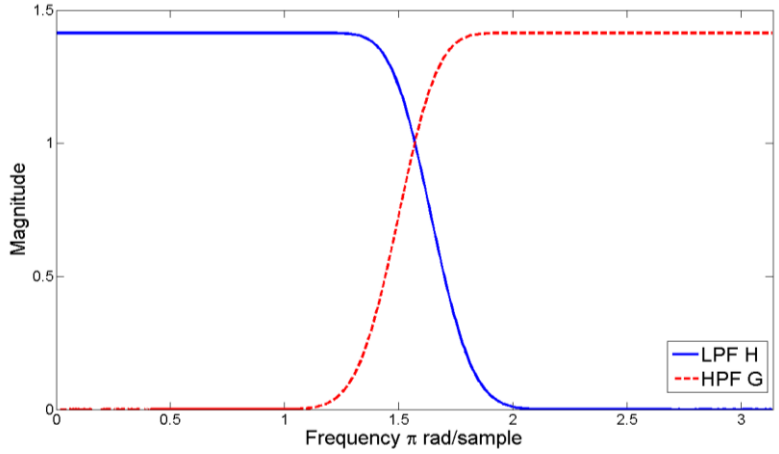

Figure 2.8: Frequency Response of Wavelet and Scaling Filter

Filtering of a signal with perfect half band pass filter removes exactly half of the frequency components from the input signal meaning that the number of samples in the filtered signal has now became redundant. In order to remove redundancy we can perform subsampling. For half-

band pass filter the filtered signal should be subsampled by 2 in order to remove redundant information. If the signal is subsampled by a larger factor we will lose information and the frequency components will be mixed up. The subsampling by factor 2 can be seen as taking every other sample of the input signal and discarding the rest of the samples, i.e.:

$$y(n) = x(2n) \tag{2.21}$$

The opposite operation to subsampling is upsampling. Upsampling increases the length of a signal by inserting zeros between each pair of samples. In contrast to subsampling, upsampling does not discard information and therefore it can always be inverted.
The upsampling by a factor 2, doubles the number of samples in a signal by inserting one zero between each pair of samples. This can be mathematically illustrated by:

$$y(m) = \begin{cases} x\left(\frac{m}{2}\right) & for\ m = 2n \\ 0 & Otherwise \end{cases} \tag{2.22}$$

2.3.2 Analysis Filter Bank

The refinement equations given in (2.13) and (2.15) can be rewritten so that the lower scale representations of the wavelet and scaling functions can be expressed in those of higher scale as [15]:

$$\begin{aligned} \varphi(2^{\alpha}t-\beta) &= \sum_n h(n)\sqrt{2}\varphi\left(2(2^{\alpha}t-\beta)-n\right) \\ &= \sum_n h(n)\sqrt{2}\varphi\left(2^{\alpha+1}t-2\beta-n\right) \\ &= \sum_{m=2\beta+n} h(m-2\beta)\sqrt{2}\varphi\left(2^{\alpha+1}t-m\right) \end{aligned} \tag{2.23}$$

$$\begin{aligned} \psi(2^{\alpha}t-\beta) &= \sum_n g(n)\sqrt{2}\psi\left(2(2^{\alpha}t-\beta)-n\right) \\ &= \sum_n g(n)\sqrt{2}\psi\left(2^{\alpha+1}t-2\beta-n\right) \\ &= \sum_{m=2\beta+n} g(m-2\beta)\sqrt{2}\psi\left(2^{\alpha+1}t-m\right) \end{aligned} \tag{2.24}$$

Using derivation carried above for wavelet and scaling function, we can express similarly DWT coefficients at scale α by coefficients at the higher scale α+1 as follows:

$$\begin{aligned}\lambda(\alpha,\beta) &= \left\langle f(t), \varphi_{\alpha,\beta}(t) \right\rangle \\ &= \int f(t) 2^{\alpha/2} \varphi(2^{\alpha} t - \beta) dt \\ &= \sum_m h(m-2\beta) \int f(t) 2^{\alpha+1/2} \varphi(2^{\alpha+1} t - m) dt \\ &= \sum_m h(m-2\beta) \lambda(\alpha+1, m)\end{aligned} \tag{2.25}$$

$$\begin{aligned}\gamma(\alpha,\beta) &= \left\langle f(t), \psi_{\alpha,\beta}(t) \right\rangle \\ &= \int f(t) 2^{\alpha/2} \psi(2^{\alpha} t - \beta) dt \\ &= \sum_m g(m-2\beta) \int f(t) 2^{\alpha+1/2} \psi(2^{\alpha+1} t - m) dt \\ &= \sum_m g(m-2\beta) \gamma(\alpha+1, m)\end{aligned} \tag{2.26}$$

Equations (2.25) and (2.26) imply that wavelet and scaling DWT coefficients at the certain scale can be calculated by taking a weighted sum of DWT coefficients from higher scales. This can be viewed as convolution between the DWT coefficients at scale α+1 with wavelet and scaling filter coefficients and subsequently subsampling each output with factor 2 to obtain new wavelet and scaling DWT coefficients at scale α. Therefore, we can describe equations (2.25) and (2.26) by a 2-channel filter bank illustrated in figure 2.9.

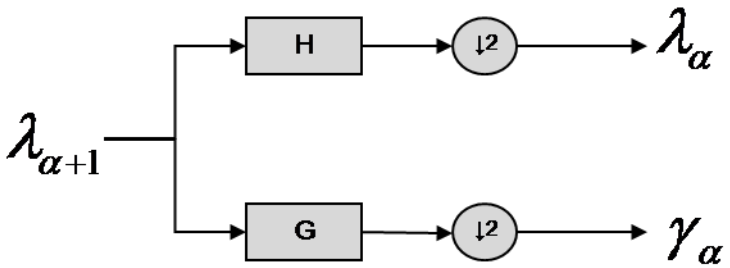

Figure 2.9: 2-Channel Analysis Filter Bank

The 2-channel filter bank first splits the input signal in two parts and filters one part with filter *H* and other with filter *G*. Both filtered signals are then subsampled by 2 and resulting signals are forwarded to the output of the 2-channel filter bank. Each output signal will therefore contain half the number of samples and will span half of the frequency band compared to the input signal. It should be noticed that the number of samples at the input of the filter bank equals the number of samples at the output.

The complete representation of the DWT can be obtained by iteration of the 2-channel filter bank and taking repeatedly scaling DWT coefficients λ as input. The iteration process starts with λ at the largest scale which is equal to the original signal. The number of stages in iteration process will determine the DWT resolution and therefore the number of channels.
The example of a two band analysis tree with three stages is graphically shown by figure 2.10. The input signal f has 512 samples and contains frequencies that lie between 0 and π. The resulting decompositions together will still contain 512 samples and span the same frequency band as the original signal but these will be decomposed in different DWT coefficients.

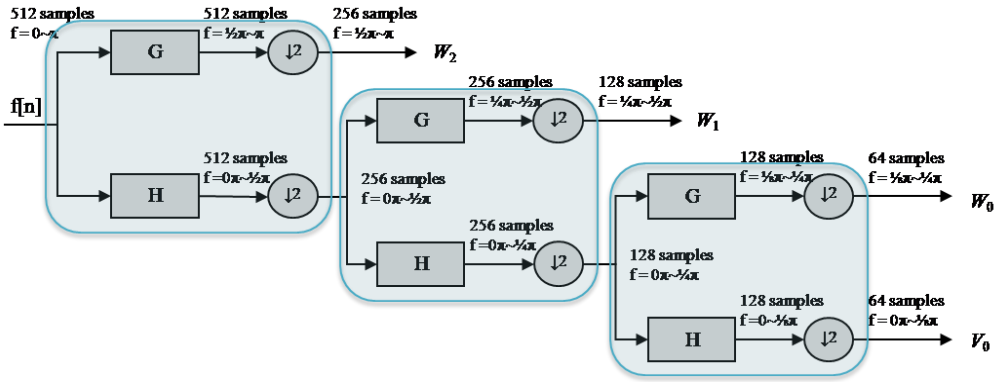

Figure 2.10: 3-Stage Analysis Tree

The subband structure of wavelet decomposition in frequency domain can be calculated using Fourier transformation. For the previous example of 3-stage analysis tree the corresponding subband structure is illustrated in figure 2.11.

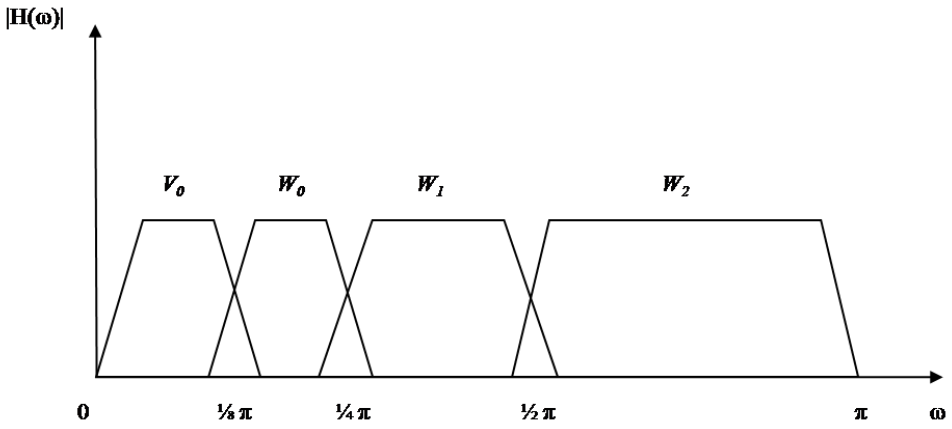

Figure 2.11: Frequency Bands for the 3-Stage Analysis Tree

2.3.3 Synthesis Filter Bank

The reconstruction formula for DWT is given in equation (2.17). If we now substitute the refinement equations for wavelet and scaling function, (2.15) and (2.13) respectively, into reconstruction equation (2.17) we get:

$$f(t)=\sum_{\beta}\lambda(\alpha,\beta)\sum_{n}h(n)2^{(\alpha+1)/2}\varphi\left(2^{\alpha+1}t-2\beta-n\right)+\sum_{\beta}\gamma(\alpha,\beta)\sum_{n}g(n)2^{(\alpha+1)/2}\varphi\left(2^{\alpha+1}t-2\beta-n\right) \tag{2.27}$$

Multiplying both sides of equation (2.27) by $\varphi(2^{\alpha+1}t-\beta')$ and taking the integral allows us to describe the DWT coefficients at higher scales by those of the lower scale as [15]:

$$\lambda(\alpha+1,\beta)=\sum_{m}\lambda(\alpha,m)h(\beta-2m)+\sum_{m}\gamma(\alpha,m)g(\beta-2m) \tag{2.28}$$

The equation (2.28) implies that the DWT coefficients at certain scale level α+1 can be reconstructed by taking a combination of weighted wavelet and scaling DWT coefficients at previous scale α. This process can be described by the 2-channel synthesis filter bank, illustrated in figure 2.12.

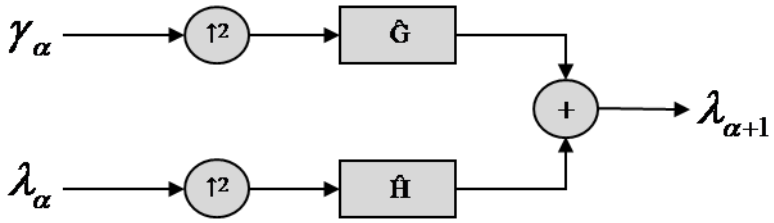

Figure 2.12: 2-Channel Synthesis Filter Bank

The 2-channel synthesis filter bank performs exactly opposite operation compared to previously discussed analysis filter bank. The wavelet and scaling DWT coefficients are first upsampled by factor 2 and after that the wavelet function DWT coefficients are filtered with HPF $\hat{G}$ while scaling function DWT coefficients are filtered with LPF $\hat{H}$. The two filtered signals are then added to each other to construct DWT coefficients at higher scale. The filters $\hat{H}$ and $\hat{G}$ are according to equation (2.28) and equations (2.25) and (2.26) time reversed version of filters H and G respectively.

The decomposition of a signal in terms of coefficients is called discrete wavelet transform. In order to reconstruct the original signal from coefficients we can apply inverse wavelet transform, abbreviated IDWT. The IDWT can be efficiently implemented by iterating the 2-channel synthesis filter bank in the same manner like we have done in the previous paragraph for the 2-channel analysis filter bank. The example of 3-stages synthesis tree is illustrates in figure 2.13.

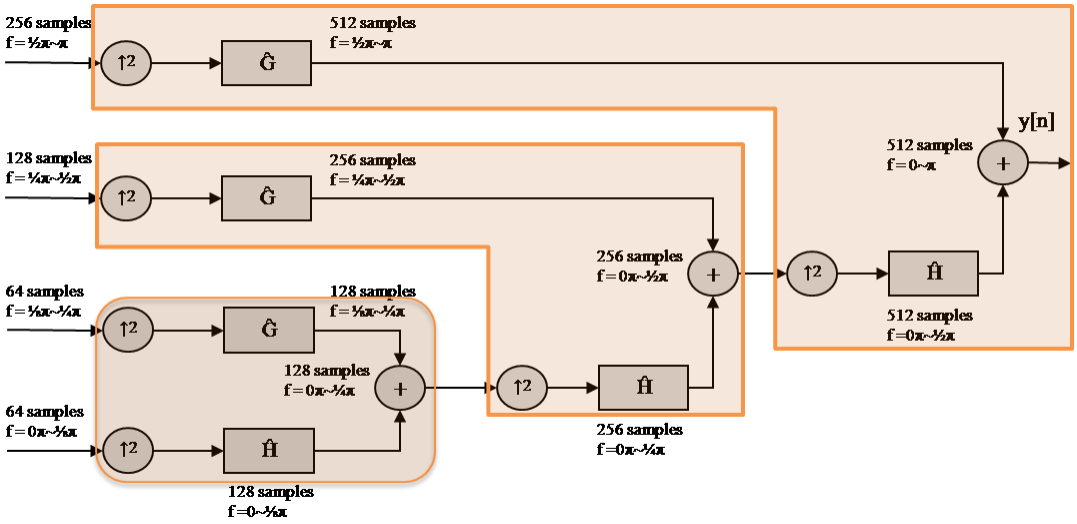

Figure 2.13: Synthesis Tree

If our primal assumption of orthogonality (2.16) is valid the reconstructed signal is simply delayed version of the input signal ($x(n) = y(n)$). The filter banks that satisfy this property are called perfect reconstruction filter banks.

2.3.4 Wavelet Packets

The resolution of discrete wavelet transform, as described so far, depends on the frequency bands. Because we are iterating the 2-channel filter bank only for the low pass output (scaling function branch), at the end of decomposition the high frequencies will have wide bandwidths while low frequencies will have narrow bandwidths, see illustration 2.11.

The wavelet packet transform on the contrary performs the iteration of the 2-channel filter bank on both sides: low pass (scaling function branch) and high pass (wavelet function branch). Because the high frequencies are decomposed in the same manner as low frequencies the wavelet packet transform has evenly spaced frequency resolution. Figure 2.14 shows the frequency bands for 3-stage wavelet packet tree.

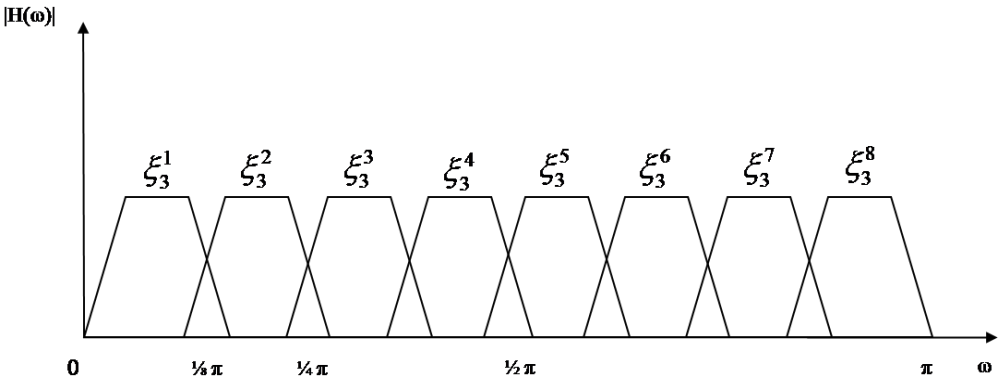

Figure 2.14: Frequency Bands for 3-Stage Wavelet Packets Tree

The filter bank structure for wavelet packet transform expands to a full binary tree. In order to make clear distinction between different sets of coefficients we will label each wavelet packet ξ by the level l which corresponds to the depth of the node in the tree and by the current position p of the node at a given level.
Wavelet packet decomposition recursively splits each parent node in two orthogonal subspaces W_l^p located at the next level:

$$W_l^p = W_{l+1}^{2p} \oplus W_{l+1}^{2p+1} \tag{2.29}$$

The subspaces given in equation (2.29) are those spanned by the basis functions of wavelet packets:

$$W_l^p = \overline{span\left\{2^{l/2}\xi_l^p(2^l t - \beta)\right\}}$$

Wavelet packet coefficients ζ at a certain level are calculated by convolving the wavelet and scaling filter with wavelet packets coefficients from previous level. This action is performed repeatedly for all wavelet packets until the full binary tree is obtain with desired depth. The equation (2.30) shows the recursive equation for wavelet packets generation. The wavelet packets coefficients $\zeta_{l+1}^{2p}(\beta)$ are generated using the scaling filter and coefficients $\zeta_{l+1}^{2p+1}(\beta)$ are created using the wavelet filter.

$$\begin{aligned}\zeta_{l+1}^{2p}(\beta) &= \sum_m h(m-2\beta)\zeta_l^p(m)\\ \zeta_{l+1}^{2p+1}(\beta) &= \sum_m g(m-2\beta)\zeta_l^p(m)\end{aligned} \tag{2.30}$$

In the regular DWT decomposition for each additional level we need only to perform single iteration of 2-channel filter bank while in wavelet packet transform the number of iterations is exponentionally proportional to the number of levels. Therefore, the wavelet packet transform has higher computational complexity when compared to regular DWT. By utilization of fast filter bank algorithm wavelet packet transform requires $O(N\log(N))$ operation, similar to FFT while DWT needs only $O(N)$ calculation [15].

Figure 2.15 illustrates the full binary tree for the 3-stages wavelet packet analysis.

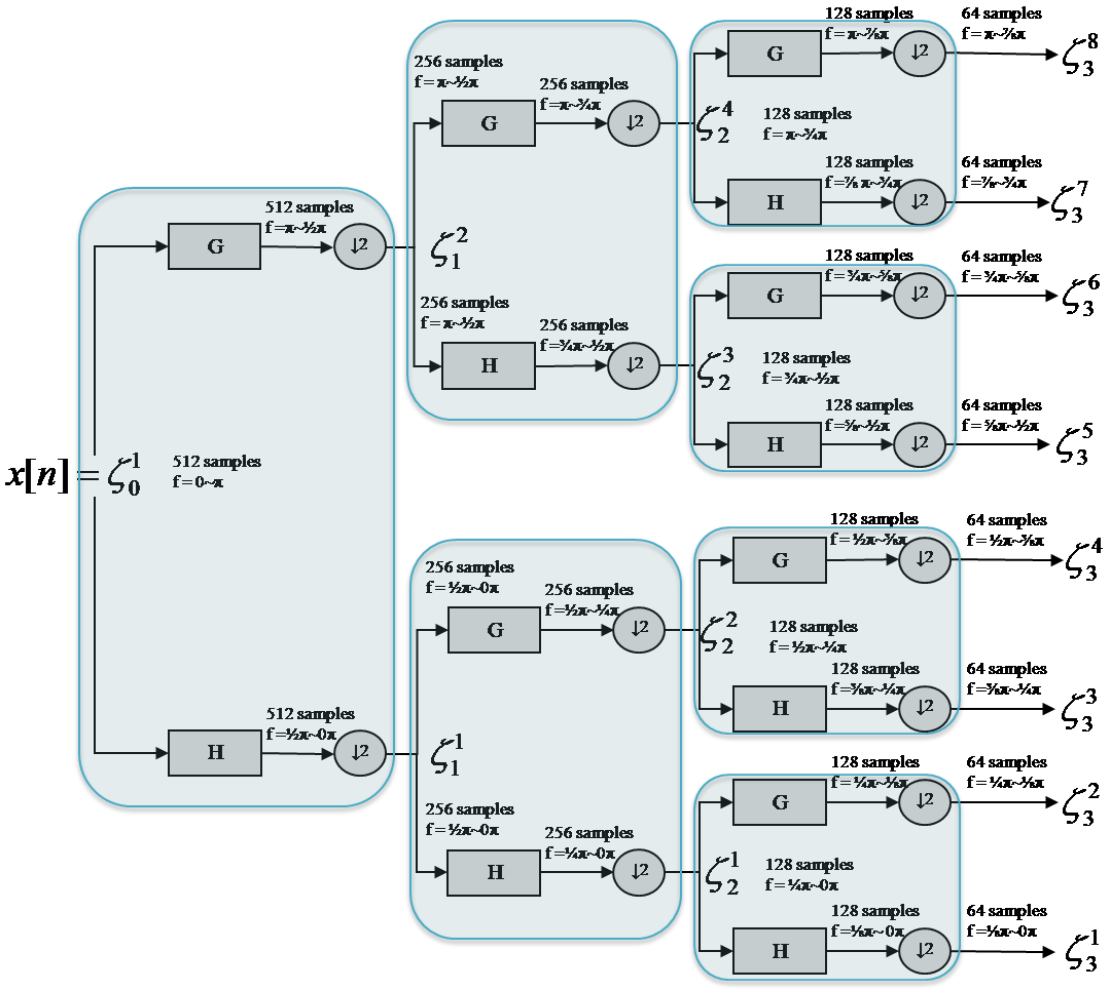

Figure 2.15: 3-Stages Wavelet Packet Analysis Tree

The reconstruction of wavelet packets is also performed in an iterative method. For each pair of wavelet packets coefficients at level l of the tree we can calculate wavelet packets coefficients at the previous level l-1 by:

$$\zeta_l^p(\beta) = \sum_m \zeta_{l+1}^{2p}(m)h(\beta - 2m) + \sum_m \zeta_{l+1}^{2p+1}(m)g(\beta - 2m) \tag{2.31}$$

Figure 2.16 illustrates the 3-stages wavelet packets synthesis tree.

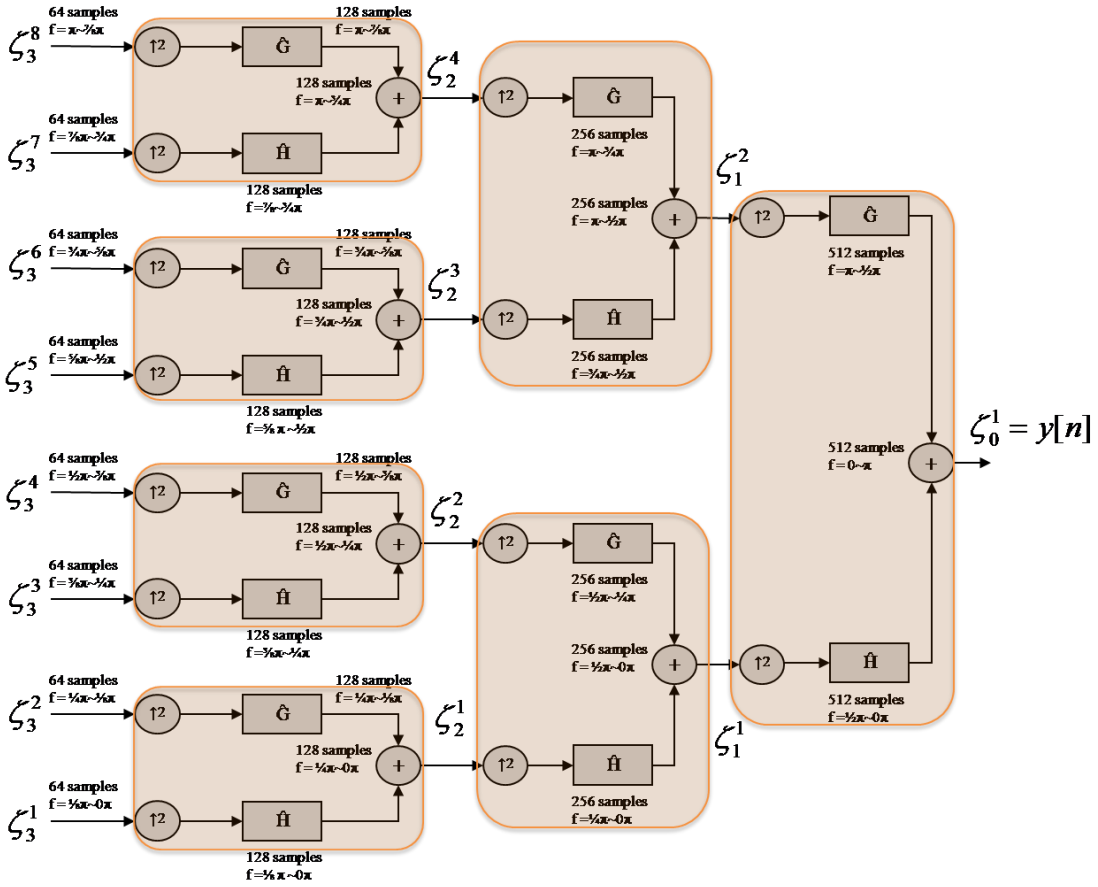

Figure 2.16: 3-Stages Wavelet Packets Synthesis Tree

2.4 Most Popular Wavelets

Today we can find quite a few wavelets in the textbooks that are recognized by most authors. Each wavelet has some distinguishing characteristics that make it more suitable for one application than other. Therefore during design of a system the careful consideration of different wavelet properties should be made with respect to the system requirements.
The selection of wavelets is generally made on following wavelet properties:

- Compact Support
- Orthogonality
- Symmetry
- *K*-Regularity/Vanishing Moments
- etc.

Compact support is defined by the length of the filter. In order to decrease computational complexity we prefer shorter filters however, filter length is closely related to other wavelet

properties like orthogonality or regularity. This means by setting other wavelet properties we automatically define minimum filter length.
Orthogonality ensures perfect reconstruction making it one of the most vital wavelet properties. For communication purposes we absolutely require orthogonal wavelets but for other applications orthogonality is occasionally too restrictive.
Symmetrical wavelets have as feature that transform of the mirror of an image is the same to the mirror of the wavelet transform. None of the orthogonal wavelets except Haar wavelet is symmetric. Although, requiring symmetric wavelets involuntarily means that wavelets are not orthogonal there are some applications that prefer symmetric wavelets above orthogonal ones. For instance image compression techniques like JPEG2000 uses biorthogonal symmetric wavelets. Because by compression of an image we discard one part of the wavelet coefficients containing high detail, the perfect reconstruction has become impossible anyhow. The fulfillment of symmetry property in JPEG2000 on the other hand results in more natural, smooth images.
K-regularity is also an important measure for wavelets because it helps reduce the number of non-zero coefficients in the high-pass sub-bands and it is one of the easiest ways to determine if a scaling function is fractal. Usually the more a wavelet has zero wavelet moments the smoother the scaling function is. However this is not a tight condition. The smoothness is actually defined by the continuous differentiability of the scaling function. There are two ways in which smoothness can be defined: local by the Hölder measure and global by the Sobolev measure. As different applications prefer one measure of smoothness above another we will here mention only the *K*-regularity.
In table 2-1 we list some of the most popular wavelets today and give their most important properties [22].

Table 2-1: Standard Wavelet Specifications

Name	Compact Support	Orthogonality		Symmetry	*K*-Regularity	Figure
Haar	2	☑		☑	1	2.17
Daubechies	L	☑	☒	far from	L/2	2.18
Symlets	L	☑	☒	near to	L/2	2.19
Discrete Meyer	102	☑		☒	1	2.20
Coiflet	L	☑	☒	near to	L/6	2.21
Bi-orthogonal	(L_1,L_2)	☒		☑	$\approx(L_1/2, L_2/2)$	2.22

The scaling and wavelet function for each of the listed wavelets in table 2-1 are illustrated in the figures 2.17 – 2.22. At the right side of these figures the corresponding frequency responses are shown for low pass and high pass filters.

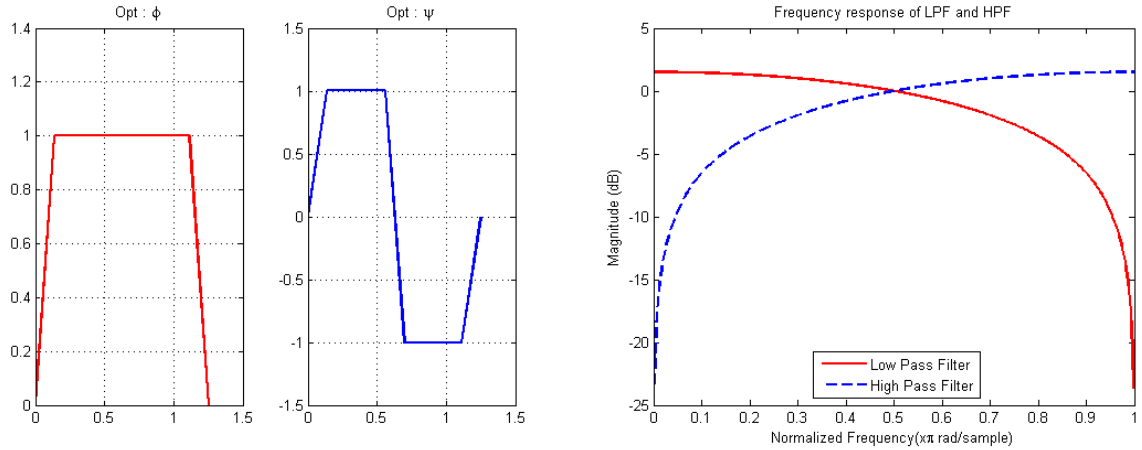

Figure 2.17: Haar Wavelet, Left: Scaling Function, Middle: Wavelet Function, Right Frequency Response of the LPF and HPF

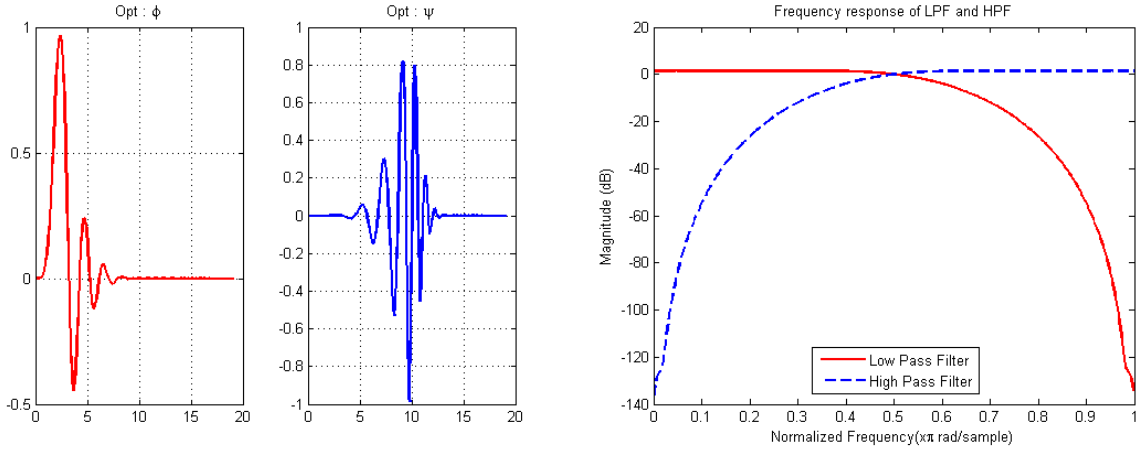

Figure 2.18: Daubechies Wavelet with 20 Coefficients, Left: Scaling Function, Middle: Wavelet Function, Right Frequency Response of the LPF and HPF

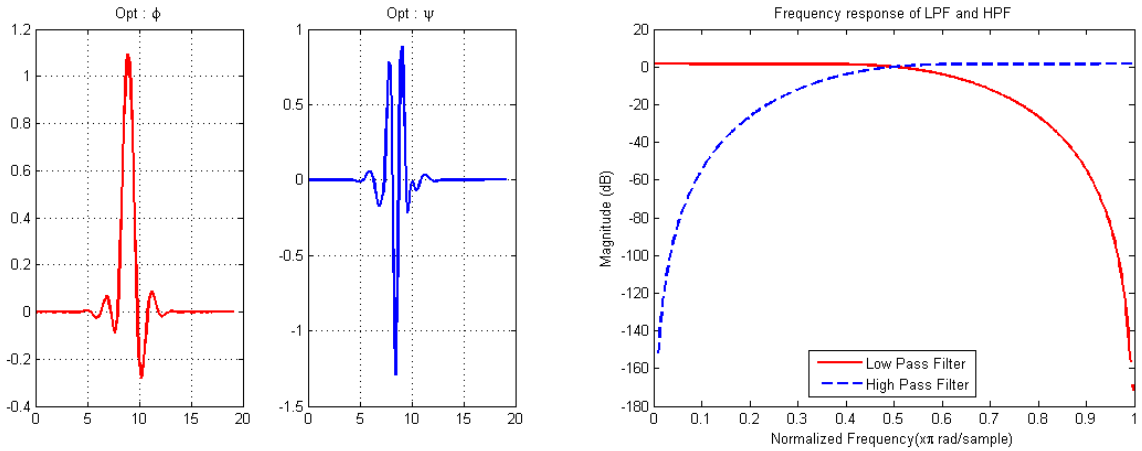

Figure 2.19: Symlets Wavelet with 20 Coefficients, Left: Scaling Function, Middle: Wavelet Function, Right Frequency Response of the LPF and HPF

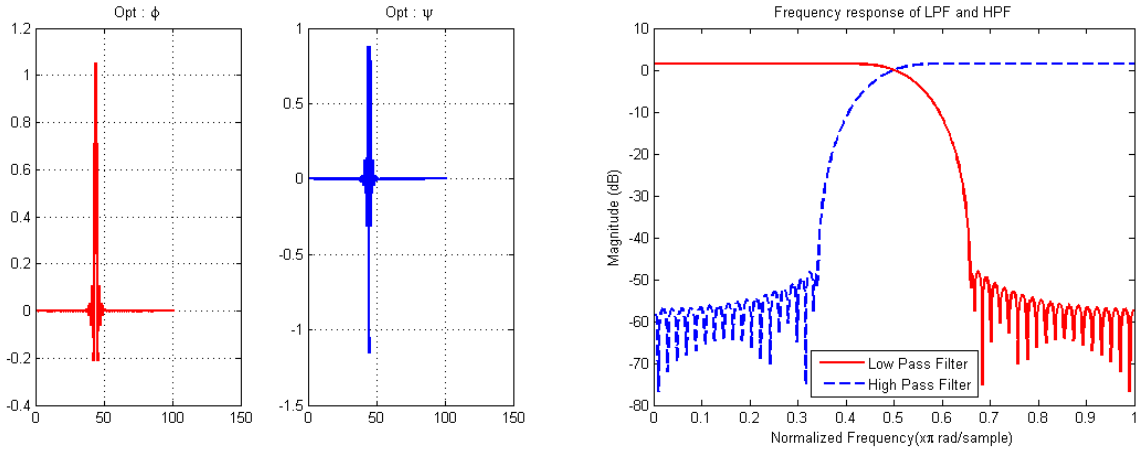

Figure 2.20: Discrete Meyer Wavelet with 102 Coefficients, Left: Scaling Function, Middle: Wavelet Function, Right Frequency Response of the LPF and HPF

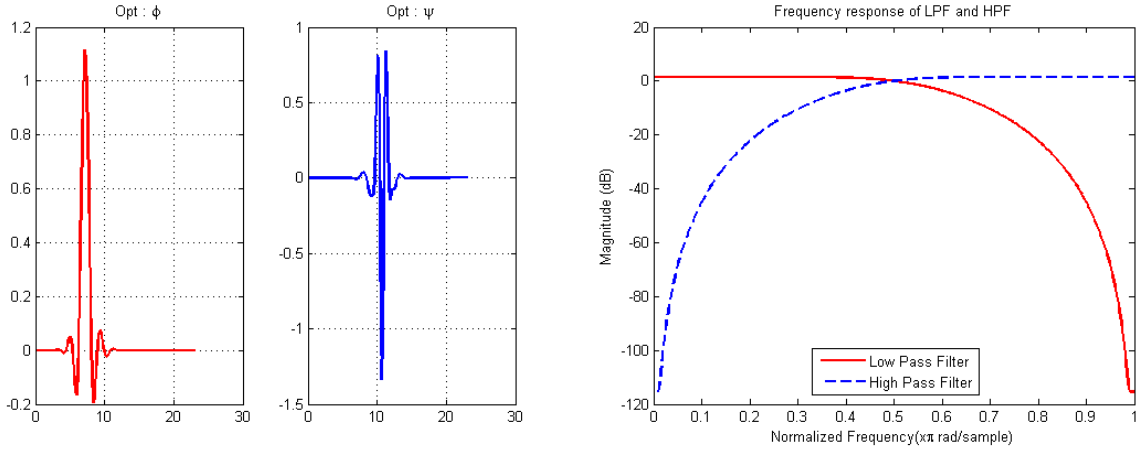

Figure 2.21: Coiflet Wavelet with 24 Coefficients, Left: Scaling Function, Middle: Wavelet Function, Right Frequency Response of the LPF and HPF

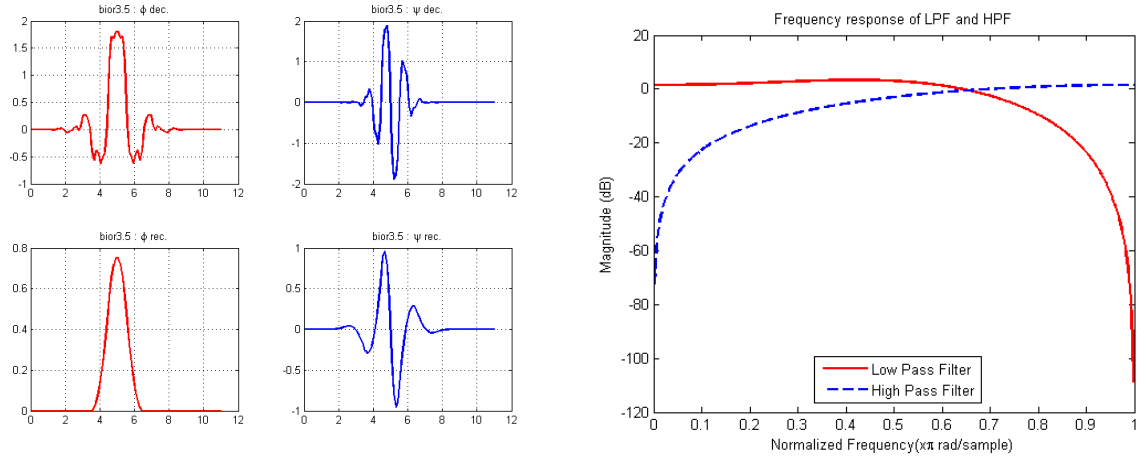

Figure 2.22: Biorthogonal Wavelet with (12, 4) Coefficients, Left: Scaling Function, Middle: Wavelet Function, Right Frequency Response of the LPF and HPF

2.5 Wavelet Packet based Multi Carrier Modulation

Wavelet Packet based Multi Carrier Modulation (WPMCM) is a multiplexing method that makes use of orthogonal wavelet packets waveforms to combine a collection of parallel signals into single composite signal. Fundamentally OFDM and WPMCM have many similarities as both use orthogonal waveforms as subcarriers and they achieve high spectral efficiency by allowing subcarriers' spectra to overlap one another. The adjacent subcarriers do not interfere with each other as long as the orthogonality between subcarriers is preserved.

The difference between OFDM and WPMCM is the shape of the subcarriers and in way they are created. OFDM makes use of Fourier bases which are static sines/cosines while WPMCM uses wavelets which offer much more flexibility. By utilization of different wavelets in WPMCM we can get different subcarriers which lead to different transmission system characteristics. Therefore, it is possible in WPMCM by selection of wavelets to change the bandwidth efficiency, frequency concentration of subcarriers, sensitivity to synchronization errors, PAPR, etc. [23] – [27].

WPMCM employs Inverse Discrete Wavelet Packet Transform (IDWPT) at the transmitter side and Discrete Wavelet Packet Transform (DWPT) at the receiver side, analogous to the IDFT and DFT used by OFDM transceivers. The IDWPT is implemented by wavelet packet synthesis tree which combines different parallel streams into a single signal. This composite signal is afterwards decomposed at the receiver using wavelet packets analysis tree or so called DWPT. The structure where synthesis tree is placed prior the analysis tree is called transmultiplexer. Figure 2.23 illustrates a 4-channel transmultiplexer.

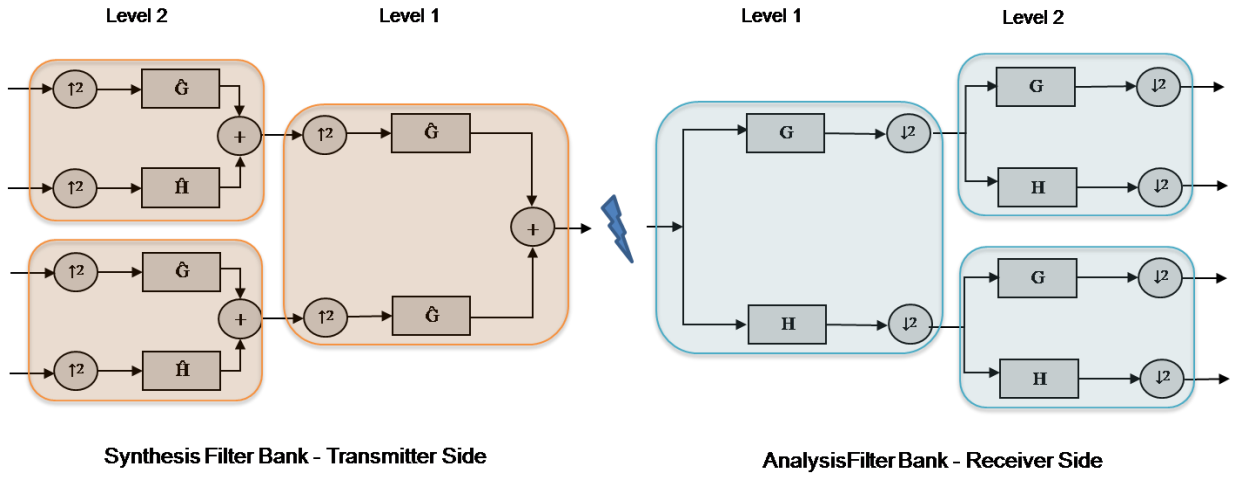

Figure 2.23: Wavelet Packets Transmultiplexer

The number of levels in synthesis and analysis trees determines the amount of subcarriers in the WPMCM system by:

$$N = 2^{l} \tag{2.32}$$

In equation (2.32) N determines the number of subcarriers and l represents the number of levels in the filter bank.

The wavelet packet synthesis and analysis tree are constructed by iteration of corresponding 2-channel filter bank, as explained in § 2.3. Therefore, the subcarriers of WPMCM are completely determined by the scaling and wavelet filter. The calculation of wavelet packet waveforms is performed in a recursive manner using filters coefficients $h(n)$ and $g(n)$ as:

$$\begin{aligned} \xi_{l+1}^{2p}(t) &= \sqrt{2}\sum_{n} h(n)\xi_{l}^{p}(t-2^{l}n) \\ \xi_{l+1}^{2p+1}(t) &= \sqrt{2}\sum_{n} g(n)\xi_{l}^{p}(t-2^{l}n) \end{aligned} \tag{2.33}$$

The subscripts l in equation (2.33) determines the level in the tree structure and superscript p can be seen as subcarrier index at a given tree depth (level l).

The filters in WPMCM cannot be arbitrary chosen and not all scaling and wavelet filters will fit the requirements for a communication system. First of all, we will only consider FIR filters because they allow wavelet packet transformation to be implemented by described fast recursive algorithm. Furthermore, we require perfect reconstruction and hence the orthogonal subcarriers. These can only be generated by filters that fulfill the orthogonality constraint. The WPMCM subcarriers are mutually orthogonal if they satisfy the following condition:

$$\left\langle \xi_{l}^{p}(t), \xi_{l}^{i}(t) \right\rangle = \sum_{k} \xi_{l}^{p}(t)\xi_{l}^{i}(t) = \delta(p-i) \tag{2.34}$$

The transmitted signal for WPMCM is composed of successively modulated WPMCM symbols that are built from a sum of modulated subcarriers. The WPMCM transmitted signal in the discrete time domain can be expressed as:

$$S(n) = \sum_{u}\sum_{k=0}^{N-1} a_{u,k}\xi_{2^{\log(N)}}^{k}(n-uN) \tag{2.35}$$

In equation (2.35) k denotes the subcarrier index and u denotes the WPMCM symbol index. The constellation symbol modulating k^{th} subcarrier in u^{th} WPMCM symbol is represented by $a_{u,k}$.

If we assume that the WPMCM transmitter and receiver are perfectly synchronized and that the channel is ideal, the detected data at the receiver can be given by:

$$
\begin{aligned}
\hat{a}_{u',k'} &= \sum_{n} R(n)\xi^{k'}_{2^{\log(N)}}(u'N-n) \\
&= \sum_{n}\sum_{u}\sum_{k=0}^{N-1} a_{u,k}\xi^{k}_{2^{\log(N)}}(n-uN)\xi^{k'}_{2^{\log(N)}}(u'N-n) \\
&= \sum_{u}\sum_{k=0}^{N-1} a_{u,k}\left(\sum_{n}\xi^{k}_{2^{\log(N)}}(n-uN)\xi^{k'}_{2^{\log(N)}}(u'N-n)\right) \\
&= \sum_{u}\sum_{k=0}^{N-1} a_{u,k}\delta(k-k') \\
&= a_{u,k}
\end{aligned}
\tag{2.36}
$$

In equation (2.36) we have used the fact that different symbols are not interfering with each other and that subcarriers with index other than *k* are not contributing, according to the orthogonality equation (2.34).

One important property of wavelet based transformation is that the waveforms used in general are longer than the transform duration of one symbol. This cause WPMCM symbols to overlap in time domain. Thanks to the orthogonality of used waveforms this overlap of the symbols does not automatically lead to Inter Symbol Interference (ISI).

The multicarrier symbols of OFDM are not overlapping each other as IDFT and DFT transform are carried out for each group of subcarriers independently. On the other hand, the use of longer waveforms in WPMCM allows better frequency localization of subcarriers while in OFDM the rectangular shape of DFT window generates large side lobes. The spectra of WPMCM and OFDM for 8 subcarriers are illustrated side by side in figure 2.24.

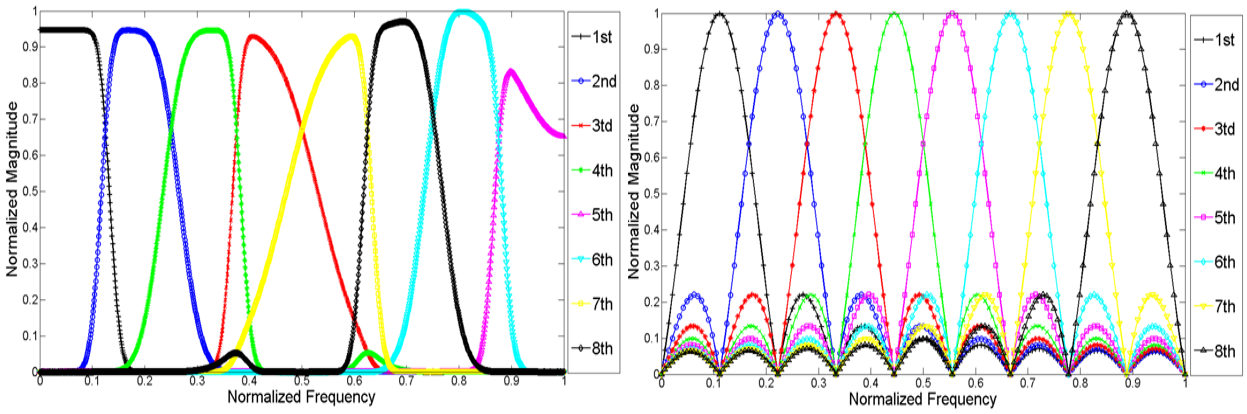

Figure 2.24: Spectrum of 8 Orthogonal Subcarriers, Left: WPMCM (Daubechies Length 20), Right: OFDM

The other non-palatable consequence of time overlap is the inability to use guard interval in WPMCM systems. Although adding a guard interval severely decreases spectral efficiency, it is effective and low complexity method to cope with dispersive channels and time offset. In contrast to OFDM, in WPMCM we will not add cyclic prefix block as it would only lead to decrease of spectral efficiency without giving any benefits.

The WPMCM transmitter and receiver block diagrams are illustrated in figures 2.25 and 2.26 respectively.

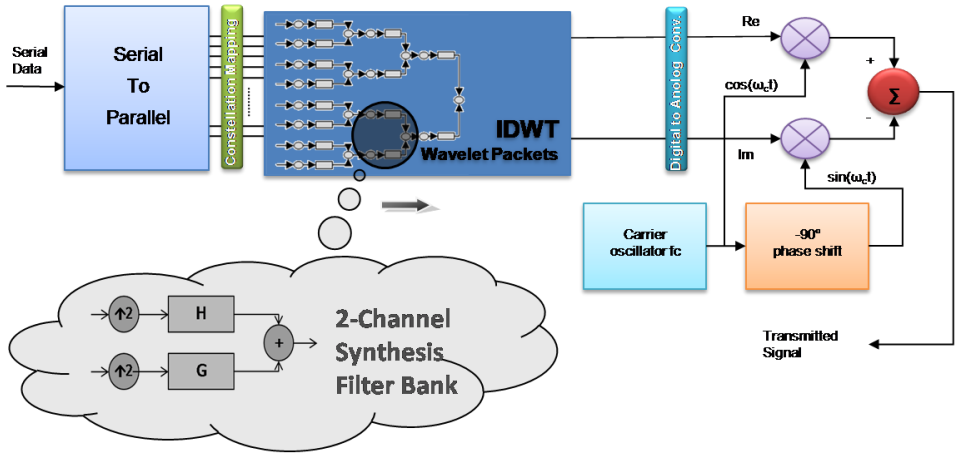

Figure 2.25: WPMCM Transmitter

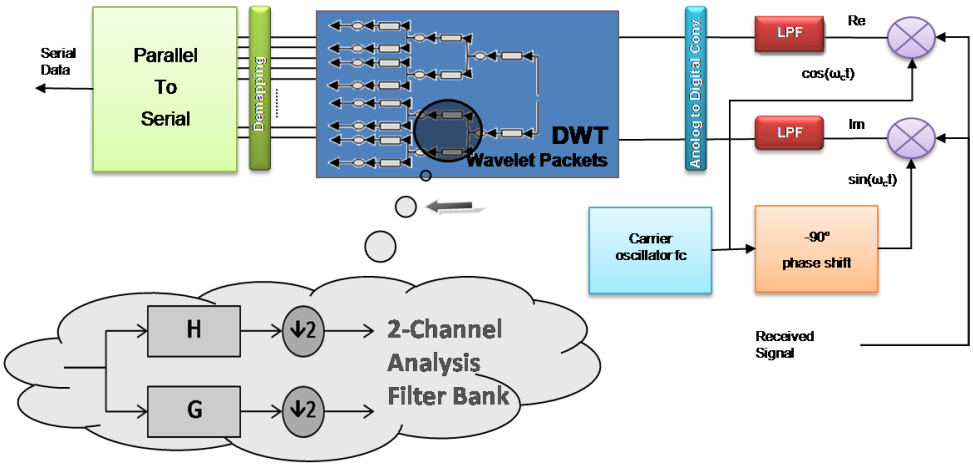

Figure 2.26: WPMCM Receiver

2.6 Conclusion

In this chapter we have discussed the basic theory of the wavelet transform and we have explained how discrete wavelet transform can be calculated with utilization of filter banks. Due to efficient implementation and the freedom they provide, wavelets have emerged in many different fields. Recently, wavelets have been also proposed as a candidate for multicarrier modulation. In this chapter we have presented WPMCM transceiver, which is one of the possible wavelet based implementation of orthogonal multicarrier system.

It is known that multicarrier systems like OFDM are very sensitive to carrier frequency offset, phase noise and time synchronization error. The WPMCM is relatively young multicarrier solution and therefore it is little known about its sensitivity to above mentioned synchronization errors.

You may be disappointed if you fail, but you are doomed if you don't try.
— Beverly Sills, 1929

3

Synchronization Errors

Multicarrier modulation techniques have gained popularity in the last decades due to higher bandwidth requirements, increased use of wireless systems in the time-dispersive environments (e.g. home, office, etc.) and lower costs of digital signal processing parts.
The principle of multicarrier modulation is to subdivide the total bandwidth into several parallel narrow subbands, giving multicarrier systems some important advantages when compared to single carrier communication systems. A few important benefits are:

- Increased symbol duration, hence better performance in dispersive channels.
- Use of several narrow subbands, therefore narrow band interference or strong frequency band attenuation only affects particular subcarriers and not the whole system.

The rapidly increasing number of new applications and lack of free spectrum restrict engineers to only consider bandwidth efficient multicarrier techniques. In order to achieve high bandwidth efficiency the subcarriers have to be closely spaced to each other, overlapping over each other. In this group of multicarrier systems belong OFDM and WPMCM, discussed in § 1.2 and § 2.5 respectively. OFDM and WPMCM have orthogonal subcarriers so that even the subcarriers overlap they do not interfere one another. However, the radio front-end induced impairments as frequency offset and/or phase noise can cause the subcarriers to lose their mutual orthogonality and to begin interfering one with another. The rise of interference level due to loss of

orthogonality among subcarriers is only experienced in multicarrier transmission. Therefore, the multicarrier systems with overlapping subcarriers are much more sensitive to the frequency offset and phase noise when compared to single carrier systems. This disadvantage of multicarrier systems sets high demands on the quality of the analog radio part, like oscillator stability. In case of OFDM the effects of frequency offset and phase noise are well documented in the literature [28] – [34] and number of synchronization techniques are reported to estimate and reduce the frequency offset and phase noise effects [35] – [39], [46], [47].
Besides the synchronization errors in form of frequency and phase misalignment, the multicarrier transceiver can also suffer from time synchronization error. Time synchronization error occurs when the start of the multicarrier symbol is incorrectly detected, selecting part of the adjacent symbol while discarding some samples at begin or at end of the useful symbol. Due to time synchronization errors the Inter Symbol Interference (ISI) arises as well as the Inter Carrier Interference (ICI). The use of guard intervals, like cyclic prefix in OFDM, can significantly improve the system performance in case of timing errors. However, the use of guard interval is not feasible solution for WPMCM systems because of time-overlapping nature of wavelet packet transform (see § 2.5).
Similarly to the frequency offset and phase noise effects on the performance of the system, also for timing errors the documentation is far more comprehensive for OFDM than for WPMCM. The sensitivity of the OFDM to the time synchronization error is reported in [42] – [44] and there are various techniques for OFDM symbol synchronization available in the literature [45] – [49].

In this chapter we will address different types of synchronization errors for the WPMCM transceiver, and compare the performance of WPMCM under these errors to OFDM. Each synchronization error will be treated separately. First we will treat the frequency offset between transmitter and receiver, after which follows the discussion of phase noise. We will finalize this chapter with discussion of time synchronization errors.

3.1 Frequency Offset in Multicarrier Modulation

The orthogonality between the subcarriers is maintained at the receiver only if the transmitter and receiver have the same reference frequency. Any offset in the frequency will result in loss of orthogonality and hence in generation of interference. The interference is the most severe consequence of frequency offset but not the only one. Besides the interference term, frequency offsets initiates attenuation and phase rotation of each subcarrier. Generally frequency offset can be caused by misalignment between receiver and transmitter local oscillator frequencies or due to Doppler shift.

The Doppler frequency shift f_d is proportional to the subcarrier frequency $f(n)$ and the relative speed between the transmitter and the receiver v_r. The Doppler shift is expressed as:

$$f_d(n) = \frac{v_r f(n)}{c} \tag{3.1}$$

In (3.1) c denotes the speed of light and it is approximately equal to 3×10^8 $^m/_s$. The frequency of each subcarrier can be calculated by taking the sum of main carrier frequency f_c and baseband subcarrier frequency f_{sc}, i.e.:

$$f(n) = f_c \pm f_{sc}(n) \tag{3.2}$$

Using equation (3.1) and (3.2) we can express the relative frequency offset due to Doppler shift as the ratio between the actual frequency offset and inter-carrier spacing as:

$$f_\varepsilon = \frac{f_d(n)}{f_c \pm f_{sc}(n)} = \frac{v_r}{c} \tag{3.3}$$

The frequency offset can be modeled at the receiver by multiplying received time-domain signal by a complex exponential whose frequency component is equal to frequency offset value. If we assume that transmitted signal is given by $S(n)$, the received signal $R(n)$ can now be written as:

$$R(n) = S(n)e^{j2\pi f_\varepsilon n/N + \phi_0} + w(n) \tag{3.4}$$

In (3.4) f_ε denotes the relative frequency offset due to local oscillator mismatch or due to Doppler shift or due to combination of both. N stand for the total number of subcarriers, ϕ_0 is initial phase and w denotes additive white Gaussian noise (AWGN). Without loss of generality, we assume for the moment that $w(n) = 0$ and $\phi_0 = 0$.

3.1.1 Frequency Offset in OFDM

In OFDM the frequency offset prevents the perfect alignment of FFT bins with the peaks of the sinc pulses i.e. subcarriers. The FFT output corresponding to the k^{th} subcarrier can be written in this case as:

$$\begin{aligned}\hat{a}_{k'} &= \frac{1}{N}\sum_{n=0}^{N-1} R(n)e^{-j2\pi\frac{k'n}{N}} \\ &= \frac{1}{N}\sum_{k=0}^{N-1} a_k \sum_{n=0}^{N-1} e^{j2\pi\frac{kn}{N}} e^{j2\pi f_\varepsilon \frac{n}{N}} e^{-j2\pi\frac{k'n}{N}} \\ &= \frac{1}{N}\sum_{k=0}^{N-1} a_k \sum_{n=0}^{N-1} e^{j2\pi\frac{(k-k'+f_\varepsilon)n}{N}}\end{aligned} \tag{3.5}$$

Using the geometric series properties the equation (3.5) can also be expressed as [34], [36]:

$$\hat{a}_{k'} = \frac{1}{N}\sum_{k=0}^{N-1} a_k \frac{\sin(\pi(k-k'+f_\varepsilon))}{\sin\left(\frac{\pi(k-k'+f_\varepsilon)}{N}\right)} e^{j\pi\left(\frac{N-1}{N}\right)(k-k'+f_\varepsilon)} \tag{3.6}$$

We can split equation (3.6) into two distinct parts:

$$\hat{a}_{k'} = a_{k'} \frac{\sin(\pi f_\varepsilon)}{N\sin\left(\frac{\pi f_\varepsilon}{N}\right)} e^{j\pi\left(\frac{N-1}{N}\right)f_\varepsilon} + \frac{1}{N}\sum_{k=0;k\neq k'}^{N-1} a_k \frac{\sin(\pi(k-k'+f_\varepsilon))}{\sin\left(\frac{\pi(k-k'+f_\varepsilon)}{N}\right)} e^{j\pi\left(\frac{N-1}{N}\right)(k-k'+f_\varepsilon)} \tag{3.7}$$

The first component of equation (3.7) stands for useful demodulated signal, which has been attenuated and phase shifted due to frequency offset. The second part of (3.7) contains the ICI term, in which contribute all other subcarriers.

3.1.2 Frequency Offset in WPMCM

The presence of the frequency offset in WPMCM transceiver cause the frequency misalignment between the waveforms of the transmitter and the receiver. The detected data at the WPMCM receiver in case of the frequency offset can be written for the k^{th} subcarrier and u^{th} symbol as:

$$\begin{aligned}\hat{a}_{u',k'} &= \sum_n R(n)\xi^{k'}_{2^{\log(N)}}(u'N-n) \\ &= \sum_n\sum_u\sum_{k=0}^{N-1} a_{f,k}\xi^{k}_{2^{\log(N)}}(n-uN)e^{j2\pi f_\varepsilon\frac{n}{N}}\xi^{k'}_{2^{\log(N)}}(u'N-n) \\ &= \sum_u\sum_{k=0}^{N-1} a_{f,k}\left(\sum_n \xi^{k}_{2^{\log(N)}}(n-uN)e^{j2\pi f_\varepsilon\frac{n}{N}}\xi^{k'}_{2^{\log(N)}}(u'N-n)\right)\end{aligned} \tag{3.8}$$

In order to shorten the derivation we are going to use different notation, first we define:

$$\Omega^{u,u'}_{k,k'} = \sum_n e^{j2\pi f_\varepsilon\frac{n}{N}}\xi^{k}_{2^{\log(N)}}(n-uN)\xi^{k'}_{2^{\log(N)}}(u'N-n) \tag{3.9}$$

Using equation (3.9) and (3.8) we can now express the output of the WPMCM receiver for the k^{th} subcarrier and u^{th} WPMCM symbol as:

$$\hat{a}_{u',k'} = a_{u',k'}\Omega^{u',u'}_{k'k'} + \sum_{u;u\neq u'} a_{u,k'}\Omega^{u,u'}_{k',k'} + \sum_u\sum_{k=0;k\neq k'}^{N-1} a_{u,k}\Omega^{u,u'}_{k,k'} \tag{3.10}$$

In equation (3.10) the first term stands for attenuated and rotated useful signal. The second term gives the ISI due to symbols transmitted on the same subchannel and the third term denotes ICI measured over the whole frame.

3.1.3 Numerical Results for Frequency Offset

The performance of WPMCM with frequency offset has been investigated by means of computer simulations and compared to the well-known OFDM. The WPMCM transceiver is simulated with different standard wavelets that are available today, an enumeration of tested wavelets and their properties is shown in Table 2-1. To simplify the analysis, the channel is taken to be additive white Gaussian noise (AWGN) and no other distortions except frequency offset is introduced. QPSK is the modulation of choice and frame size is set to 100 multicarrier symbols, each consisting of 128 subcarriers. Furthermore, the simulated system has no error estimation or correction capabilities nor are guard intervals or guard bands used. Any deviation from these specifications will be explicitly stated.
An overview of simulation set-up is given in table 3-1.

Table 3-1: Simulation Setup Frequency Offset

	WPMCM	OFDM
Number of Subcarriers	128	128
Number of Multicarrier Symbols per Frame	100	100
Modulation	QPSK	QPSK
Channel	AWGN	AWGN
Oversampling Factor	1	1
Guard Band	-	-
Guard Interval	-	-
Frequency Offset	f_ε= 5-10%	f_ε= 5-10%
Phase Noise	-	-
Time Offset	-	-

- does not apply

Figure 3.1 illustrates the bit error rate (BER) of OFDM and WPMCM transceivers with relative frequency offset of 5% with regard to $^1/_T$ spacing.
BER curves of different wavelets and OFDM show similar performance but due to frequency offset they all lie far from theoretical curve. The biorthogonal wavelet is the exception with a very poor performance compared to the other systems. This is due to the fact that the biorthogonal wavelet does not fulfill orthogonality condition (refer eq. 2.34) and therefore even without frequency offset it suffers from ICI and ISI.

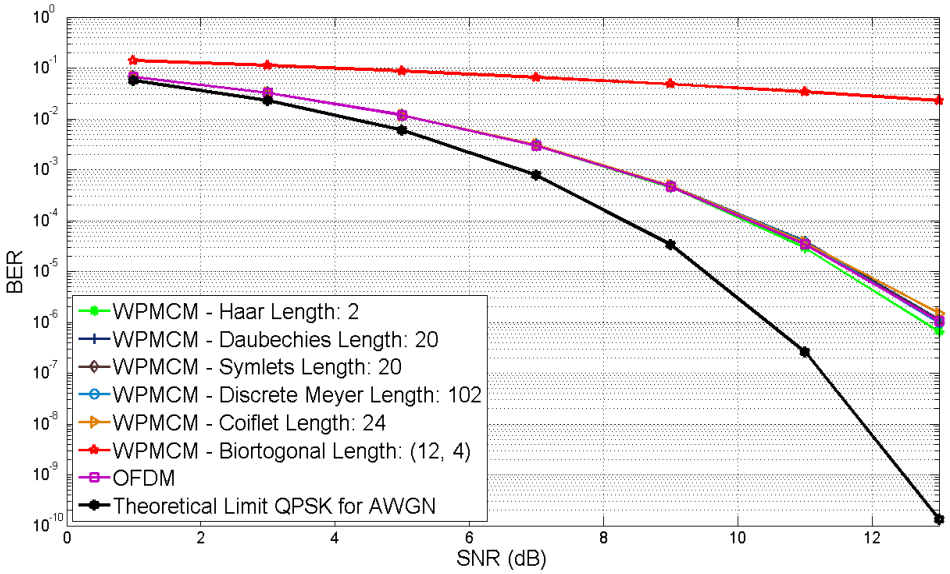

Figure 3.1: BER for WPMCM with Different Wavelets and OFDM under Relative Frequency Offset of 5%

In figure 3.2 the BER is shown for different values of relative frequency offset varying from 0 to 40%. During this simulation we kept SNR constant at 16 dB.

Again we can see that the performances of majority of the wavelets are very similar to that of OFDM. The biorthogonal wavelet has obviously a poor performance, while Haar wavelet slightly outperforms other wavelets and OFDM. The figure 3.2 implies that WPMCM and OFDM are both very sensitive to the frequency offset, since small variations of frequency offset degrade the system performance significantly.

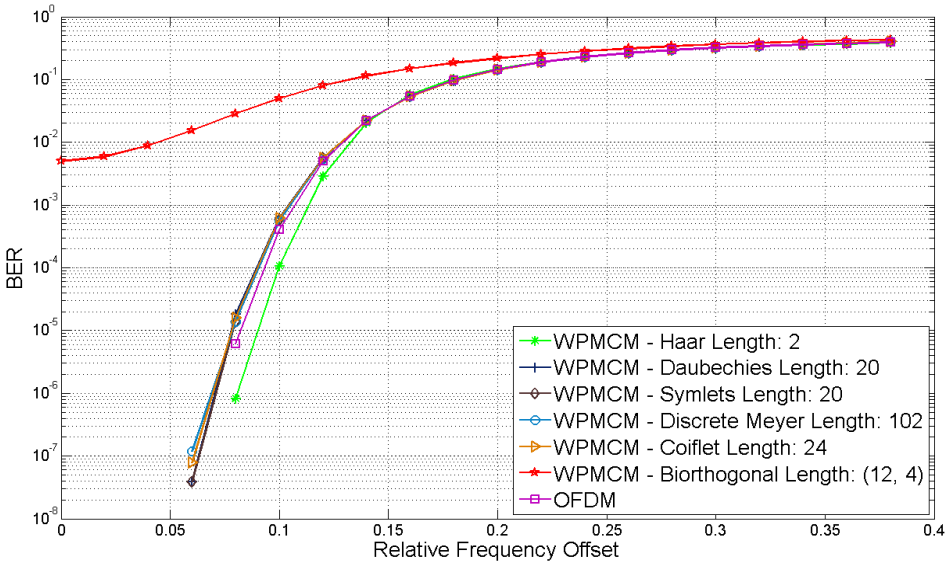

Figure 3.2: BER vs. Relative Frequency Offset for WPMCM and OFDM in AWGN Channel (SNR = 16 dB)

The figure 3.3 is obtained during simulation where we investigate the influence of the amount of subcarriers in combination with frequency offset on the BER. All WPMCM transceivers are now simulated with the same wavelet but with different number of subcarriers. We arbitrarily chose the Daubechies wavelet with 20 coefficients. Furthermore the relative frequency offset is set to 10% and again we use AWGN channel.
The degradation of WPMCM's BER in the presence of frequency offset is dependent on the number of subcarriers. This is straightforward when the absolute frequency offset is fixed [28], as for the more subcarriers in a given bandwidth the subcarrier spacing decreases and hence the relative frequency offset increases. However, in the figure 3.3 the relative frequency offset with respect to inter-carrier spacing is kept constant and there are still noticeable differences in the number of subcarriers used. The WPMCM with more subcarriers are slightly more susceptible to the frequency offset. This sensitivity decreases with increasing the number of subcarriers. From figure 3.3 we can also see that the performances of WPMCM with 64 and 128 subcarriers are almost identical for a given relative frequency offset.

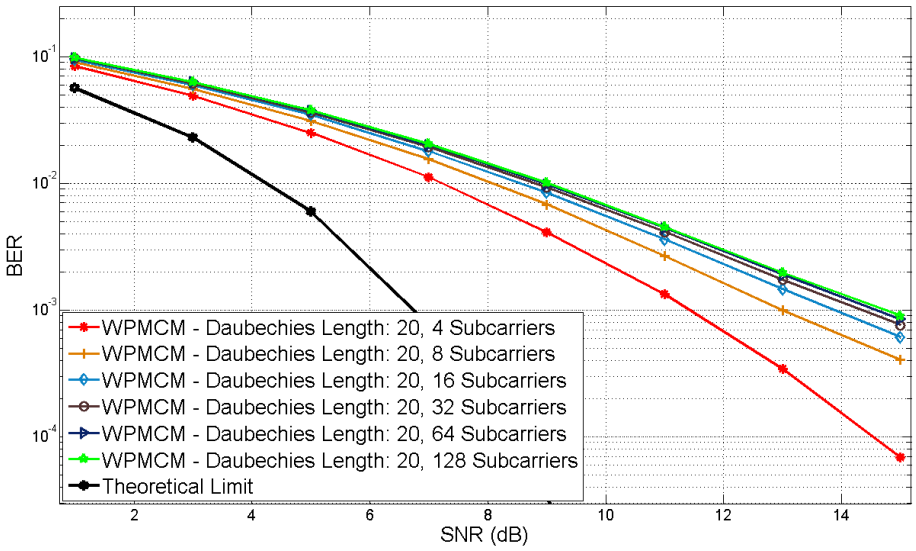

Figure 3.3: BER for WPMCM with Different Number of Subcarriers and Relative Frequency Offset of 10%

Frequency offset in WPMCM does not only lead to ICI inside one symbol but across the whole frame. Therefore, it is important to see the effect of the frame size in combination with the frequency offset. These results are illustrated in figure 3.4.
Figure 3.4 shows that the amount of multicarrier symbols in a frame does not affect the performance of WPMCM in the presence of frequency offset. The extraordinarily bad performance of WPMCM transceiver that uses frame size of just 5 multicarrier symbols is caused by the relatively long filter. We make use of periodic extension in order to deal with excessive length caused by the convolution. The problem occurs when the filter is longer than the frame. Accordingly the filtered data does not fit anymore in the available space and a part of the samples has to be discarded.

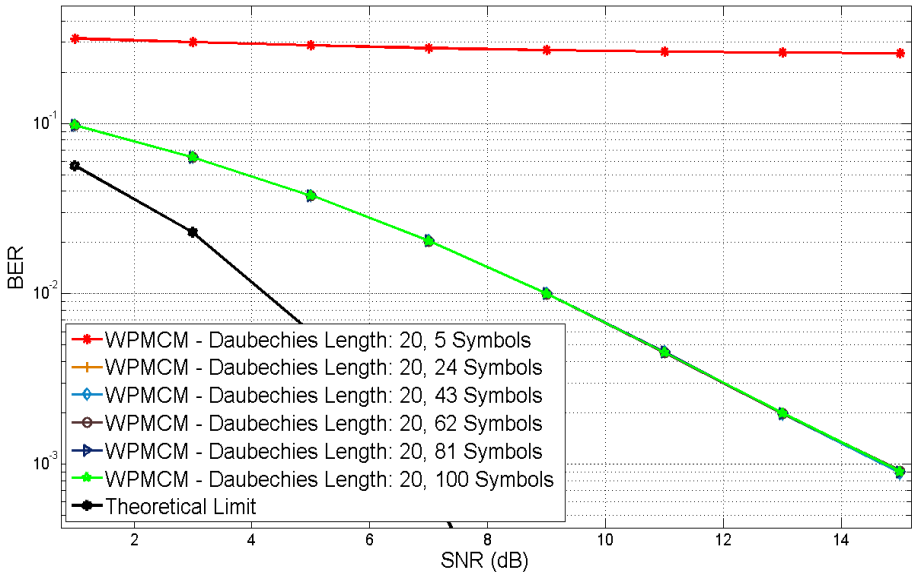

Figure 3.4: BER for WPMCM with Different Number of Multicarrier Symbols/Frame and Relative Frequency Offset of 10%

The influence of the filter's length in combination with the frequency offset on the BER is illustrated in figure 3.5. This simulation is performed for AWGN channel and the relative frequency offset of 10%. For a second time, we arbitrary choose the Daubechies wavelet but now we alter the number of filter's coefficients and fix the number of subcarriers to 128. In case of Daubechies wavelet the amount of wavelet zero moments is indisputably related to the length of the filter, and hence for each doubling of filters' coefficients we also double the number of wavelet zero moments.

The BER curves shown in figure 3.5 are all superimposed one over another, suggesting that the filter's length and number of wavelets' zero moments have no noticeable influence on the system performance in the case of frequency offset.

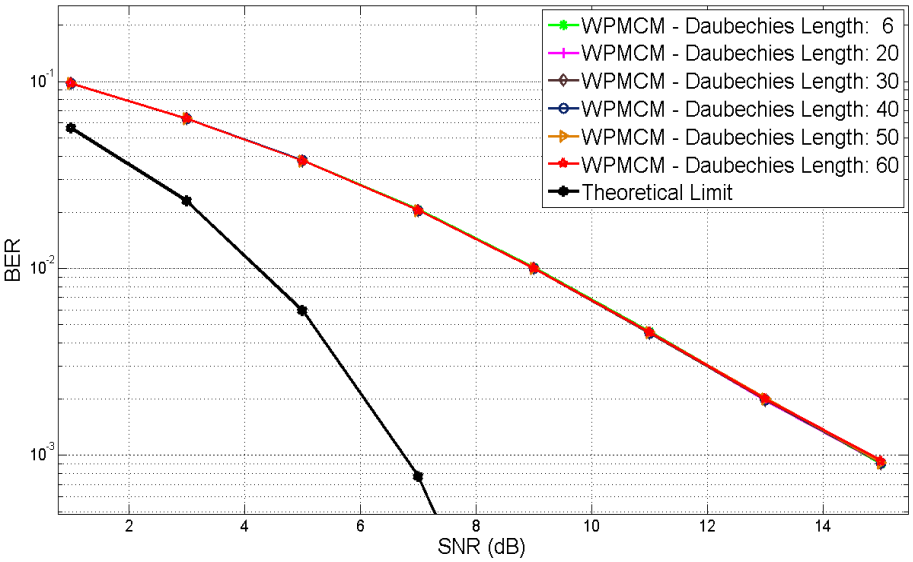

Figure 3.5: BER for WPMCM using Daubechies Wavelets of Different Lengths and Relative Frequency Offset of 10%

The effect of frequency misalignment between transmitter and receiver on the constellation points is depicted in the figure 3.6, for the relative frequency offset of 5%. In order to highlight the effect of frequency offset we assumed for the moment an ideal channel without any noise.
The main consequence of the frequency offset is the scattering of the constellation points around reference positions due to interference. Other consequences are the anti-clockwise rotation of all constellation points and almost negligible attenuation.

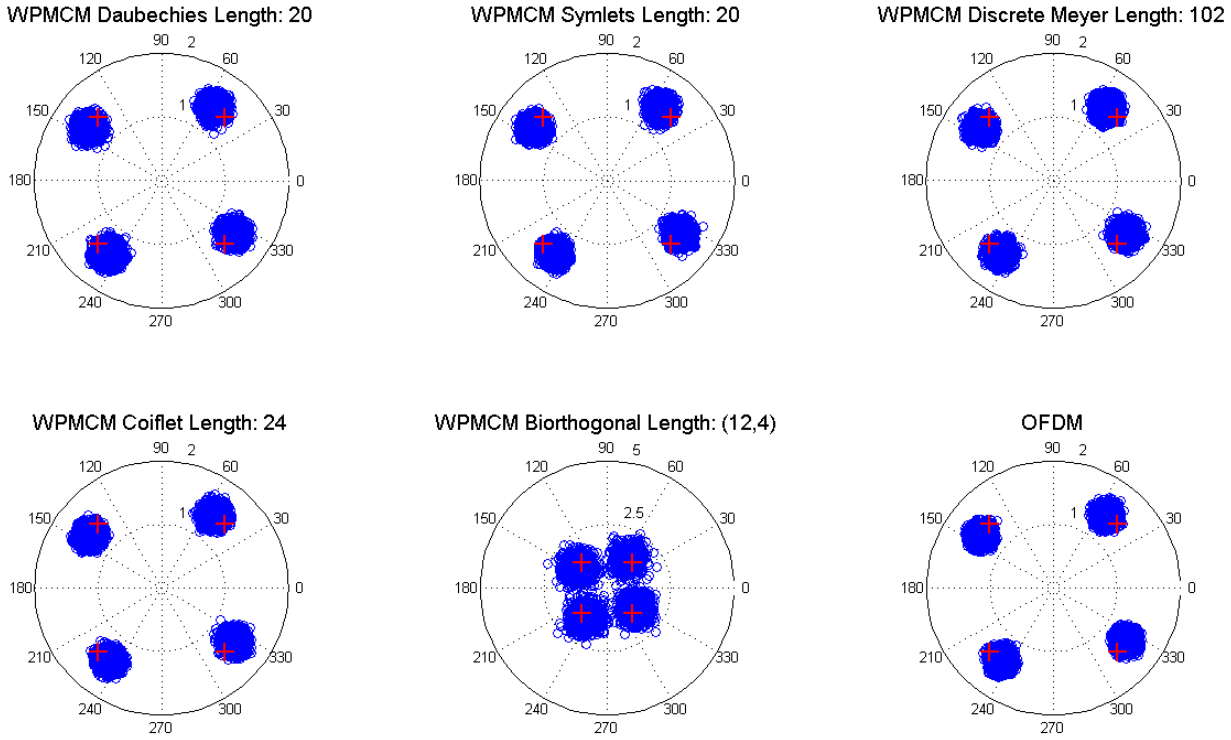

Figure 3.6: Constellation Points in the Presence of Relative Frequency Offset of 5%

The last set of figures in this section shows the dispersion of the subcarriers energy due to a frequency offset. For clarity we limited the number of subcarriers to 16 and the frame size to 30 multicarrier symbols. The channel is assumed to be ideal so that all exposed disturbance of the subcarriers is the consequence of the frequency offset. Figure 3.7 is obtained by transmission of just one non-zero pilot subcarrier while all other subcarriers in the frame are set to zero.
In an ideal situation, without any frequency offset, the only subcarrier with non-zero value will be the pilot subcarrier regardless of which system we use: WPMCM or OFDM. However, the frequency offset result in loss of orthogonality and subcarriers begin to interfere one with another. In OFDM interference due to frequency offset is limited to inside the multicarrier symbol where ICI occurs. The other OFDM symbols in this case are not affected. The WPMCM, on the other hand, has overlapping symbols and an offset in frequency results in both ICI and ISI. In figure 3.7 we therefore observe that the energy of the pilot subcarrier located in the 5^{th} subcarrier and 5^{th} symbol is spread almost across the whole frame. This is in agreement with the theoretical derivation carried in § 3.1.1 and § 3.1.2.

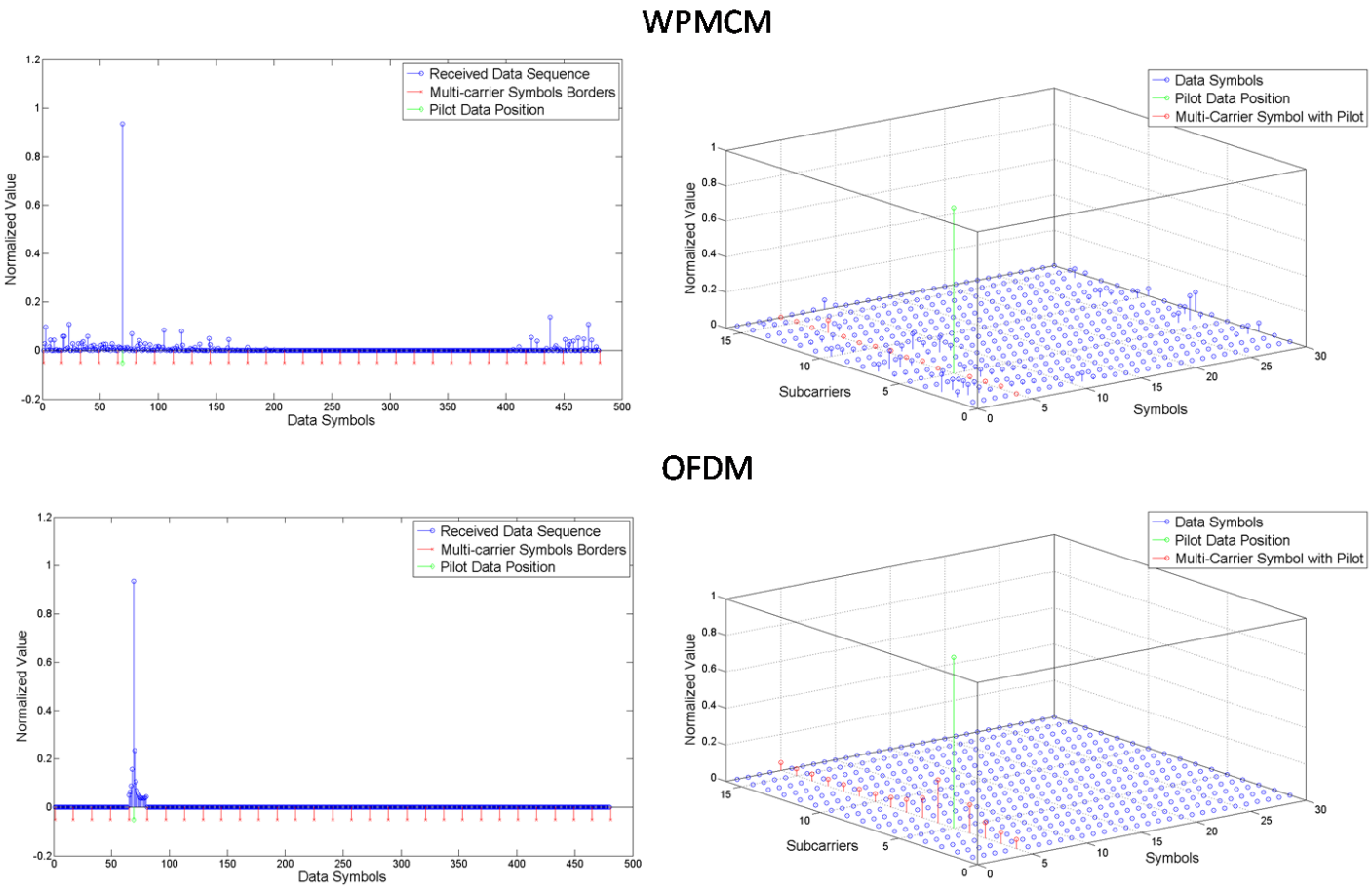

Figure 3.7: Received Subcarriers Spectral Energy in a Frame in Presence of the Frequency Offset; Up: WPMCM with Daubechies wavelet, Down: OFDM

3.2 Phase Noise in Multicarrier Modulation

The ideal local oscillator would have a single carrier with constant amplitude and frequency. However, the outputs of practical local oscillators are degraded due to factors such as thermal noise, causing the oscillator's central frequency to fluctuate a bit. This uncertainty in the actual frequency or the phase of the signal is referred to as phase noise.

Multicarrier transmission is very vulnerable to phase noise since phase noise can cause the loss of orthogonality between subcarriers. The influence of the phase noise on multicarrier transmission can be divided into two parts:

- Common Phase Error (CPE): Attenuates and rotates all constellation symbols by the same angle.
- Interference: Contribution of all other subcarriers.

Phase noise can be represented as a parasitic phase modulation of the oscillator's signal. In the literature there are different models used for the phase noise. Majority of these models are described in terms of power spectral density (PSD). In ideal case the PSD of the local oscillator would be a single pulse (delta function) at the central frequency. Due to imperfections of the oscillator (fluctuations), the PSD of the practical oscillator is distributed over a wider frequency band with highest concentration around oscillator's central frequency. The single side band PSD of free running oscillator can be estimated by the Lorentzian function [50], like one illustrated in figure 3.8.

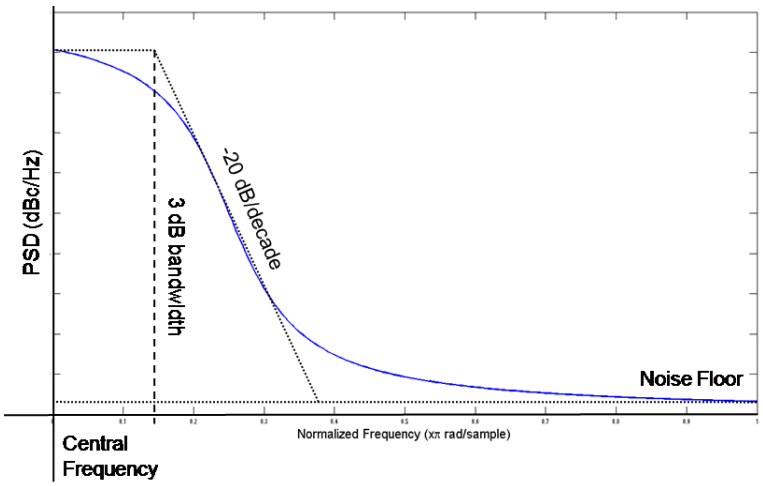

Figure 3.8: Single Side Band PSD of the Oscillator Process

In this thesis we model the phase noise as a zero mean white Gaussian process ϕ_w with finite variance $\sigma_w{}^2$ [29]. The autocorrelation function of the phase noise is given by:

$$R_{\phi_w}(m) = \sigma_w^2 \delta(m) \tag{3.11}$$

Using (3.11) we can express the power spectral density of phase noise as:

$$S_{\phi_w}(f) = \sum_{m=-\infty}^{\infty} R_{\phi_w}(m) e^{-j2\pi fm} \tag{3.12}$$

In order to get the desired phase noise bandwidth we perform low pass filtering with filter F_ϕ. The PSD from (3.12) now becomes:

$$S_{\phi b}(f) = S_{\phi_w}(f) \left| F_\phi(f) \right|^2 \tag{3.13}$$

By changing the corner frequency $f_{c\phi}$ of the filter used we can adjust the phase noise bandwidth. Low value of corner frequency results in narrow bandwidth while higher value spread the phase noise.
In the last stage of the model we add phase noise floor to the signal. Similarly to the main phase noise contribution, the phase noise floor is also modeled as a zero mean Gaussian process with finite variance σ_{wn}^2, which is relatively low compared to σ_w^2. The phase noise floor is not correlated so that it spans the whole available bandwidth and has flat PSD.
The total phase noise can now be expressed as a sum of bandwidth limited main noise contribution ϕ_b and phase noise floor ϕ_{wn} as:

$$\phi(n) = \phi_b(n) + \phi_{wn}(n) \tag{3.14}$$

Using the phase noise model given in (3.11–3.14) we can write the received signal $R(n)$ that has been affected by phase noise and AWGN channel as:

$$R(n) = S(n)e^{j\phi(n)} + w(n) \tag{3.15}$$

Without loss of generality, we assume for the moment that $w(n) = 0$.

3.2.1 Phase Noise in OFDM

When an OFDM transceiver experience some phase noise, we can express the demodulated signal at the receiver's output as:

$$\begin{aligned}\hat{a}_{k'} &= \frac{1}{N}\sum_{n=0}^{N-1} R(n)e^{-j2\pi\frac{k'}{N}n} \\ &= \frac{1}{N}\sum_{k=0}^{N-1} a_k \sum_{n=0}^{N-1} e^{j2\pi\frac{k}{N}n} e^{j\phi(n)} e^{-j2\pi\frac{k'}{N}n} \\ &= \frac{1}{N}\sum_{k=0}^{N-1} a_k \sum_{n=0}^{N-1} e^{j\phi(n)} e^{j2\pi\frac{(k-k')n}{N}}\end{aligned} \tag{3.16}$$

We can simplify the analysis for phase noise by splitting the demultiplexed signal in useful part and disturbance part. In order to do this we will assume that phase noise is sufficiently small so that it can be approximated by [29]:

$$e^{j\phi(n)} \approx 1 + j\phi(n) \tag{3.17}$$

Using approximation (3.17) we can express the demodulated OFDM signal (3.16) for the k^{th} carrier as:

$$\begin{aligned}\hat{a}_{k'} &\approx \frac{1}{N}\sum_{k=0}^{N-1} a_k \sum_{n=0}^{N-1} e^{j2\pi\frac{(k-k')n}{N}} + \frac{j}{N}\sum_{k=0}^{N-1} a_k \sum_{n=0}^{N-1} \phi(n) e^{j2\pi\frac{(k-k')n}{N}} \\ &\approx a_{k'} + \frac{j}{N}\sum_{k=0}^{N-1} a_k \sum_{n=0}^{N-1} \phi(n) e^{j2\pi\frac{(k-k')n}{N}} = a_{k'} + I_\phi(k)\end{aligned} \tag{3.18}$$

The first component of (3.18) stands for correctly demodulated symbol and second term I_ϕ stands for disturbance which is added to the each subcarrier. Two distinct scenarios are possible with the phase noise:

1. If *k' = k*: *Common Phase Error (CPE)*
   The disturbance term from equation (3.18) can now be written as:

$$\begin{aligned}I_\phi(k') &= \frac{j}{N}\sum_{k=0}^{N-1} a_k \sum_{n=0}^{N-1} \phi(n) \\ &= j \ \Phi \ a_{k'}\end{aligned} \tag{3.19}$$

   The error, given in equation (3.19), causes the constellation points to be rotated by an angle Φ. This angle is common for all subcarriers so that all constellation points will be rotated by the same angle. Here, the rotation angle Φ is defined by the average phase noise given as:

$$\Phi = \frac{1}{N}\sum_{n=0}^{N-1} \phi(n) \tag{3.20}$$

   The common phase error (CPE) is only dependent on low frequencies of the phase noise spectrum up to the frequency of the inter-carrier spacing.

2. If *k' ≠ k*: *Inter Carrier Interference (ICI)*
   The disturbance term from equation (3.18) can now be written as:

$$I_{\substack{\phi \\ k\neq k'}}(k) = \frac{j}{N}\sum_{k=0;k\neq k'}^{N-1} a_k \sum_{n=0}^{N-1} \phi(n) e^{j2\pi\frac{(k-k')n}{N}} \tag{3.21}$$

   The error in equation (3.21) consists of contribution from all other subcarriers in an OFDM symbol, and it is known as ICI. The magnitude of ICI as a result of phase noise is dependent only at the phase noise components that have high frequencies. In general, the phase noise that causes ICI contains frequencies which are larger than inter-carrier spacing frequency.

3.2.2 Phase Noise in WPMCM

The detected data at the WPMCM receiver in presence of the phase noise can be written for the k^{th} subcarrier and u^{th} symbol as:

$$\begin{aligned}\hat{a}_{u',k'} &= \sum_{n} R(n)\xi^{k'}_{2^{\log(N)}}(u'N-n) \\ &= \sum_{n}\sum_{u}\sum_{k=0}^{N-1} a_{u,k}\xi^{k}_{2^{\log(N)}}(n-uN)e^{j\phi(n)}\xi^{k'}_{2^{\log(N)}}(u'N-n) \\ &= \sum_{u}\sum_{k=0}^{N-1} a_{u,k}\left(\sum_{n}\xi^{k}_{2^{\log(N)}}(n-uN)e^{j\phi(n)}\xi^{k'}_{2^{\log(N)}}(u'N-n)\right)\end{aligned} \tag{3.22}$$

Using same assumption like we have done for phase noise analysis in OFDM (3.17), we can approximate the equation (3.22) by:

$$\begin{aligned}\hat{a}_{u',k'} &\approx \sum_{u}\sum_{k=0}^{N-1} a_{u,k}\left(\sum_{n}\xi^{k}_{2^{\log(N)}}(n-uN)\xi^{k'}_{2^{\log(N)}}(u'N-n)\right)+ \\ &\quad j\sum_{u}\sum_{k=0}^{N-1} a_{u,k}\left(\sum_{n}\xi^{k}_{2^{\log(N)}}(n-uN)\phi(m)\xi^{k'}_{2^{\log(N)}}(u'N-n)\right) \\ &\approx a_{u',k'} + j\sum_{u}\sum_{k=0}^{N-1} a_{u,k}\left(\sum_{n}\xi^{k}_{2^{\log(N)}}(n-uN)\phi(m)\xi^{k'}_{2^{\log(N)}}(u'N-n)\right) \\ &\approx a_{u',k'} + I_{\phi}(u,k)\end{aligned} \tag{3.23}$$

The first component of (3.23) stands for correctly demodulated symbol and second term I_{ϕ} stands for disturbance which is added to the each subcarrier. Similarly to the OFDM, we can also in WPMCM indicate two distinct situations in presence of phase noise, i.e.:

1. If *k' = k and f' = f*: *Common Phase Error (CPE)*
   The disturbance term from equation (3.23) can now be written as:

$$\begin{aligned}I_{\phi}(u',k') &= \frac{j}{N}\sum_{k=0}^{N-1} a_{u,k}\sum_{n=0}^{N-1}\phi(n) \\ &= j\ \Phi\ a_{u',k'}\end{aligned} \tag{3.24}$$

   The equation (3.24) describes the rotation of constellation points by an angle Φ, which is common for all subcarriers. Rotation angle Φ is dependent on the average value of phase noise sequence and it is given in equation (3.20).

2. If $k' \neq k$ *or/and* $f' \neq f$: *Inter Carrier Interference and Inter Symbol Interference (ICI/ISI)*
   The disturbance term from equation (3.23) can now be written as:

$$I_{\phi}(u,k) = j \sum_{\substack{u \neq u';k \neq k'}} \sum_{u;u \neq u'} \sum_{k=0;k \neq k'}^{N-1} a_{u,k} \left(\sum_{n} \xi^{k}_{2^{\log(N)}}(n-uN)\phi(m)\xi^{k'}_{2^{\log(N)}}(u'N-n) \right) \qquad (3.25)$$

   The equation (3.25) stands for the interference, caused by the phase noise. In contrary to the OFDM in an AWGN channel, the phase noise in WPMCM raises the ICI and ISI levels. This is due to overlapping nature of the wavelet transform.

Different frequency components of the phase noise have different impacts on the CPE and ICI/ISI terms. If the phase noise bandwidth is very concentrated near the central frequency the CPE term will dominate, but when the phase noise bandwidth is somewhat more spread the ICI/ISI term will soon take over. Using already defined model for phase noise (3.11 – 3.14), we can control the phase noise bandwidth by the corner frequency of the filter.

3.2.3 Numerical Results for Phase Noise

The performance degradation associated with phase noise has been evaluated by the computer simulations using almost identical set-up as for the frequency offset. More details on the set-up can be found in the § 3.1.3.
An overview of simulation parameters is given in table 3-2.

Table 3-2: Simulation Setup Phase Noise

	WPMCM	OFDM
Number of Subcarriers	128	128
Number of Multicarrier Symbols per Frame	100	100
Modulation	QPSK	QPSK
Channel	AWGN	AWGN
Oversampling Factor	1	1
Guard Band	-	-
Guard Interval	-	-
Frequency Offset	-	-
Phase Noise	σ_w^2= -10 dBc, σ_{wn}^2= -20 dBc, $f_{c\phi} = 0.1$	σ_w^2= -10 dBc, σ_{wn}^2= -20 dBc, $f_{c\phi} = 0.1$
Time Offset	-	-

- does not apply

The different effects of the phase noise on the WPMCM and OFDM are best illustrated by the constellation points' diagram and the PSD of the phase noise.
At the left side of the figure 3.9 we can see the PSD of the phase noise which has relatively low corner frequency. The dominant effect of such phase noise is the common phase error, which results in the rotation of all constellation points.
The PSD of the phase noise with relatively high corner frequency is illustrated in the figure 3.10. Now the rotation behavior is not more visible but the interference between subcarriers is much more pronounced.

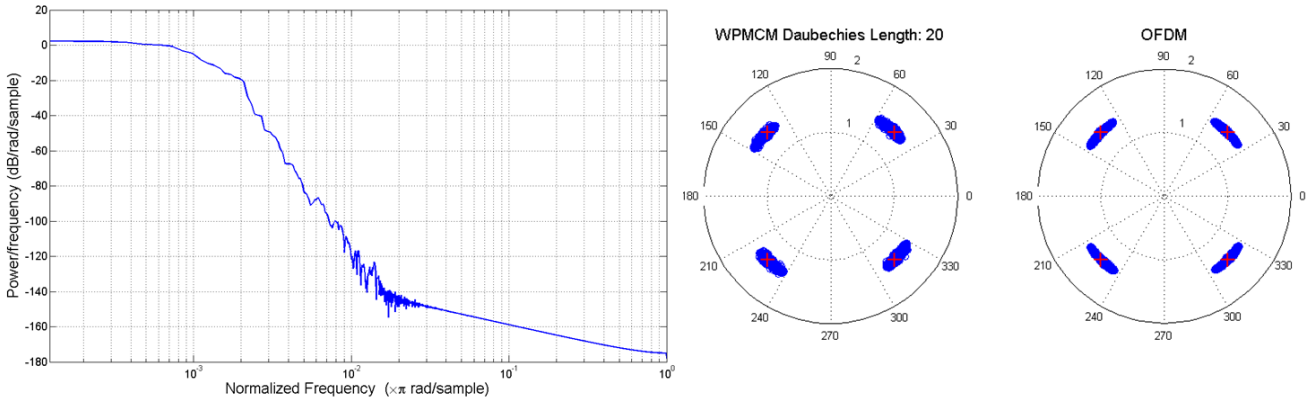

Figure 3.9: Phase Noise (Narrow Band); Left: PSD, Right: WPMCM and OFDM Constellation Points

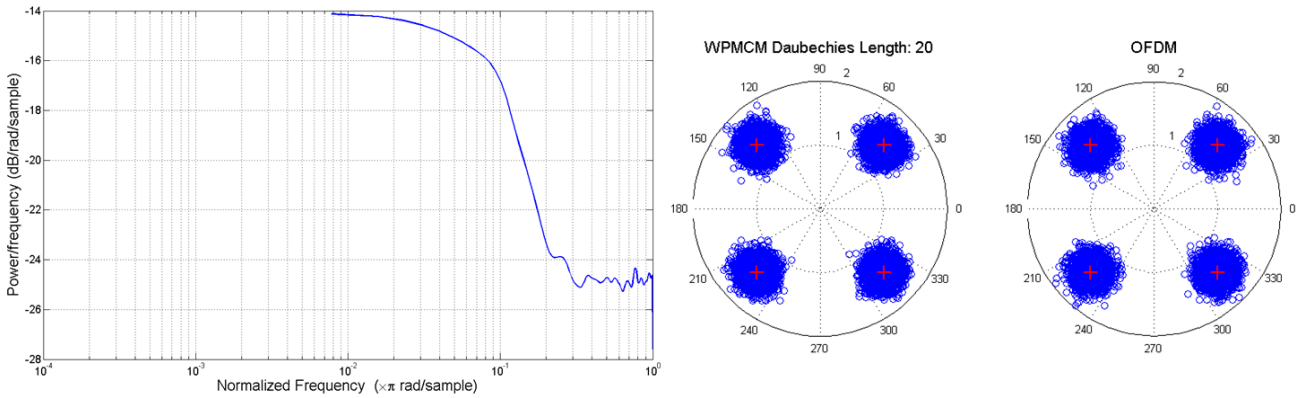

Figure 3.10: Phase Noise (Wide Band); Left: PSD, Right: WPMCM and OFDM Constellation Points

Both effects of the phase noise are important and depending on the system one or the other can be the limiting factor for the system performance. In the literature there are many adequate correction approaches available for the CPE [40] – [41] but the estimation and correction of the interference is much harder to realize. Therefore, we will limit the following part of this paragraph to the performance analysis of the WPMCM and OFDM in the presence of phase noise that causes interference. In order to achieve this, we set the phase noise bandwidth to 10% of the total available bandwidth and the variance to -10 dBc (decibel relative to the carrier). The PSD of the phase noise will look similar to one illustrated at the left side of the figure 3.10.

Figure 3.11 shows the bit error rate (BER) of WPMCM and OFDM in presence of phase noise. The illustrated behaviors of BER curves are similar to each other with the exception of biorthogonal wavelet. The poor performance of biorthogonal wavelet, as already mentioned, is due to unfulfilled perfect reconstruction constraint.

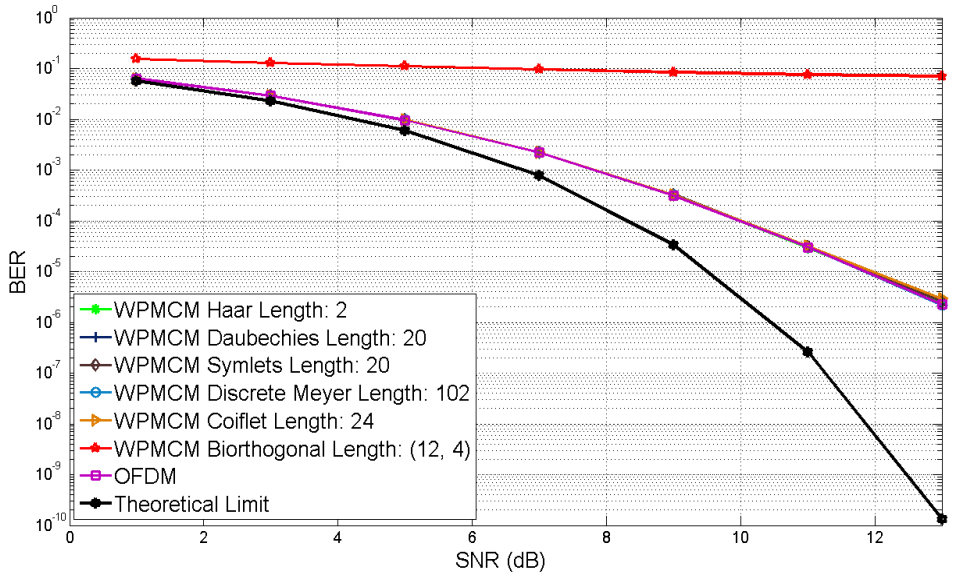

Figure 3.11: BER for WPMCM with Different Wavelets and OFDM under Phase Noise with Relative Bandwidth of 10% and variance of -10 dBc

Figure 3.12 illustrates the effect of the phase noise variance on the BER. This figure is obtained using an AWGN channel with 16 dB SNR while phase noise variance is varied from -10 to 20 dBc with step-size of 5 dBc.

It is natural that the phase noise variance and the performance degradation are closely related. The sensitivity of WPMCM and OFDM to the variance of the phase noise is confirmed by figure 3.12.

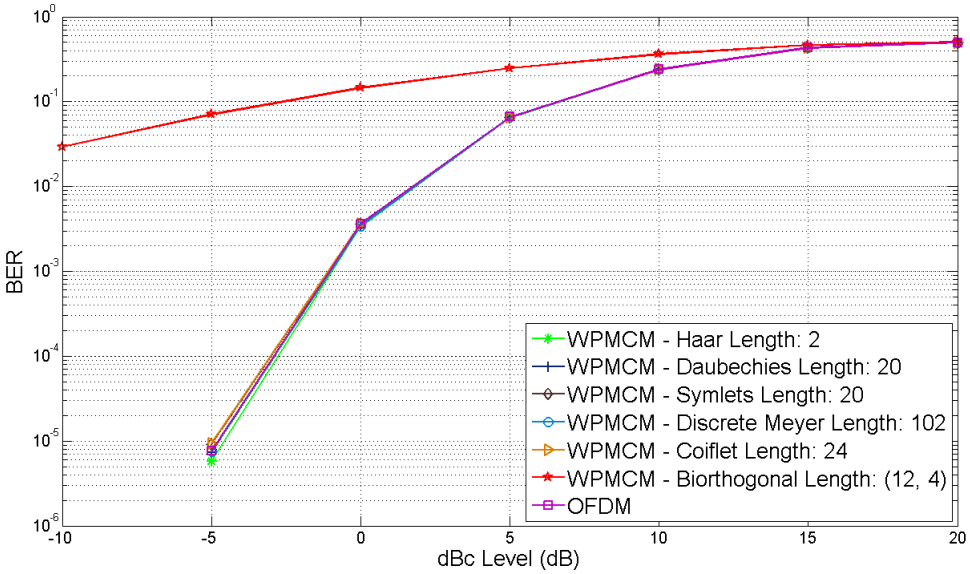

Figure 3.12: BER vs. Phase Noise Variance for WPMCM and OFDM in AWGN Channel (SNR = 16 dB)

Figure 3.13 shows the performance of the WPMCM with phase noise when the number of subcarriers and symbols in the frame is altered.
The simulation results haven't shown any essential connection between performance degradation and the number of subcarriers nor the number of symbols per frame. The results would be different if we set the corner-frequency to a smaller value, because the inter-carrier spacing depends on the number of subcarriers, for low number of subcarriers dominant CPE term will dominate while for high number of subcarriers the interference will be the major term [29], [51].

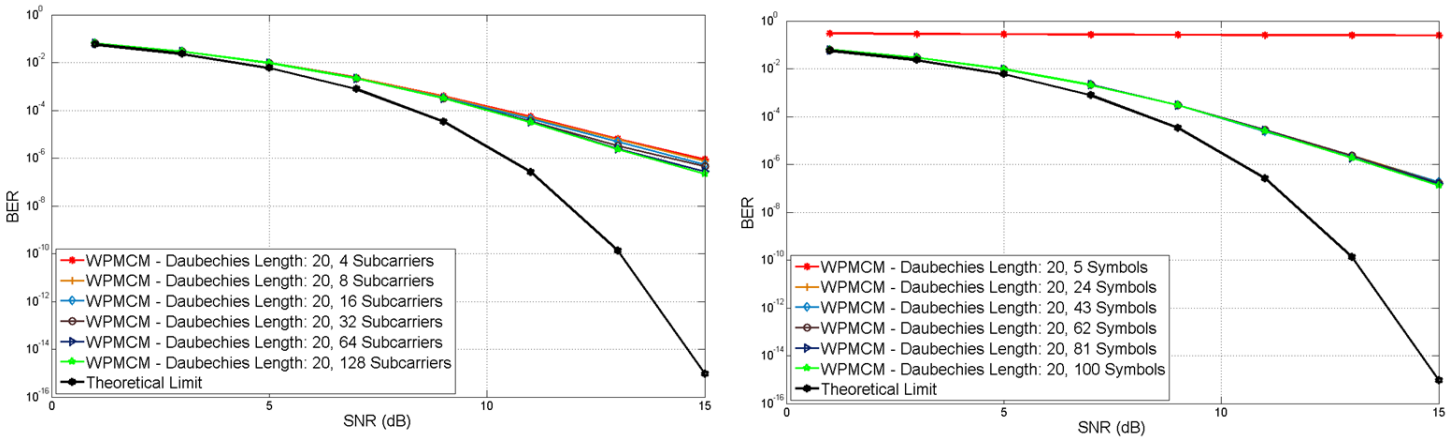

Figure 3.13: BER for WPMCM with Phase Noise;
Left: Different Number of Subcarriers, Right: Different Number of Symbols/Frame

Figure 3.14 illustrates the influence of filter's length and number of zero wavelet moments in combination with the phase noise on the BER.
Similar to the frequency offset there are no noticeable influences of the filter's length and number of wavelets' zero moments on the system performance when operating under a phase noise.

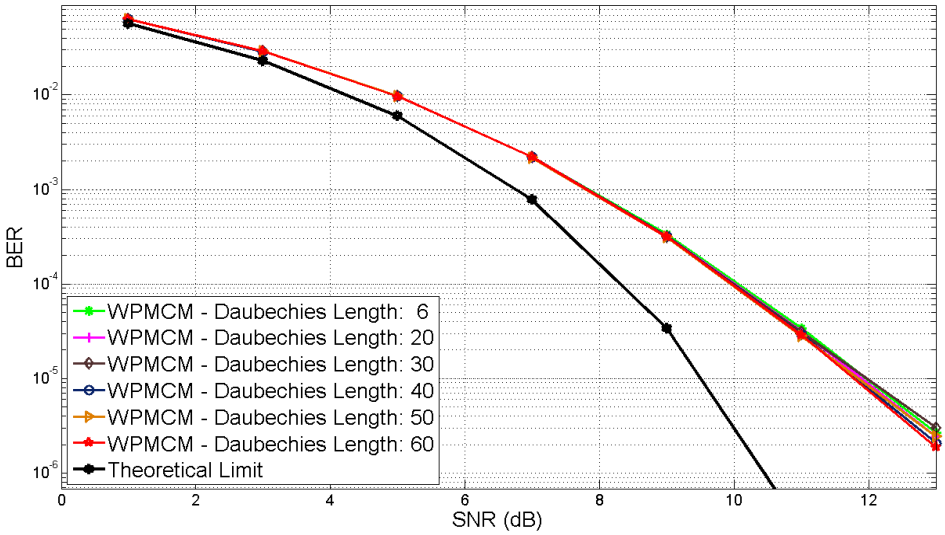

Figure 3.14: BER for WPMCM using Daubechies Wavelets of Different Lengths under Influence of Phase Noise

For the completeness of the analysis we show in figure 3.15 the effect of the phase noise on the constellation points, but now for all discussed wavelets and OFDM. The clearly visible scattering of the constellation points around the reference positions is caused by the phase noise, as the channel is assumed to be ideal and no other disturbances were introduced.

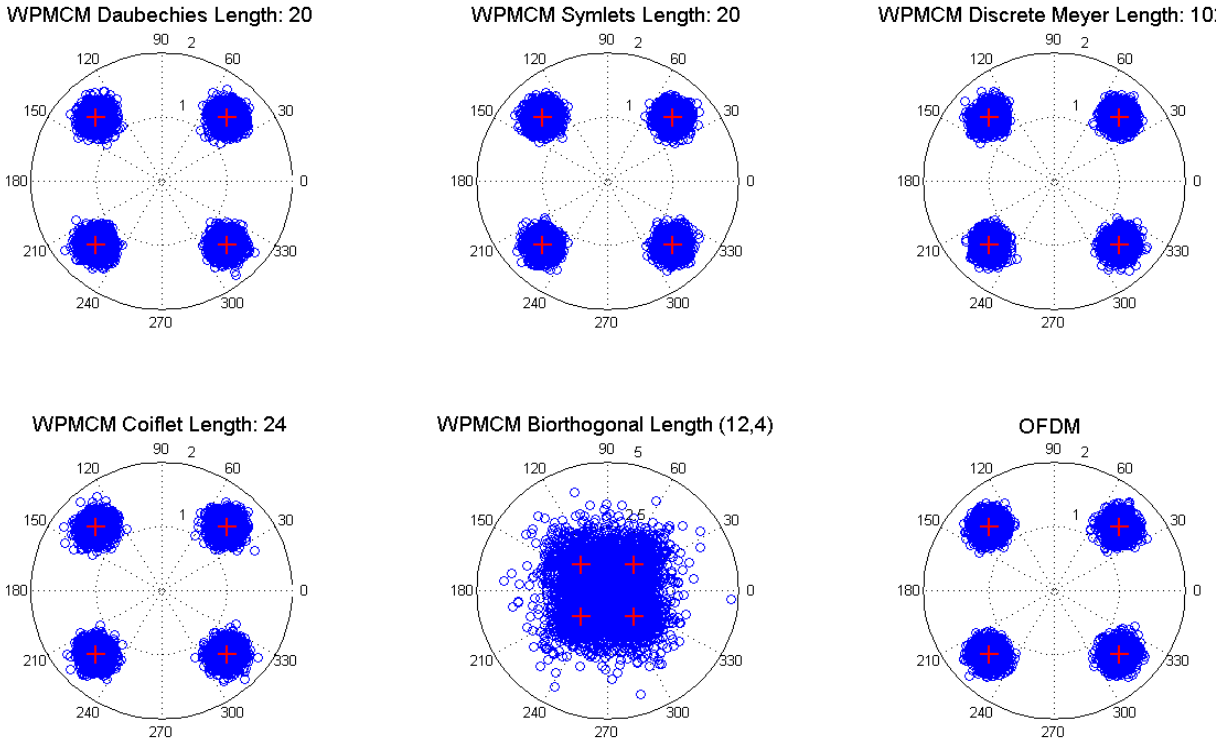

Figure 3.15: Constellation Points in the Presence of Phase Noise

The spreading of subcarrier energy due to phase noise is illustrated in figure 3.16 for the similar simulation set-up as used in Figure 3.7.

Phase noise result in loss of orthogonality and subcarriers begin to interfere with each other. In OFDM interference due to phase noise is limited to the multicarrier symbol where ICI occurs. The other OFDM symbols in this case are not affected. The WPMCM, on the other hand, has overlapping symbols and phase noise, besides ICI, also results in ISI. In figure 3.16 we therefore observe that energy of the pilot subcarrier located at the 5^{th} subcarrier and 5^{th} symbol is spread almost across the whole frame. This is in agreement with the theoretical derivation carried out in § 3.2.1 and § 3.2.2.

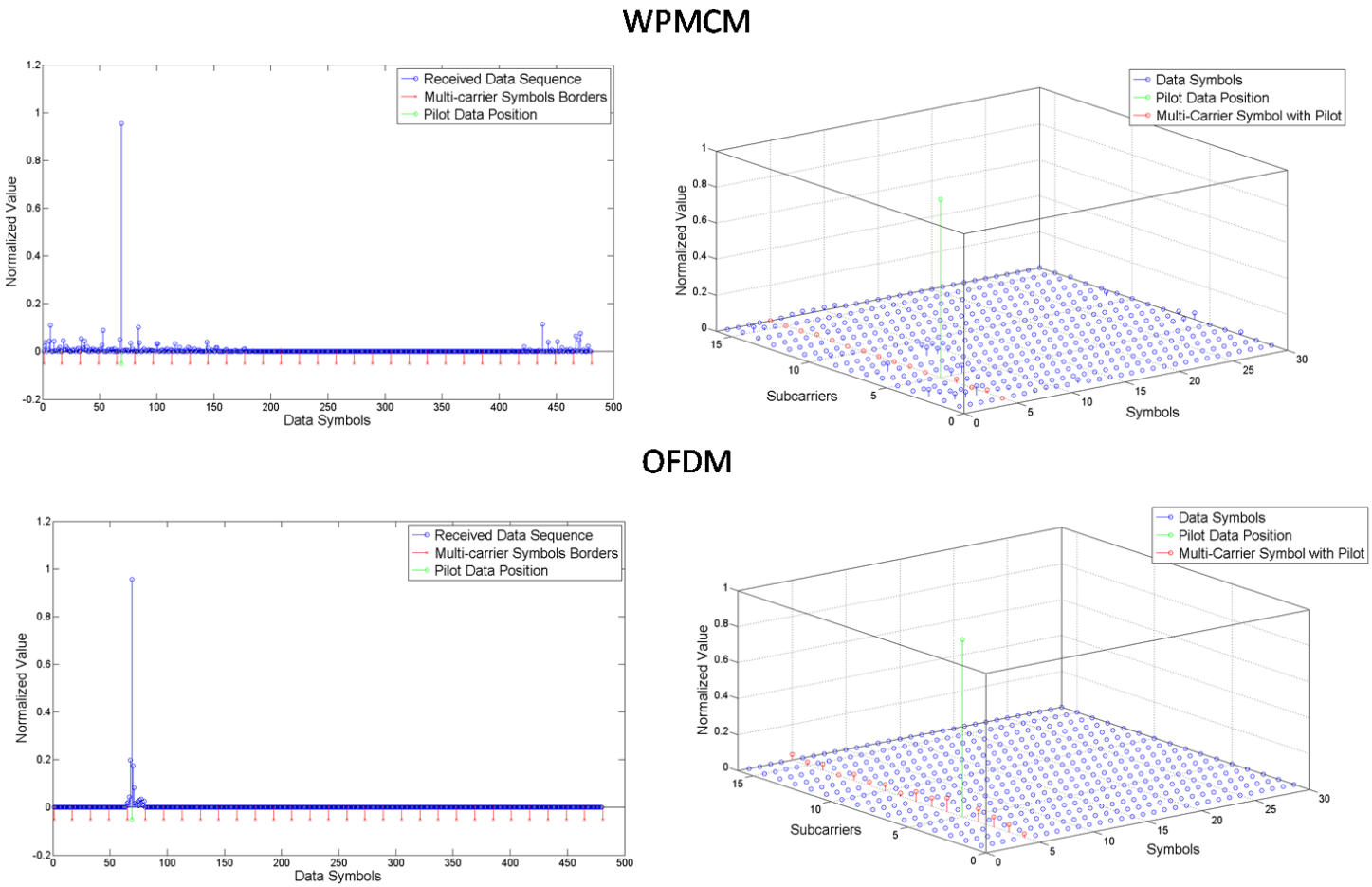

Figure 3.16: Received Subcarriers Spectral Energy in a Frame in presence of Phase Noise; Up: WPMCM with Daubechies wavelet, Down: OFDM

3.3 Time Offset in Multicarrier Modulation

One of the major concerns of a multicarrier system is their vulnerability to timing synchronization errors, which occur when multi-carrier symbols are not perfectly aligned at the receiver. Because of the time offset samples outside a WPMCM or OFDM symbol get erroneously selected, while useful samples at the beginning or at the end of that particular symbol get discarded.

The time synchronization error is modeled by shifting the received data samples by a time offset value t_ε to the left or right, depending on the sign of the t_ε. If we assume that transmitted signal is given by $S(n)$, the received signal $R(n)$ in presence of time synchronization error can be expressed as:

$$R(n \pm t_\varepsilon(k)) = S(n) + w(n) \tag{3.26}$$

Without loss of generality, we assume for the moment that $w(n) = 0$.

Time offset degrades the performances of multicarrier transceivers for the greatest part by introducing inter-symbol interference (ISI) and inter-carrier interference (ICI). WPMCM and OFDM share many similarities as both are orthogonal multicarrier systems but in case of timing error there is a major difference that causes different behaviors for each transmission scheme.
The actual length of the WPMCM symbols is defined by the wavelet used and in general it is significantly longer than the OFDM symbol. This excessive length of WPMCM symbols does not cause frame size to grow by allowing symbols to overlap one another. In case of time offset this overlap of the symbols in WPMCM causes each symbol to interfere with several other symbols while in OFDM each symbol can only interfere with one adjacent symbol.
The second important difference between the two transmission schemas is the use of the guard interval between the symbols. OFDM uses cyclic prefix that significantly improves its performance when time errors occur, assuming that time offset is not exceeding the size of cyclic prefix and that the direction of time shift is towards the cyclic prefix. The WPMCM, on the other hand, cannot benefit from such guard interval since the WPMCM symbols overlap one another.

3.3.1 Time Offset in OFDM

Cyclic prefix is effective and low complexity method to cope with dispersive channels and time synchronization errors in OFDM transceivers. OFDM is often accommodated with cyclic prefix but rarely with cyclic postfix. This means that we have two distinct situations that can occur under time synchronization errors, depending on the direction of the time offset.

- Time synchronization error away from own cyclic prefix (to the right).
- Time synchronization error towards own cyclic prefix (to the left).

Time Offset Away From the Cyclic Prefix
Figure 3.17 illustrates 3 OFDM symbols (u-1, u, u+1) where FFT window is misaligned to the right, i.e. away from the cyclic prefix. Each OFDM symbol consists of N data samples and an extension of N_{CP} samples representing cyclic prefix. The FFT window in illustrated situation will contain N-t_ε data samples ((t_ε+1), (t_ε+2), … N) of the considered u^{th} OFDM symbol, missing first t_ε samples. Instead t_ε samples (1, 2, … t_ε) of the next (u+1)th OFDM symbol will be erroneously selected.

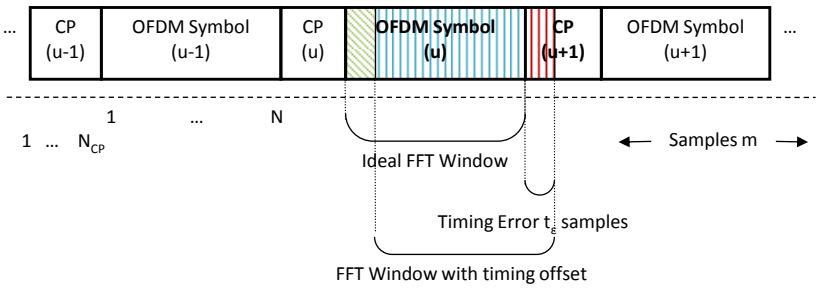

Figure 3.17: Timing Offset Away from Cyclic Prefix (to the right)

An OFDM system that is affected by timing error and where samples of neighboring symbol are wrongly selected experience severe degradation of the performance. The demodulated OFDM signal after FFT can be written as:

$$\begin{aligned}\hat{a}_{u',k'} &= \frac{N-t_\varepsilon}{N} a_{u',k'} e^{j2\pi\frac{k'}{N}t_\varepsilon} \\ &+ \frac{1}{N}\sum_{n=0}^{N-1-t_\varepsilon}\sum_{k=0;k\neq k'}^{N-1} a_{u',k} e^{j2\pi\frac{k(n+t_\varepsilon)}{N}} e^{-j2\pi\frac{k'n}{N}} \\ &+ \frac{1}{N}\sum_{n=N-t_\varepsilon}^{N-1}\sum_{k=0}^{N-1} a_{u+1,k} e^{j2\pi\frac{k(n-N+t_\varepsilon)}{N}} e^{-j2\pi\frac{k'n}{N}}\end{aligned} \tag{3.27}$$

The first component of equation (3.27) represents useful signal which is attenuated and phase shifted by a term proportional to subcarrier index *k'*. The second component of (3.27) gives ICI and the third component stands for ISI with next symbol.

Time Offset Towards the Cyclic Prefix

The other situation occurs when we have time offset towards the symbols own cyclic prefix, i.e. to the left. Figure 3.18 illustrates such a scenario. In this case FFT window consists of first N-t_ε samples (1, 2, … (N- t_ε)) of the considered u^{th} OFDM symbol and the last t_ε samples of the own cyclic prefix. We assume for the convenience that $t_\varepsilon < N_{CP}$.

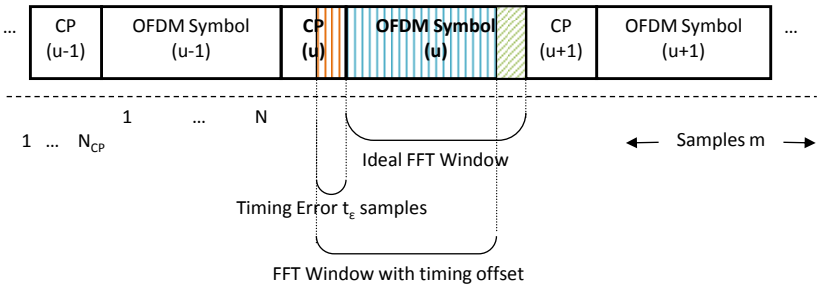

Figure 3.18: Timing Offset Towards Cyclic Prefix (to the left)

The demodulated OFDM signal affected by time offset in the direction of symbol's own cyclic prefix is given in equation (3.28), for case when $t_\varepsilon < N_{CP}$.

$$\hat{a}_{u',k'} = a_{u',k'} e^{-j2\pi\frac{k't_\varepsilon}{N}} \tag{3.28}$$

Thanks to the cyclic prefix the orthogonality is preserved and ISI and ICI terms have disappeared. The timing error towards the cyclic prefix results therefore in pure phase shift.

The common consequence of time-offset in OFDM, regardless of offset direction, is the introduction of phase shift. The phase shift in equations (3.27) and (3.28) is linearly proportional

to the subcarrier index and the value of time offset. The rotation angle $\Phi_t(k)$ due to timing error is given by:

$$\Phi_t(k) = \frac{2\pi k t_\varepsilon}{N} \tag{3.29}$$

The subcarriers with higher frequencies experience greater phase shifts. In case of coherent QPSK modulation even the small timing offset such as $t_\varepsilon = 1$ results in a phase rotation of constellation symbols in order of $0 < \Phi_t(k) < 2\pi$. The subcarrier with the highest frequency will therefore experience a phase shift of almost 360 degrees. If this phase shift is not corrected the majority of the detected data would be corrupted even without ICI or ISI.
The phase rotation due to timing error can be usually revised by pilot-symbol-aided channel estimation techniques or by use of differential constellation mapping [9], [42], [44]. In this thesis we employ differential quadrature phase shift keying (DQPSK) in order to overcome this problem. In the DQPSK scheme the data is modulated on the basis of phase difference between two consecutive constellation symbols, thereby ensuring that adjacent subcarriers experience a phase shift which is independent of the carrier position. The phase rotation of constellation point k is determined by applying a phase shift of $\Delta\Phi$ to the previous constellation symbol k-1. The difference in phase shift $\Delta\Phi$ is determined by the unmodulated data value assigned to subcarrier k, in case of DQPSK phase shift can be written as:

$$\Delta\Phi_b = \frac{2(b-1)\pi}{4}, \quad b \in 1\ldots 4 \tag{3.30}$$

The phase difference between two consecutive DQPSK constellation symbols under timing errors becomes:

$$\Delta\phi_{k,k-1} = e^{j\left(\Delta\Phi_b - \frac{2\pi t_\varepsilon}{N}\right)} \tag{3.31}$$

Using DQPSK modulation in presence of timing error therefore results in a phase shift that is depending on the value of the time offset but not anymore on the value of subcarrier index k. The rotation angle $\Phi_t(k)$ due to timing error becomes:

$$\Phi_t(k) = \frac{2\pi t_\varepsilon}{N}, \quad differential - PSK \tag{3.32}$$

Figure 3.19 illustrates the rotations of constellation points for received OFDM signal using QPSK and DQPSK modulation. We have assumed here an ideal channel and a time offset of $t_\varepsilon = 1$ samples towards the cyclic prefix.

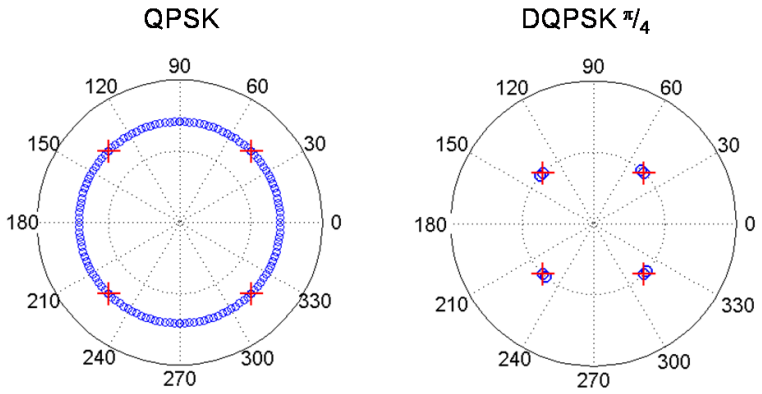

Figure 3.19: OFDM Received Constellation Points with Timing Error of t_ε=1 and an Ideal Channel; Left: QPSK, Right: DQPSK $\pi/4$

DQPSK modulation is a simple solution to overcome the problem of phase shift under time synchronization errors. However, DQPSK modulation requires about 2 to 3 dB higher SNR when compared to coherent QPSK to obtain the same BER performance in AWGN channel.

3.3.2 Time Offset in WPMCM

The WPMCM transceivers are not employing guard intervals and therefore the direction of time offset is inconsequential. The demodulated signal under influence of time offset t_ε can be written as:

$$\begin{aligned}\hat{a}_{u',k'} &= \sum_n R(n)\xi^{k'}_{2^{\log(N)}}(u'N-n+t_\varepsilon)\\ &= \sum_n\sum_u\sum_{k=0}^{N-1} a_{u,k}\xi^{k}_{2^{\log(N)}}(n-uN)\xi^{k'}_{2^{\log(N)}}(u'N-n+t_\varepsilon)\\ &= \sum_u\sum_{k=0}^{N-1} a_{u,k}\left(\sum_n \xi^{k}_{2^{\log(N)}}(n-uN)\xi^{k'}_{2^{\log(N)}}(u'N-n+t_\varepsilon)\right)\end{aligned} \tag{3.33}$$

In order to shorten the derivation we are going to use different notation, first we define:

$$\Omega^{u,u'}_{k,k'}(t_\varepsilon) = \sum_n \xi^{k}_{2^{\log(N)}}(n-uN)\xi^{k'}_{2^{\log(N)}}(u'N-n+t_\varepsilon) \tag{3.34}$$

The equation (3.34) represents the autocorrelation and the cross-correlation of the WPMCM waveforms, depending on subcarrier index k. When $k = k'$ the two subcarrier waveforms are time-reversed images of each other and equation (3.34) gives the autocorrelation sequence of the waveform k. In the other cases when $k \neq k'$ the two waveforms correspond to different subcarriers and equation (3.34) stands for the cross-correlation between waveforms k and k'.
Using equation (3.33) and (3.34) we can now express the output of the WPMCM receiver for the k^{th} subcarrier and u^{th} WPMCM symbol as:

$$\hat{a}_{u',k'} = a_{u',k'}\Omega_{k'k'}^{u',u'} + \sum_{u;u\neq u'} a_{u,k'}\Omega_{k',k'}^{u,u'} + \sum_{u}\sum_{k=0;k\neq k'}^{N-1} a_{u,k}\Omega_{k,k'}^{u,u'} \quad (3.35)$$

In equation (3.35) the first term stands for attenuated useful signal. The second term gives the ISI due to symbols transmitted on the same subchannel and the third term denotes ICI measured over the whole frame.

The received constellation points of WPMCM under time synchronization errors don't experience linear phase rotation, opposed to OFDM where rotation of constellation points is proportional to subcarrier index. The WPMCM signal in presence of timing error will however be attenuated and it will suffer from ISI and ICI.

3.3.3 Numerical Results for Time Offset

The performances of WPMCM and OFDM in presence of timing synchronization errors are investigated by means of simulations. The time offset is modeled as a discrete uniform distribution between -2 and 2 samples, i.e. $t_\varepsilon \in [-2,-1,0,1,2]$.

The designed parameters deviate to some extent from these used for frequency offset and phase noise. First of all, DQPSK modulation scheme is used instead of QPSK modulation in order to prevent OFDM constellation points to experience to large phase shifts. Secondly, in OFDM we use cyclic prefix of 16 samples that is placed in front of OFDM symbols, in WPMCM we don't use any guard interval. Due to utilization of cyclic prefix the spectral efficiency of OFDM is decreased by 12.5% while spectral efficiency of WPMCM has remained unchanged. Finally, we employ the oversampling in order to magnify the difference in performance between various systems and wavelets.

An overview of simulation parameters is given in table 3-3.

Table 3-3: Simulation Setup Time Synchronization Error

	WPMCM	OFDM
Number of Subcarriers	128	128
Number of Multicarrier Symbols per Frame	100	100
Modulation	DQPSK	DQPSK
Channel	AWGN	AWGN
Oversampling Factor	15	15
Guard Band	-	-
Guard Interval	-	CP (length: 16)
Frequency Offset	-	-
Phase Noise	-	-
Time Offset	t_ε= 2	t_ε= 2

Figure 3.20 illustrates the bit error rates (BER) of OFDM and WPMCM transceivers over AWGN channel for uniformly distributed timing offset of t_ε = 2 samples.

The OFDM system performs much better under time synchronization errors when compared to the WPMCM, partly due to exploit of cyclic prefix and cancellation of phase rotation by DQPSK modulation scheme. The WPMCM cannot profit from these revisions and therefore show poor performance in presence of timing error. Once again biorthogonal wavelet has highest BER due to unfulfilled perfect reconstruction condition.

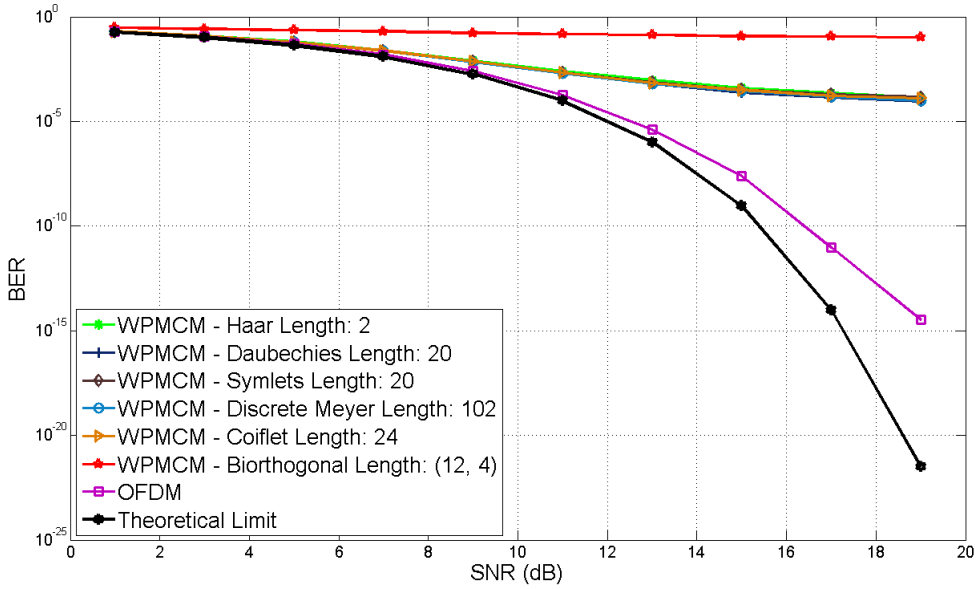

Figure 3.20: BER for WPMCM with Different Wavelets and OFDM under Time Synchronization Errors (t_ε=2)

In figure 3.21 the BER is shown for different values of time offset varying from -15 to 12 samples. The time offset in this simulation is modeled as one-sided uniform distribution in order to highlight the importance of cyclic prefix for OFDM. The value of time offset is given by $t_\varepsilon \in [0,\ldots,t_\varepsilon]$ for timing error to the right and by $t_\varepsilon \in [-t_\varepsilon,\ldots,0]$ for the timing error to the left. During this simulation we kept SNR constant at 10 dB.

The direction of time offset is inconsequential for WPMCM systems as can be seen at figure 3.21. The BER curves of WPMCM are almost perfect mirror images with respect to the origin. This does not hold for OFDM, since we can see clearly that the negative timing offset (towards the own cyclic prefix) result in much lower BER when compared to the positive timing offsets (away from the own cyclic prefix). Due to use of cyclic prefix the misalignment of FFT window between the boundaries of extended symbols does not cause interference. However when time offset exceeds the length of cyclic prefix the ICI and ISI terms reappear.

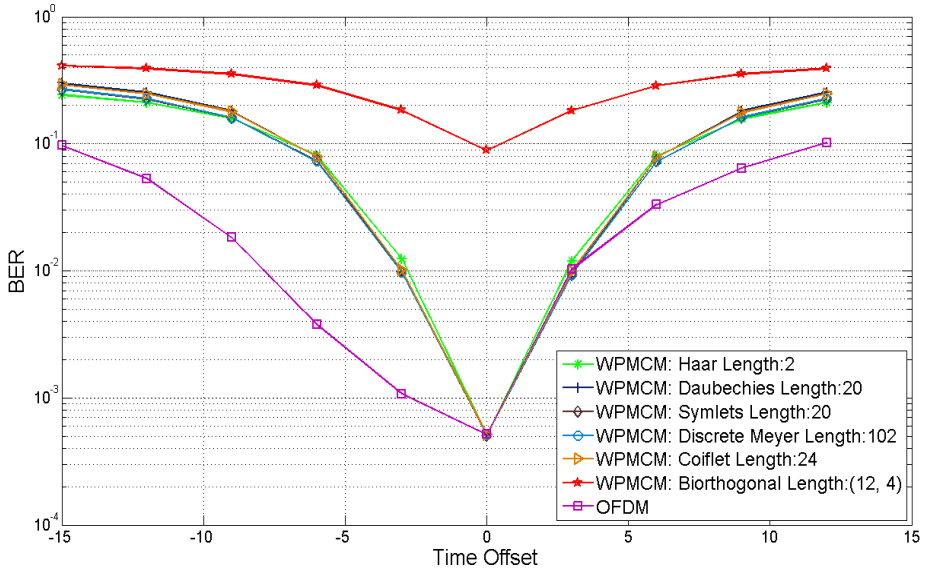

Figure 3.21: BER vs. Time Offset for WPMCM and OFDM in AWGN Channel (SNR = 10 dB)

Figure 3.22 shows the performance of the WPMCM in presence of time synchronization error when the number of subcarriers and symbols in the frame is altered.

The left side of figure 3.22 reveals that under timing error the performance of WPMCM is depending on the number of subcarriers. For increasing number of WPMCM subcarriers the BER significantly decreases. We recall from the first chapter that the symbol duration of multicarrier system is proportional to the number of subcarrier used. Therefore, larger number of subcarriers means longer symbol duration and hence smaller relative time offset with respect to multicarrier symbol length.

The simulation results performed for different number of WPMCM symbols haven't shown any essential connection between BER performance and the number of symbols, when we assume that the number of symbols in a frame is exceeding the filter's length.

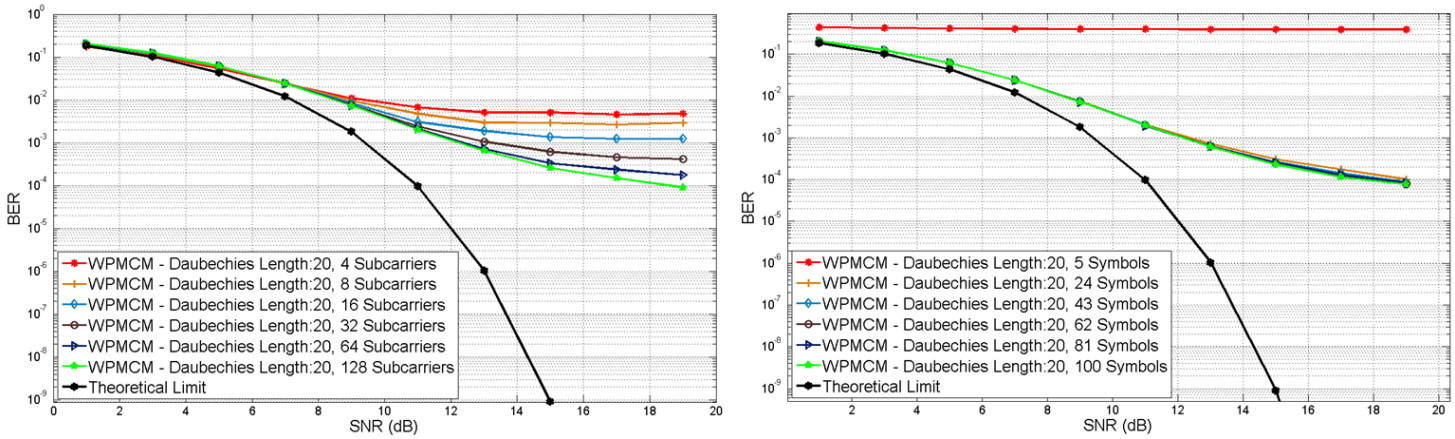

Figure 3.22: BER for WPMCM with Timing Error;
Left: Different Number of Subcarriers, Right: Different Number of Symbols

Figure 3.23 illustrates the influence of filter's length and number of zero wavelet moments in combination with timing error on the BER.
Daubechies filter with 6 coefficients and 3 wavelet zero moments has slightly higher BER when compared to longer filters from the same family. However, when length of the filters is further increased the BER curves become closely spaced and therefore we can conclude that there is no significant relation between the BER and filter's length in presence of timing errors.

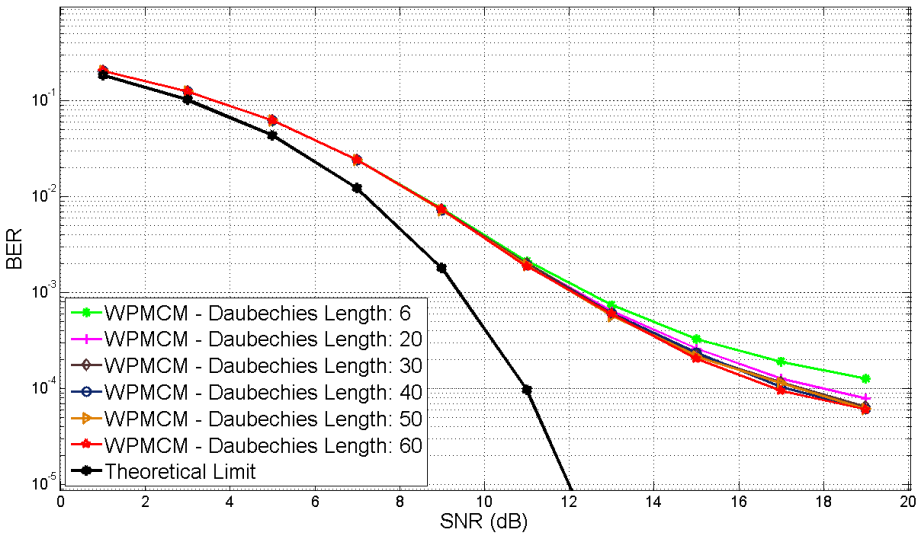

Figure 3.23: BER for WPMCM using Daubechies Wavelets of Different Lengths under Influence of Timing Error

The effect of time synchronization error on the constellation points is depicted in the figure 3.24. In order to highlight the effect of time synchronization error we assumed for the moment an ideal channel without any noise.
The main consequence of the time offset is the scattering of the constellation points around reference positions due to interference. OFDM has more concentrated constellation points than any tested WPMCM system, which indicates that the signal to interference ratio (SIR) of OFDM is higher than SIR of WPMCM under timing errors.

Figure 3.25 illustrates the spreading of subcarrier energy due to time synchronization error for the similar simulation set-up as used in Figure 3.7.
The timing error in OFDM results in ISI between successive symbols and ICI. If the cyclic prefix is used the ICI and ISI terms are cancelled for time offset towards the symbols own cyclic prefix, i.e. time offset to the left. This can be also seen at figure 3.25 where energy of the pilot symbol is spread into the subsequent symbol (ISI) but not into the previous symbol. Furthermore, energy of pilot subcarrier is also spread across the other subcarriers located in the same symbol (ICI).
In case of WPMCM the energy of single pilot is spread across a number of symbols, where subcarriers close to the pilot subcarrier contain the greatest part of interfering energy, regardless of the symbol index.

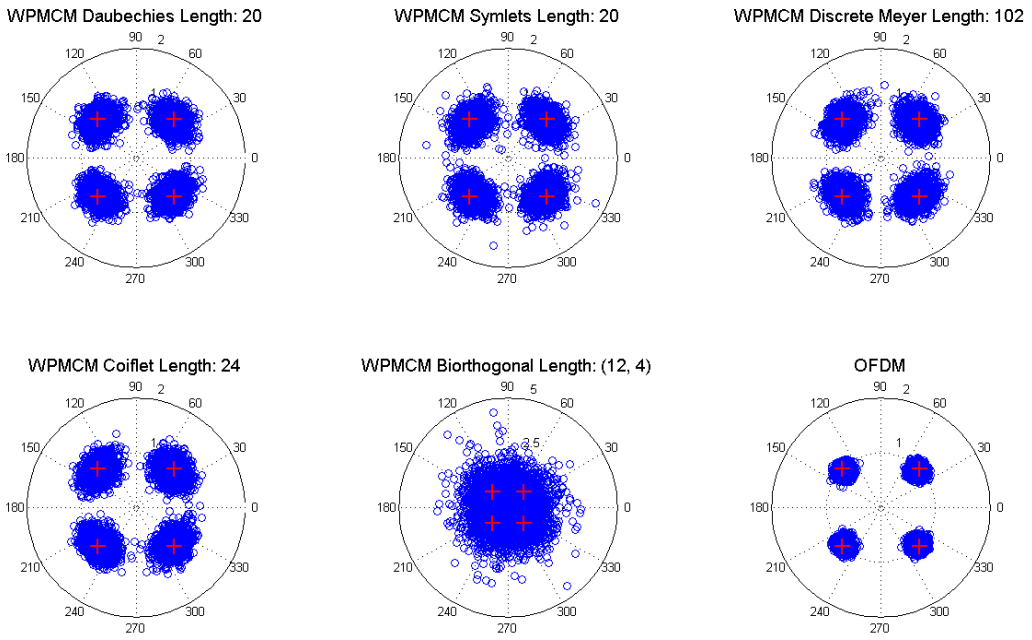

Figure 3.24: Constellation Points in the Presence of Timing Error

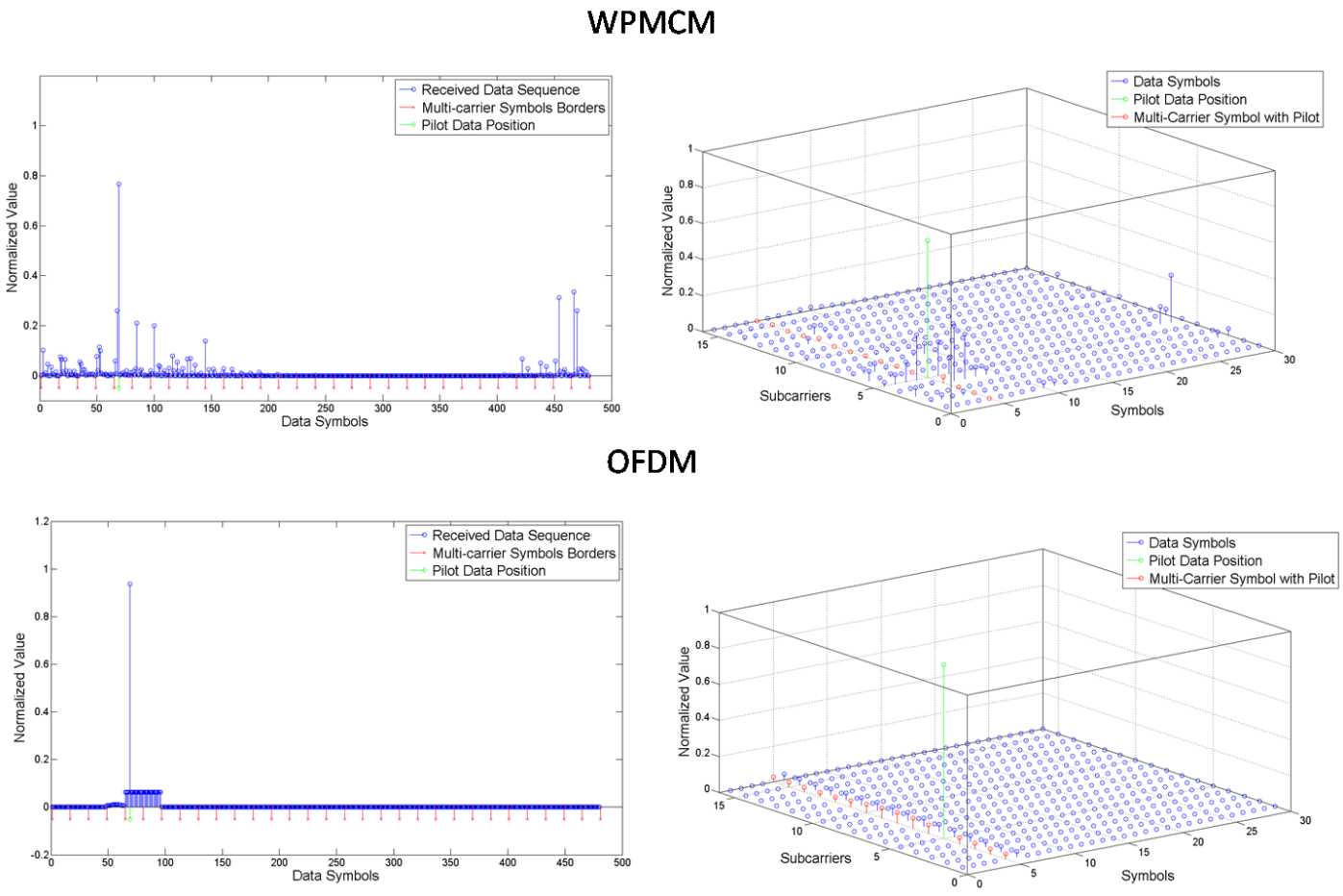

Figure 3.25: Received Subcarriers Spectral Energy in a Frame in presence of Timing Error; Up: WPMCM with Daubechies wavelet, Down: OFDM

3.4 Conclusion

In this chapter we have studied the effects of frequency offset, phase noise and time synchronization error on WPMCM and OFDM transceivers. The frequency offset and phase noise lead to the loss of orthogonality and subcarriers begin to interfere with each other. In OFDM interference is limited to ICI but in WPMCM the frequency offset and phase noise cause ICI as well as ISI. The effect of time synchronization error was also discussed. Akin to OFDM, we have found that timing error in WPMCM contain two components: ICI and ISI. There are however significant differences between both schemes in presence of timing error. Firstly, the ISI in OFDM arises only between successive symbols while in WPMCM a number of symbols interfere one with another. Secondly, the timing error in OFDM results in rotation of constellation symbols that is proportional to subcarrier frequency but in WPMCM the rotation behavior is absent.

The effects of frequency offset, phase noise and time synchronization errors were also examined by the simulations studies. Several well-known wavelets such as Daubechies, Symlets, discrete Meyer, Coiflet and biorthogonal wavelet were applied and studied. The sensitivity of WPMCM and OFDM are quite similar in presence of frequency offset and phase noise. However, time synchronization error is found to be a major drawback of WPMCM transceiver. The simulations have shown that OFDM has much lower BER under timing errors when compared to WPMCM. This is partially caused due to use of cyclic prefix in OFDM and utilization of differential modulation scheme. The wavelets used during these simulations are standard wavelets that were developed for other applications such as image processing or compression, and hence not possibly suitable for telecommunication purposes. Therefore, in the next chapter we will present the design process which we have established to design new wavelets that minimize timing-error interference.

It is an experience like no other experience I can describe, the best thing that can happen to a scientist, realising that something that's happened in his or her mind exactly corresponds to something that happens in nature. It's startling every time it occurs. One is surprised that a construct of one's own mind can actually be realised in the honest to goodness world out there. A great shock and a great joy.
— Leo Kadanoff

4

Optimal Wavelet Design

The WPMCM transceivers are exceptionally sensitive and vulnerable to the time synchronization errors, which cause inter symbol and inter carrier interference. The conventional communication systems, like OFDM, exploit cyclic prefix or guard intervals to greatly mitigate the effect of the timing error. In the previous chapters we have seen that the WPMCM's subcarriers overlap in both: time and frequency domain. Therefore use of simple guard interval in WPMCM cannot prevent ICI and ISI from occurring when symbols are not correctly aligned at the receiver. Fortunately, WPMCM provides other benefits such as freedom to choose the shape and properties of the waveforms. It is well known that the attributes of a multicarrier modulation system greatly depends on the set of waveforms it uses. In WPMCM transceivers these waveforms are determined by the underlying filter coefficients used. By adapting the filter coefficients we can conceive the WPMCM transceiver that best suits an engineering requirement [52] – [54]. In this chapter the wavelet design for telecommunications application is proposed using modern optimization-based techniques. This method is used to design a new filter, which minimize the energy of the timing error interference.

The design of a wavelet system is bounded by multiple constraints. Besides the design objectives there are other constraints on wavelet bases that should be considered in order to guarantee that the designed wavelet is valid. The most important constraints are listed below ordered by their significance:

- Wavelet Existence and Compact Support
- Orthonormality
- *K*-Regularity

At initial stage we have a number of degrees of freedom that can be used to design a wavelet system. Fulfillment of each constraint consumes one or more degrees of freedom leaving less space for other criteria. Therefore the constraints should be carefully selected and deliberated according to the design specifications.

The remainder of this chapter is organized as follows. Section 4.1 describes the criteria for the two-channel filter bank. Time offset in WPMCM is discussed in § 4.2 where the objective function is derived. In § 4.3 the optimization problem is formulated and in § 4.4 the numerical results of optimal filter under the timing error are shown. Finally brief conclusion of this chapter is given in § 4.5.

4.1 Filter Criteria for Two-Channel Filter Bank

Multiresolution analysis of wavelet theory allows construction of compactly supported orthonormal waveletes by succesively iterating discrete two-band paraunitary filter banks. Time and frequency limited wavelet and scaling function can hence be represented by discrete half-band low and high-pass filters with filter coefficients $h(n)$ and $g(n)$ respectively.
The number of channels in WPMCM is determined by the number of iterations to be performed of the two-channel filter bank. Regardless of the desired number of channels the WPMCM bases can be derived from only 'one' fundamental filter. This is due to strict relationship that has to be fulfilled between the impulse responses of wavelet and scaling filter in a two channel filter bank. The wavelet filter is obtained by shifting the spectrum of scaling filter by π, which is equivalent to multiplication of $h(n)$ by $(-1)^n$ in time domain. Furthermore, in order to guarantee the orthogonality between filters the coefficients are reversed. In frequency domain the responses of the two filters appear as the mirror images of each other with respect to the mirror-frequency of $\frac{1}{2}\pi$. Equations (4.1) and (4.2) show the relationship between the wavelet and scaling filters.

$$g(n) = (-1)^n h(L-1-n) \tag{4.1}$$

$$h(n) = (-1)^{1-n} g(L-1-n) \tag{4.2}$$

In equations (4.1) and (4.2) L denotes the length of the filters.

The transfer function of synthesis filtering followed by analysis filtering will besides the useful signal also contain an aliasing term. In order to cancel undesired aliasing, the filters in synthesis

filter bank have to be chosen according to filters present in analysis filter bank. In Fourier domain we can express the relationship between the filters in two filter banks as:

$$\tilde{H}_1(\omega) = \tilde{G}_0(\omega + \pi) \tag{4.3}$$

$$\tilde{G}_1(\omega) = \tilde{H}_0(\omega + \pi) \tag{4.4}$$

In equations (4.3) and (4.4) $\tilde{G}_0$ and $\tilde{H}_0$ belong to analysis filter bank while $\tilde{G}_1$ and $\tilde{H}_1$ belong to synthesis filter bank.

Because of the relationships between the scaling- and wavelet filter as well as between the analysis and synthesis filter banks, the design of only one fundamental filter is required. In the following part of this chapter we will therefore discuss the design of scaling filter. Once the scaling filter coefficients are obtained we can calculate the wavelet filter coefficients using formula (4.1) and synthesis filters using equations (4.3) and (4.4).

4.1.1 Wavelet Existence and Compact Support

The coefficients outside the defined region are set to zero so that the filter banks used to derive wavelets are of the finite length. Other basic requirement for discrete wavelet system is fulfilment of the wavelet existence condition:

$$\sum_{n=0}^{L-1} h(n) = \sqrt{2} \tag{4.5}$$

Equation (4.5) represents the normalization of the scaling filter which implies that not just any set of coefficients will support a solution. In order for coefficients $h(n)$ to be valid scaling filter they have to satisfy wavelet existence condition. The foundations of this property are given in the Appendix A.
The equality (4.5) imposes one linear constraint on the filter coefficients $h(n)$.

4.1.2 Orthonormality or Paraunitary Condition

The paraunitary condition is essential for many reasons. Firstly, it is a prerequisite for generating orthonormal wavelets. Secondly, it automatically ensures perfect reconstruction of the decomposed signal i.e., the original signal can be reconstructed without amplitude or phase or aliasing distortion. A rational transfer function $A(z)$ is said to be paraunitary when it obeys the relation $\tilde{A}(z)A(z) = 1$. Here $\tilde{A}(z)$ is the paraconjugate of $A(z)$ and is given by $\tilde{A}(z) = A^*(z^{-1})$, where the superscript * denotes the conjugation of the coefficients. In order to satisfy the paraunitary constraint the scaling filter coefficients need to be self-orthogonal at even shift, that is:

$$\sum_{n=0}^{L-1} h(n)h(n-2m) = \delta(m) = \begin{cases} 1 & if \quad m = 0 \\ 0 & otherwise \end{cases} \tag{4.6}$$

In equation (4.6) δ denotes the Kronecker delta function. The origin of this property is given in the Appendix B.
The orthogonality condition imposes in total $^{L}/_{2}$ non-linear constraints on the filter coefficients $h(n)$. Together, properties (4.5) and (4.6) are necessary and sufficient conditions for the wavelets to be realized leaving $^{L}/_{2}$-1 degrees of freedom for other design criteria. However, other conditions might be essential to guarantee the generation of regular and well shaped wavelets. Quite often the designed wavelets can be irregular or even fractal shaped. In order to ensure smoothness or regularity of the wavelets the additional condition of *K*-regularity will be defined.

4.1.3 *K*-Regularity/Vanishing Moments

The *K*-regularity property was briefly introduced in § 2.4. This property gives a rough measure of the wavelet's smoothness. The regularity condition requires that the wavelet is locally smooth and concentrated in both, the time and frequency domains. It is normally quantified by the number of times a wavelet is continuously differentiable. The simplest regularity condition is the "flatness" constraint which is stated on the low pass filter. A LPF is said to satisfy K^{th} order flatness if its transfer function $H(z)$ contains K zeroes located at the Nyquist frequency (z = -1 or $\omega = \pi$). For some $Q(z)$ with no poles or zeros at (z = -1) this can be written as [10]:

$$H(z) = \left(\frac{1+z^{-1}}{2}\right)^{K} Q(z) \tag{4.7}$$

where

$$\begin{aligned} H(z) &= \sum_{n} h(n)z^{-n} \\ Q(z) &= \sum_{n} q(n)z^{-n} \end{aligned} \tag{4.8}$$

Parameter K in equation (4.7) is called the regularity order. In equations (4.7) and (4.8) the functions $H(z)$ and $Q(z)$ stand for the z-transforms of scaling and q-filter, respectively.

The number of zeros of the transfer function is related to the fact that the differentiability of a function is tied to how fast its Fourier transform magnitude drops off as frequency goes to infinity. Because $H(z)$ is a low-pass and by letting it have high order zero at Nyquist frequency, the Fourier transform of the scaling function should drop off rapidly and therefore scaling

function should be smooth. The Fourier transforms of the scaling function and filter are given by equations (4.9) and (4.10) respectively.

$$\Phi(\omega) = \left[\prod_{k=1}^{\infty}\left[\frac{1}{\sqrt{2}}H\left(\frac{\omega}{2^k}\right)\right]\right]\Phi(0) \tag{4.9}$$

$$H(\omega) = \sum_n h(n)e^{-j\omega n} \tag{4.10}$$

The k^{th} derivative of $H(\omega)$ evaluated at Nyquist frequency can be written as:

$$H^{(k)}(\pi) = \sum_n (2\pi j)^k n^k (-1)^n h(n) \tag{4.11}$$

Therefore in time domain we can impose regularity condition (4.7) by:

$$\sum_{n=0}^{L-1} n^k (-1)^n h(n) = 0 \quad for \quad k = 0,1,\ldots,(K-1) \tag{4.12}$$

Each wavelet has at least regularity order of 1 due to fulfillment of wavelet existence condition. By setting $K > 1$ we can impose extra regularity but because of previous constraints the regularity order for a filter of length L is limited by:

$$1 \le K \le \frac{L}{2} \tag{4.13}$$

K-Regularity condition requires additional K-1 constraints on filter coefficients $h[n]$. An extreme case exist where all remaining degrees of freedom are used to design maximally regular filters for a given filter length. Such filters are designed by [10].

4.2 Designing Best Bases to Tackle Time Synchronizations Errors

The degrees of freedom that remain after satisfying wavelet existence (4.5), orthonormality (4.6) and K-regularity (4.12) constraints can be used to design a scaling filter, which has minimal timing error interference.

The information carried by the waveforms that overlap one another can only be correctly decoded if the used waveforms have large distances in relation to each other, i.e. the cross-correlation between the waveforms is as small as possible. In WPMCM this is achieved through the orthogonality, where generated waveforms form an orthogonal set. Therefore, in disturbance free environment the cross-correlations of WPMCM waveforms equals zero and perfect

reconstruction is possible despite the time and frequency overlap. The timing error on the other hand leads to the loss of the orthogonality between the waveforms and consequently they begin to interfere one with another. The inter symbol and inter carrier interference can be expressed for a timing error t_ε as:

$$\Omega_{\substack{k,k' \\ k\neq k'}}^{u,u'}(t_\varepsilon) = \sum_n \xi^k_{2^{\log(N)}}(n-uN)\xi^{k'}_{2^{\log(N)}}(u'N-n+t_\varepsilon) \tag{4.14}$$

For $t_\varepsilon = 0$ and $k \neq k'$ the value of equation (4.14) will equal 0 due to orthogonality property of the waveforms (2.34). However, in presence of timing error the orthogonality property does not hold anymore and each waveform will be affected by the joint contribution of other waveforms. In § 3.3.2 an exhaustive treatment of the subject can be found.
The objective function for minimizing the interference energy in presence of timing error can now be written as:

$$\text{MINIMIZE:} \quad \sum_{u,k;k\neq k'} \left|\Omega_{k,k'}^{u,u'}(t_\varepsilon)\right|^2 \quad \textit{with respect to } \{h(n), g(n)\} \tag{4.15}$$

The waveforms in WPMCM are created by the tree structured filter bank where the end terminals of the tree correspond to the final waveforms used. Using Parseval's theorem of energy conservation (Appendix C) it can be easily confirmed that the total energy at each level is equal, regardless of the tree's depth. Therefore, minimizing the interfering energy at the origin of the tree will automatically lead to the decrease of total interfering energy at the higher tree levels. This property allows us to consider only elementary two-channel filter bank in our design process. The two-channel filter bank consists from the scaling and wavelet filters, which are unambiguously related to the WPMCM's waveforms through equation (2.33). Therefore, we should be able to minimize deleterious effects of time synchronization errors in WPMCM by minimizing the following objective function:

$$\begin{aligned}\sum_\tau \left|r_{hg}\right|^2 &= \sum_\tau \left|\sum_n h(n)g(n-\tau)\right|^2 \\ &= \sum_\tau \left|\sum_n h(n)\left((-1)^n h(L-n-\tau)\right)\right|^2\end{aligned} \tag{4.16}$$

4.3 Problem Formulation

The design problem of minimizing the interference energy due to timing error can now be defined as an optimization problem with objective function (4.16) and constraints (4.5), (4.6) and (4.12), i.e.

$$\text{MINIMIZE:} \quad \sum_{\tau} \left| r_{hg} \right|^2 \quad \textit{with respect to } h(n) \tag{4.17}$$

$$\text{SUBJECT TO:} \quad \begin{aligned} &\sum_{n=0}^{L-1} h(n) = \sqrt{2} \\ &\sum_{n=0}^{L-1} h(n)h(n-2m) = \delta(m) \quad \textit{for } m = 0,1,\ldots,\left(\frac{L}{2}-1\right) \\ &\sum_{n=0}^{L-1} n^k (-1)^n h(n) = 0 \quad \textit{for } k = 0,1,\ldots,(K-1) \end{aligned} \tag{4.18}$$

The objective function (4.17) as majority of the constraints in (4.18) is non-linear. Therefore, the optimization problem as given above can only be solved by general purpose solvers. The main disadvantage of such solvers is that they are susceptible to being trapped by the local minima. In order to overcome this difficulty, some authors have suggested multiple starting point techniques or branch-and-bound method [55]. Nevertheless, general purpose algorithms cannot guarantee that the found result is a global minimum and furthermore when number of constraints increases these algorithms often fail to provide a valid solution.

The optimization problems with convex objective function and constraints can be solved much more efficiently by the semidefinite programming. In the next part of this paragraph we will briefly discuss semidefinite programming and we will attempt to express our problem in the convex form.

4.3.1 SemiDefinite Programing

SemiDefinite Programming (SDP) is a subfield of convex optimization, which can efficiently exploit interior point methods to find an optimal solution [56], [57]. The main advantages of convex optimization methods are that they always achieve global minimum without being trapped in the local minima, and that they can determine explicitly the feasibility of a given set of constraints. SDP algorithms can be used to solve linear, quadratic and semidefinite problems, which all are part of convex optimization problems.

The optimization problems in SDP can be described as minimization of an objective linear function over the intersection of the semidefinite cone with an affine space. This cone is shaped by constraints that form a set of positive symmetric semidefinite matrices, called Linear Matrix Inequality (LMI) constraint [58]. LMI gives boundaries of feasible region in which SDP solver tries to find an optimal solution for the objective function or prove infeasibility. This region is generally non-smooth and non-linear but it has to be convex in order to be solvable by SDP [59] – [62].

Some set C is said to be convex if the line segment between any two arbitrary selected points in C lies also in C. In case of points X_1 and X_2 we can show convexity by:

$$\Gamma X_1 + (1-\Gamma) X_2 \in C \quad \textit{for} \quad X_1, X_2 \in C \ \textit{and} \ 0 \le \Gamma \le 1 \tag{4.19}$$

The example of convex and non-convex set is illustrated by figure 4.1. For each two points in pentagon the line segment lies in the defined set and therefore blue figure (left) is convex. The red figure (right) is obviously not convex since two points X_1 and X_2 are within the set but the line which connects them is partially not contained in the set.

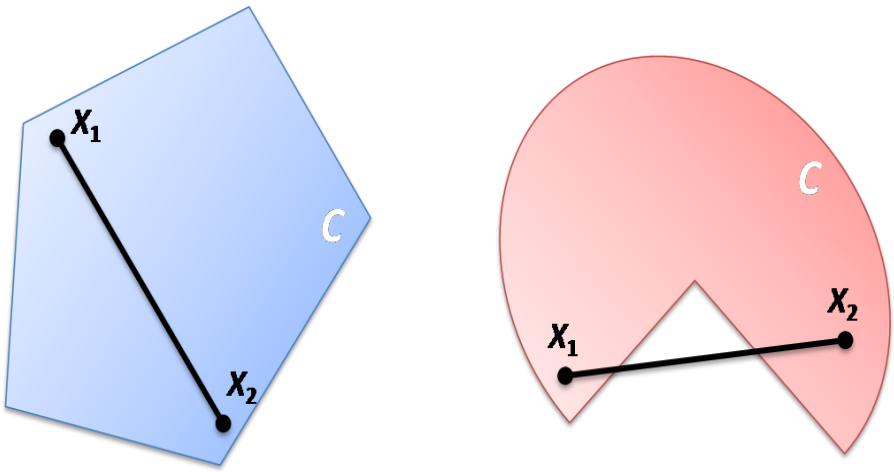

Figure 4.1: Convexity; Left: Convex Set, Right: Non-Convex Set

The minimization of timing error interference is unfortunately not a convex optimization problem. Therefore, in order to use SDP solvers the original non-convex problem has to be revised first [63].

4.3.2 Conversion of Non-Convex Problem

The optimization problem, stated in (4.17) and (4.18), can be converted into a convex form by rewriting the objective and constraints as convex functions of the scaling filter's autocorrelation [64] – [66]. The autocorrelation sequence $r_h(n)$ of scaling filter $h(m)$ is given by:

$$r_h(n) = \begin{cases} \sum_{m=0}^{L-n-1} h(m)h(m+n) & n \geq 0 \\ r_h(-n) & n < 0 \end{cases} \tag{4.20}$$

4.3.2.1 Wavelet Existence and Compact Support

The constraint that ensures wavelet existence and compact support has been given earlier by equation (4.5). The same constraint can be expressed in terms of autocorrelation sequence $r_h(n)$ by imposing following condition:

$$\sum_{n=-L+1}^{L-1} r_h(n) = 2 \tag{4.21}$$

Because autocorrelation is a symmetric function we only need to consider positive indices n. Using the properties of symmetry and orthonormality condition at instance $n = 0$, we can rewrite equation (4.21) as:

$$\sum_{n=1}^{L-1} r_h(n) = \frac{1}{2} \tag{4.22}$$

4.3.2.2 Orthonormality or Paraunitary Condition

The double shift orthogonality condition (4.6) can also be easily expressed in terms of $r_h(n)$, making use of symmetry property we can express the orthogonality constraint as:

$$r_h(2n) = \delta(n) = \begin{cases} 1 & if\ n = 1 \\ 0 & otherwise \end{cases} \quad for\ n = 0,1,\ldots,\left(\frac{L-1}{2} - 1\right) \tag{4.23}$$

In contradiction to original orthogonality constraint (4.6) which was not convex, the new constraint (4.23) is composed from a set of linear equalities and is therefore convex.

4.3.2.3 K-Regularity/Vanishing Moments

The K-Regularity constraint (4.12) requires from transfer function $H(z)$ to have K zeros at Nyquist frequency ($\omega = \pi$). In terms of autocorrelation function this is equivalent to having twice as much zeros at frequency $\omega = \pi$, since the corresponding frequency response is given by:

$$\left|H(\omega)\right|^2 = \left|\frac{1+e^{j\omega}}{2}\right|^{2K} \left|Q(\omega)\right|^2 \tag{4.24}$$

Making again use of symmetry property we can omit $n < 0$ indices and therefore we only need to impose K-1 regularity constraints on $r_h(n)$:

$$\sum_{n=1}^{L-1} (-1)^n n^{2k} r_h(n) = 0 \quad for\ k = 1,2,\ldots,K-1 \tag{4.25}$$

4.3.2.4 Spectral Factorization

The reformulated optimization problem consists of the objective function and the constraints that are functions of sequence $r_h(n)$ and therefore the solution to such problem is given in the form of optimal autocorrelation. In order to obtain optimal filter we need to find those filter coefficients that correspond to the optimal autocorrelation. There are infinitely many time domain sequences which share the same autocorrelation but using spectral factorization algorithms we are able to

extract the unique minimum-phase time domain coefficients. The spectral factorization of an autocorrelation sequence $r_h(n)$ can be performed as long as the log-function of Fourier transform $R_h(\omega)$ remains in $\mathbb{R}$, see Appendix D for more detail about Kolmogorov spectral factorization algorithm. Therefore, spectral factorization requires an additional constraint:

$$R_h(\omega) \geq 0 \quad for\ \omega \in (0, \pi) \tag{4.26}$$

where

$$\begin{aligned} R_h(\omega) &= \sum_{n=0}^{L-1} r_h(n) e^{-j\omega n} \\ &= r_h(0) + 2\sum_{n=1}^{L-1} r_h(n) \cos \omega n \end{aligned} \tag{4.27}$$

Constraint (4.26) contains an infinite number of linear inequalities and needs therefore to be sampled before it can be applied to an optimization program. This can be achieved by replacing continuous variable ω by a discrete variable $\omega_i = {}^{i\pi}/_{d}$, which is defined on a finite set $i = [0,\ldots,d]$. The value for d should be set sufficiently large, typically $15n$. The constraint (4.26) can hence be approximated by:

$$R_h\left(\frac{i\pi}{m}\right) \geq 0 \quad for\ \ i \in [0,\ldots,m] \tag{4.28}$$

4.3.2.5 Objective Function

The original objective is a non-convex function of the filters coefficients $h(n)$ and needs to be translated into autocorrelation domain to fit the new perspective. The autocorrelation function of scaling filter is given by equation (4.20) and correspondingly the autocorrelation of wavelet filter can be expressed as:

$$\begin{aligned} r_g(n) &= \sum_{m=0}^{L-n-1} g(m) g(m+n) \quad for \quad n \geq 0 \\ &= \sum_{m=0}^{L-n-1} \Big((-1)^m h(L-m)\Big)\Big((-1)^{m+n} h\big(L-(m+n)\big)\Big) \\ &= (-1)^n r_h(n) \end{aligned} \tag{4.29}$$

The sum of squares of a cross-correlation between two functions equals the inner product of the autocorrelation sequences of these two functions, see Appendix E for the prove. This property together with orthogonality limitation (4.23) is used to rewrite (4.16) in terms of $r_h(n)$. The equation (4.30) shows the new objective where only the right side of autocorrelation and cross-correlation is taken into account.

$$\begin{aligned}\sum_{n=0}^{L-1}\left|r_{hg}(n)\right|^2 &= \sum_{n=0}^{L-1} r_h(n) r_g(n) \\ &= \sum_{n=0}^{L-1} r_h(n)\left((-1)^n r_h(n)\right) \\ &= \sum_{n=0}^{N/2}\left(r_h(2n+1)\right)^2 - \left(r_h(2n)\right)^2 \\ &= \sum_{n=0}^{N/2}\left(r_h(2n+1)\right)^2 - 1\end{aligned} \tag{4.30}$$

The original non-convex problem given by (4.17) and (4.18) can be transformed into a convex optimization problem by using identities (4.22), (4.23), (4.25) and (4.30), i.e.,

$$\text{MINIMIZE:} \quad \sum_{n=0}^{N/2}\left(r_h(2n+1)\right)^2 \quad \textit{with respect to } r_h(n) \tag{4.31}$$

$$\begin{aligned}&\sum_{n=1}^{L-1} r_h(n) = \frac{1}{2} \\ &r_h(2n) = \delta(n) \quad \textit{for } n = 0,1,\ldots,\left(\frac{L-1}{2}-1\right) \\ \text{SUBJECT TO:} \quad &\sum_{n=1}^{L-1}(-1)^n n^{2k} r_h(n) = 0 \quad \textit{for } k = 1,2,\ldots,K-1 \\ &\left((r_h(0) + 2\sum_{n=1}^{L-1} r_h(n)\cos\left(\frac{i\pi n}{d}\right)\right) \geq 0 \quad \textit{for } i \in [0,\ldots,d]\end{aligned} \tag{4.32}$$

4.4 Numerical Results

The optimal filter in accordance with (4.31) and (4.32) can be found using semi definite programming (SDP). Today there exist several generic SDP solvers under which SeDuMi [67]. SeDuMi is an additional Matlab® package that can be used for linear, quadratic and semidefinite programming. Normally it requires a problem to be described in a primal standard form but with Yalmip toolbox [68] the optimization problems can be directly expressed in a higher level language.

We have developed a filter optimization program that incorporates most of the available optimization routines for Matlab® and which relies on Yalmip to translate the problem into the standard form.

In the filter design discussed here we have selected SeDuMi optimization algorithm and we have set the length of the optimal filter to 20 coefficients. However, it is obviously possible to design

longer or shorter filters. Another parameter that can be chosen, besides the length of a filter, is the regularity. Regularity has to be equal or larger than 1 ensuring that wavelet existence constraint is satisfied, while it may not exceed $^{L}/_{2}$ in order to remain in feasible region. If the selected value for regularity is close to the upper limit, less degrees of freedom will be left for the optimization of the objective function. On the other hand imposing small regularity can result in highly irregular wavelets. Here we have chosen for regularity-order 5, which is a compromise between optimization space and wavelet regularity.
The GUI of the wavelet filter design program is illustrated in figure 4.2

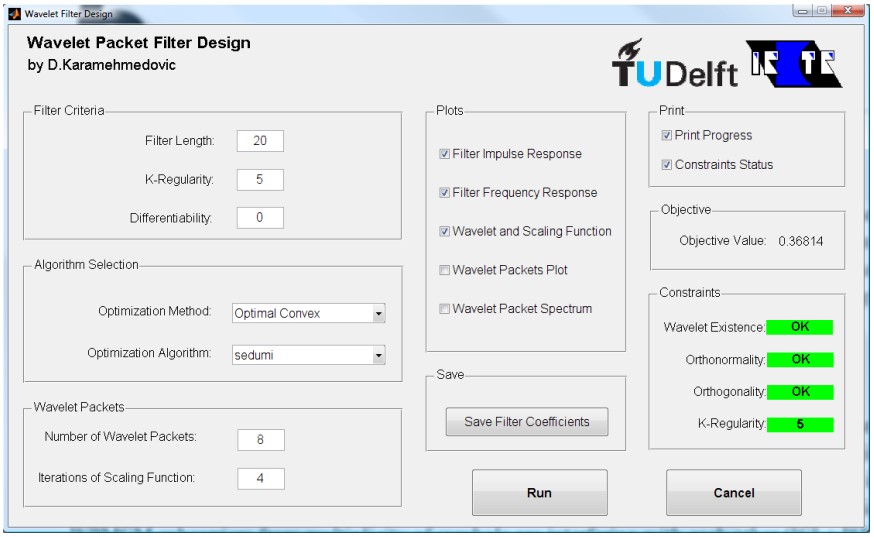

Figure 4.2: Wavelet Packet Filter Design Program

Table 4-1 shows optimal wavelet at the side of 'standard' wavelets, which have been also discussed in previous chapters. It is clear that the value of the objective function for optimal wavelet is considerably reduced in comparison with 'standard' wavelets.

Table 4-1: Wavelet Specification

Name	Length	*K*-Regularity	$\sum_{n=0}^{N/2}\left(r_h(2n+1)\right)^2$
Haar	2	1	-
Daubechies	20	10	0.41955
Symlets	20	10	0.41955
Discrete Meyer	102	1	0.45722
Coiflet	24	4	0.41343
Optimal	20	5	0.36814

The impulse response of the designed optimal filter is illustrated in figure 4.3 and numerical values of filter coefficients are given in table 4-2. Although the optimal filter is designed in autocorrelation domain, shown minimum-phase time domain coefficients satisfy all original constraints (4.5), (4.6) and (4.12)

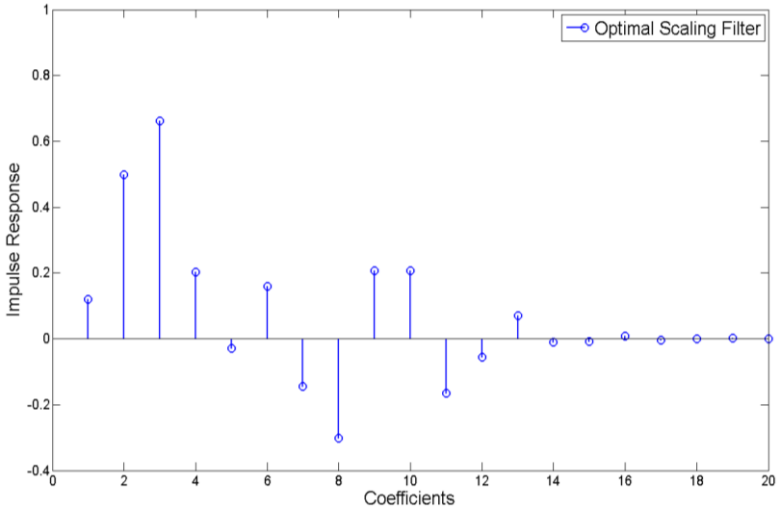

Figure 4.3: Impulse Response of the Optimal LPF with 20 coefficients

Table 4-2: Optimal Filter Coefficients

0.119881851613898	0.498287367999060	0.660946808777660	0.203191803677134
-0.0291516906888238	0.159448121842196	-0.144908809151642	-0.301681615791117
0.206305798368833	0.205999004857997	0.165410385138750-	-0.0566148032177797
0.0712828626076334	-0.00958254794419582	-0.00839405084469072	0.00912479119304040
-0.00498653232060994	-0.000694408819538431	0.00154092796305564	-0.000370932610232259

The wavelet and scaling function corresponding to the optimal filter are illustrated in figure 4.4. It is quite clear that the scaling function and the wavelet function of optimal filter are not as smooth as scaling and wavelet function of Daubechies filters with the same number of coefficients, (refer Figure 2.18). This is because Daubechies filter has twice as high regularity-order when compared to the optimal filter. In optimal filter remaining degrees of freedom, which haven't been used for *K*-regularity constraint, are exploited for minimization of the objective function.

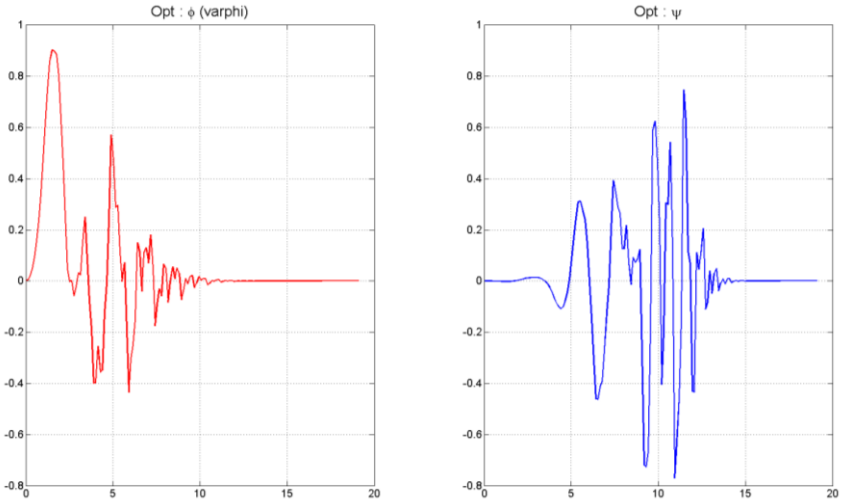

Figure 4.4: Optimal Filter; Left: Scaling Function, Right: Wavelet Function

The frequency response of the optimal filter is illustrated in figure 4.5.

The optimization process has compromised the frequency selectivity of the designed filter to some extent. However, more frequency selective filters can be designed by increasing the filter's length in the optimization program.

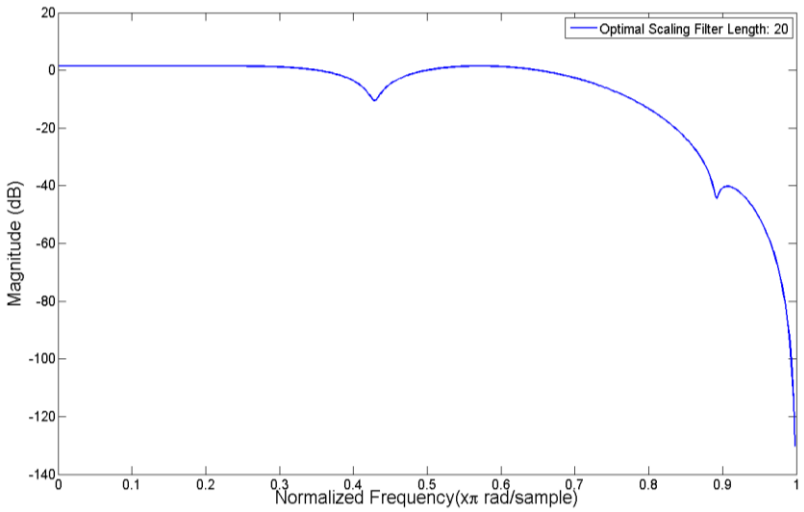

Figure 4.5: Frequency Response in dB of the Optimal Filter

The performance of optimal wavelet in presence of timing synchronization errors is examined by means of computer simulations. For the purpose of comparison we have also included 'standard' wavelets and OFDM in the analysis. The time offset is modeled as a discrete uniform distribution between -2 and 2 samples, i.e. $t_\varepsilon \in$ [-2, -1, 0, 1, 2]. Furthermore, an oversampling with factor 15 is applied in order to magnify the difference between different systems and different wavelets. An overview of important simulation parameters is given in table 4-3.

Table 4-3: Simulation Setup Time Synchronization Error

	WPMCM	OFDM
Number of Subcarriers	128	128
Number of Multicarrier Symbols per Frame	100	100
Modulation	DQPSK	DQPSK
Channel	AWGN	AWGN
Oversampling Factor	15	15
Guard Band	-	-
Guard Interval	-	-
Frequency Offset	-	-
Phase Noise	-	-
Time Offset	t_ε= 2	t_ε= 2

- does not apply

Figure 4.6 shows the Bit Error Rate (BER) performances of WPMCM system with different kind of wavelets and OFDM, under assumption of AWGN channel and time discrepancy between transmitter and receiver.

Figure 4.6 reveals that the designed optimal wavelet has better BER performance in presence of timing error when compared to performances of 'standard' wavelets. However, OFDM remains superior to WPMCM based systems if symbols at the receiver are not correctly synchronized. This is due to fact that under time synchronization errors the ISI in OFDM arises only between two adjacent symbols while in the case of WPMCM several symbols are interfering with each other.

Table 4-4 shows the reduction of required SNR of designed optimal wavelet over 'standard' wavelets in presence of timing errors. The shown improvement is evaluated at BER of 10^{-4}.

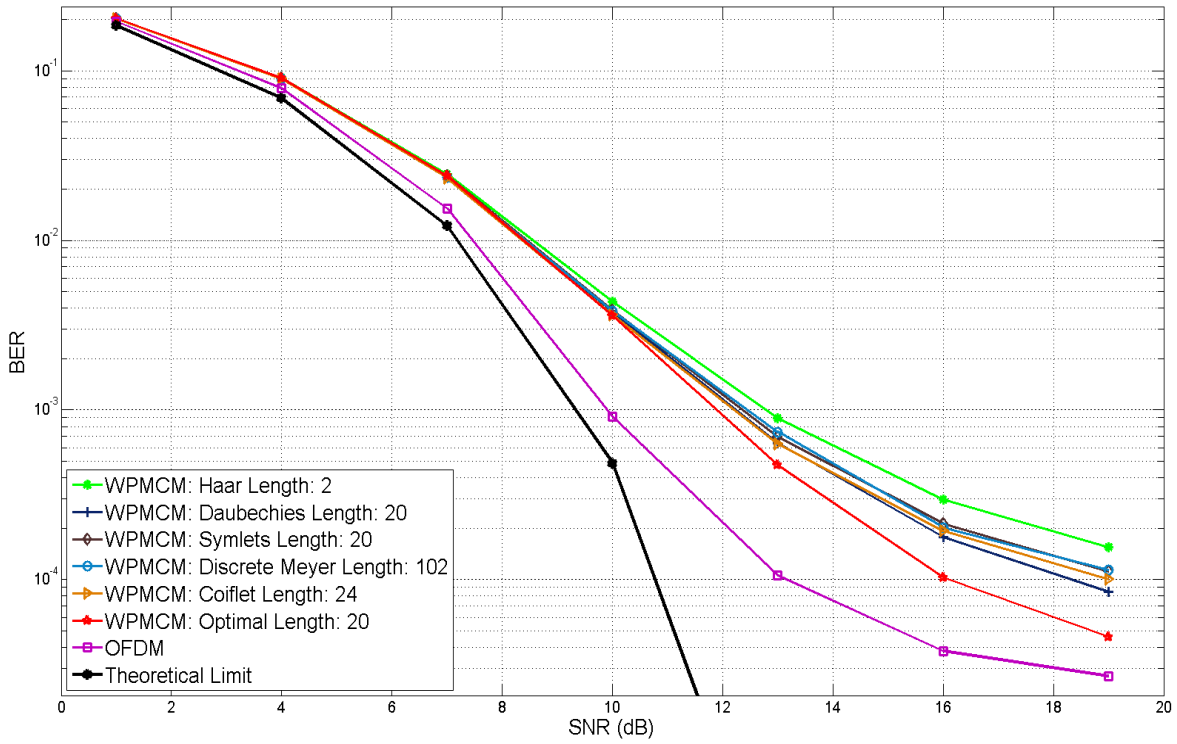

Figure 4.6: BER Performance of Different Wavelets and OFDM under Time Synchronization Errors

Table 4-4: Performance Improvement of Designed Optimal Wavelet over Standard Wavelets in Presence of Timing Errors (measured at BER of 10^{-4})

Wavelet Name	Haar	Daubechies	Symlets	Discrete Meyer	Coiflet
Improvement	5.03 dB	2.17 dB	3.25 dB	3.25 dB	2.98 dB

BER and Mean Square Error (MSE) calculated for different values of time offset are shown in figures 4.7 and 4.8, respectively. Because the direction of timing error is inconsequential for WPMCM based system the time offset is modeled as uniform distribution between -t_ε and t_ε samples with t_ε going from 1 to 5 samples.
From figures 4.7 and 4.8 it is evident that our optimal wavelet is less sensitive to the time synchronization errors when compared to other simulated wavelets.

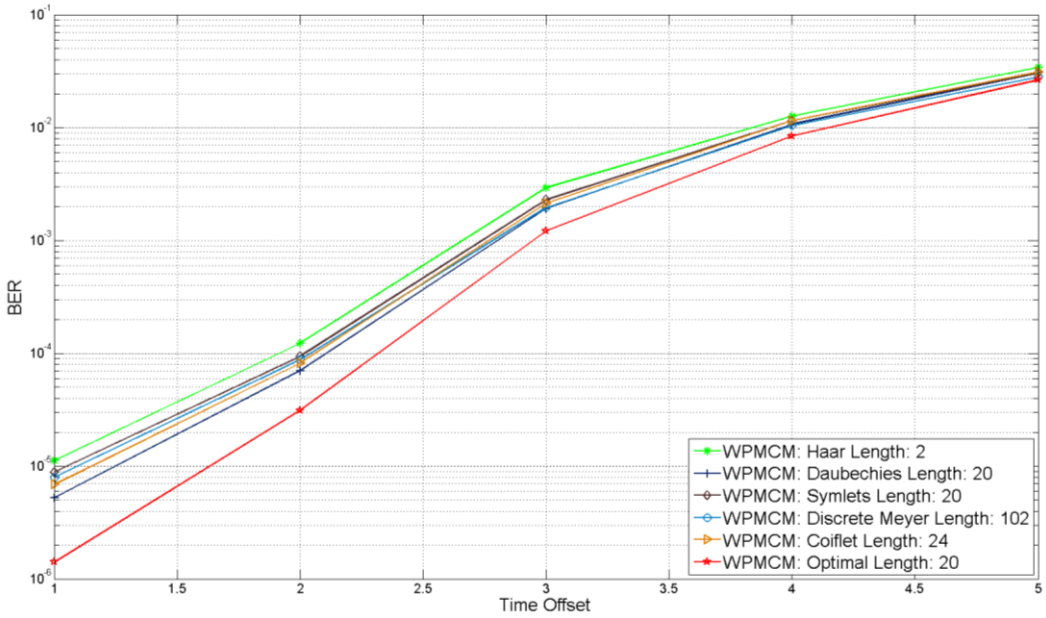

Figure 4.7: BER vs. Time Offset for WPMCM in AWGN channel (SNR = 20dB)

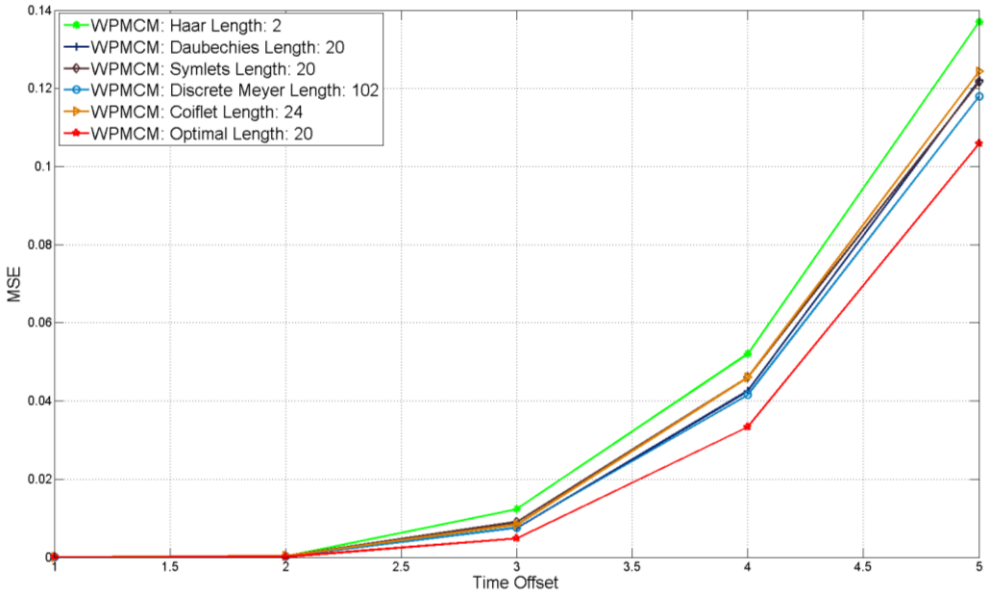

Figure 4.8: MSE vs. Time Offset for WPMCM in AWGN channel (SNR = 20dB)

In figure 4.9 and 4.10 the spreading of subcarriers energy due to time synchronization error is illustrated. For the clarity we limited the number of subcarriers to 16 and frame size to 30 multicarrier symbols. From total 480 subcarriers which can be found in each frame, we are setting one pilot subcarrier to non-zero value while remaining 479 subcarriers are set to zero. The channel is assumed to be ideal in order to emphasize the effect of timing error.

As expected, it can be seen from the figures that the amplitudes of interfering subcarriers is highly reduced by employing optimal filter. Furthermore it can be noticed that for the Haar wavelet the ISI is only limited to the neighboring symbols, comparable to the OFDM case. In contrast to other orthogonal wavelets, waveforms generated by the Haar wavelet are not overlapping one another in time domain. Despite no-time-overlapping waveforms the performance of Haar wavelets is not superior to other orthogonal wavelets due to increased ICI.

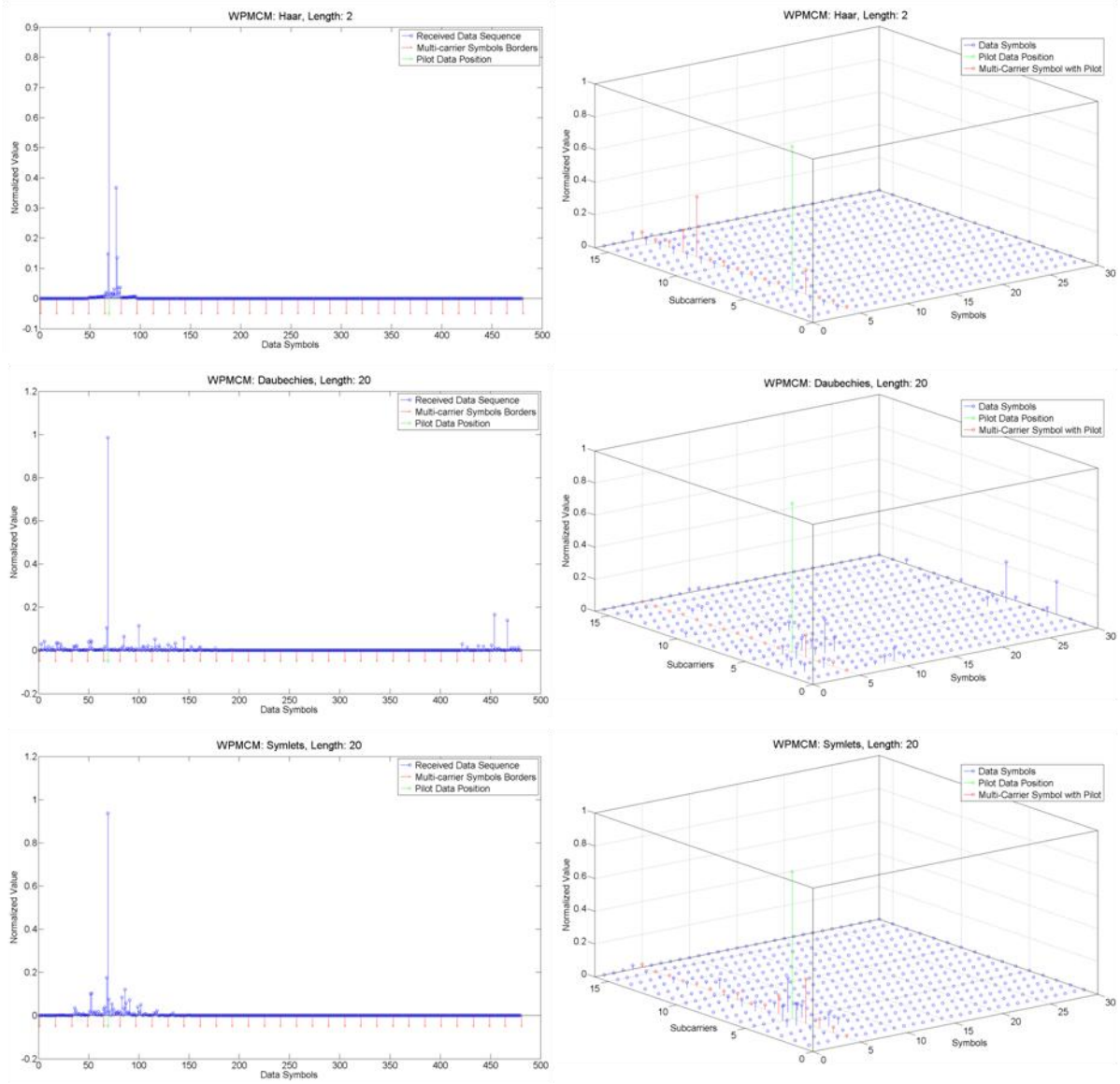

Figure 4.9: Received Spectral Energy in a Frame in presence of Timing Error; Haar, Daubechies and Symlet Wavelet

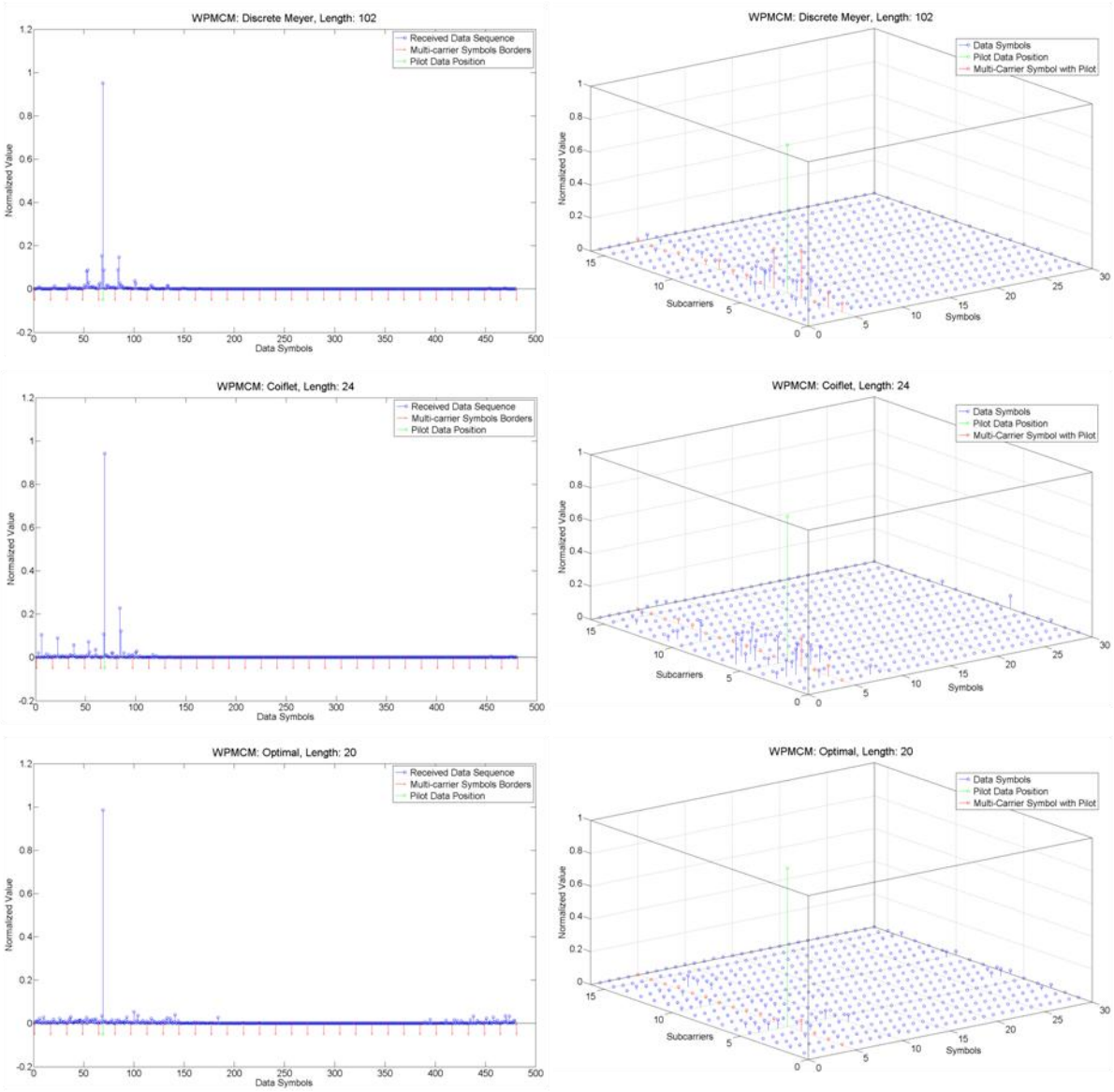

Figure 4.10: Received Spectral Energy in a Frame in presence of Timing Error; Discrete Meyer, Coiflet and Optimal Wavelet

In table 4-5 the values of interference variance and maximal interference amplitude ratio in relation to signal amplitude is given. These values are obtained for constant time offset and one pilot subcarrier.

Table 4-5: Interference Variance and Max. Interference Amplitude Ratio

Wavelet Name	Haar	Daubechies	Symlets	Discrete Meyer	Coiflet	Optimal Wavelet
Interference Variance (10^{-5})	5.1088	3.0751	3.0721	3.1651	3.0639	2.8775
Max. Interference to Signal Amplitude	14.14 %	8.36 %	7.97 %	6.66 %	8.25 %	4.51 %

4.5 Conclusion

WPMCM can offer more flexibility and adaptability to the system designers but the major drawbacks of WPMCM remain in its high sensitivity to timing discrepancies when compared to the competing OFDM technique.

In this chapter we have presented the design of dedicated wavelets which are less sensitive to the timing errors. The design process is described as an optimization problem with an objective to minimize timing error interference energy. In order to obtain the global minimum, the original non-convex constraints and objective function are translated into the autocorrelation domain. Using the new formulation the design problem is expressed as a convex optimization problem and efficiently solved by the semi definite programming technique. The imposed constraints ensure that the designed wavelets are orthonormal and that they satisfy the wavelet existence condition. Furthermore, designers can make tradeoff between the number of vanishing moments and optimization space.

The simulation results of multicarrier transmission system revealed that the designed wavelet has a significantly better performance under time synchronization errors when compared to standard wavelets, such as discrete Meyer, Daubechies, etc. However, by the optimization process the frequency selectivity of wavelet is compromised and therefore a deliberated tradeoff between frequency selectivity and timing sensitivity should be made.

It is worth mentioning that the wavelet design method described here can also be used for other design criteria by merely altering the objective function.

Any piece of knowledge I acquire today has a value at this moment exactly proportional to my skills to deal with it. Tomorrow, when I know more, I recall that piece of knowledge and use it better .
— Mark Von Doren, 1894-1972

5

Conclusions and Further Research

In this thesis work we have addressed the sensitivity of novel Wavelet Packed based Multi-Carrier (WPMCM) transmission system to the carrier frequency offset, phase noise and time synchronization errors. Furthermore, we have proposed a filter design framework that facilitates the development of new optimized wavelet bases according to the preferred design criteria.

5.1 Key Research Conclusions

The core conclusions of this effort can be summarized in the following points:

- Spectral efficient multicarrier transceivers as WPMCM and OFDM are vulnerable to carrier frequency offset which causes subcarriers to lose their mutual orthogonality and begin to interfere one with another. In OFDM performance degradation due to frequency offset is limited to the interference among the subcarriers within one OFDM symbol (ICI), while in WPMCM subcarriers from multiple symbols interfere with each other (causing ICI + ISI). This dissimilarity in the interference behavior is due to the manner in which the subcarriers in wavelet and Fourier based systems are created. The signals generated by OFDM overlap only in frequency domain while WPMCM generated signals overlap in both frequency and time domain.

- Secondly, the impact of phase noise on the performance of WPMCM and OFDM was analyzed. We found that two different scenarios can occur in presence of phase noise, depending on the phase noise bandwidth. If the phase noise bandwidth is small compared to inter-carrier spacing the dominant effect will be a constant rotation of constellation symbols. On the other hand, when phase noise bandwidth is greater than the inter-carrier spacing the rotational behavior is less pronounced but instead the interference dominates. Quite similar to the frequency offset, the interference due to the phase noise corrupts the OFDM signal only with ICI while WPMCM signals are corrupted with ICI and ISI.

- Thirdly, we studied the problem of the time offset. Under time synchronization errors OFDM can take advantage of cyclic prefix to greatly reduce the generation of interference as opposed to WPMCM which cannot benefit from such constructions due to time overlap of the symbols. Nevertheless, cyclic prefix in OFDM fails to prevent interference from occurring if offset value is larger than the size of the prefix or when offset is in the opposite direction with regard to symbol's own prefix. When parts of the neighboring symbols get erroneously selected at the OFDM or WPMCM receiver windows, the demodulated signal will be distorted by ISI and ICI. In OFDM, ISI arises only due to neighboring multicarrier symbols, while in WPMCM more than two multicarrier symbols contribute to the ISI generation.

- To confirm our theoretical findings, we built a simulation set-up where performance of WPMCM was examined in the presence of carrier frequency offset, phase noise and time synchronization error. Several well-known wavelets such as Daubechies, Symlets, discrete Meyer, Coiflets and biorthogonal wavelet were applied and studied. For the purpose of comparison, we have also included OFDM in our numerical analysis.
  Simulations studies have shown that the performance degradation of WPMCM and OFDM are quite similar in the presence of carrier frequency offset and phase noise. However, time synchronization error is found to be a major drawback of WPMCM transceivers. Therefore, we focused our attention on the time synchronization error and attempted to find a solution for the large performance gap between WPMCM and OFDM transceivers under timing errors.

- The attributes of a WPMCM transceiver greatly depends on the underlying wavelet it uses. 'Standard' wavelets which are developed for other applications are not suitable for multicarrier modulation. As means to overcome the problem of WPMCM's sensitivity to time offset, we designed a new wavelet filter which reduces the timing error interference.

- The design of a wavelet filter is subject to the multiple constraints. Besides the objective to minimize the timing error interference, there are also general constraints on wavelet bases that should be fulfilled in order to guarantee the validity of designed wavelets. The

all-embracing solution for the design problem was found by means of semi definite programming (SDP).
We expressed our filter design criteria as a convex optimization problem and subsequently we used SDP algorithm to obtain optimal solution, i.e. filter with minimized timing error interference.

- Simulations of WPMCM transceiver proved that the newly designed optimum filter has a better performance under time synchronization errors when compared to 'standard' wavelets such as Daubechies, Symlets, discrete Meyer, Coiflets, etc.

In short the results of this thesis work confirmed WPMCM to be a very flexible communication system whose actual characteristics can be tailored according to the engineering requirements. We used the unique features offered by wavelets to tailor and customize new filters, to make WPMCM transmission less sensitive to time synchronization errors. The wavelet filter design template developed in this work can also be used for other design goals by merely altering the objective function. This approach hopefully will pave the way for the development of other wavelet filters which can for instance decrease frequency offset and phase noise sensitivity, reduce Peak-to-Average Power Ration (PAPR), increase spectral efficiency, etc.
An added advantage of using wavelet theory for Multicarrier modulation is in the possibility of improving transmission security. Because newly designed wavelets are unique in nature, the transmitted signal can only be decoded by the WPMCM receiver which is acquainted with filter coefficients used by the WPMCM transmitter.

5.2 Recommendations for Further Research

Although the theory of wavelet transform has been well-evolved and documented over the past years, the use of wavelets in the communication systems is still in the early stage of the development. Therefore, there remain several important issues and concepts that are worth investigating.
The first suggestion concerns time offset correction. In this thesis the vulnerability of WPMCM to time synchronization errors was addressed and optimal wavelet filter design, which reduces WPMCM's timing error sensitivity, was proposed and implemented. Nevertheless, the fact remains that we cannot use guard intervals and that only moderate timing errors are acceptable. For this reason, a robust frame synchronization algorithm is needed to detect and correct large time offsets.
A second interesting topic would be to implement a dynamic spectrum allocation in WPMCM, which can help increase the system capacity by allocating spectrum resources according to the actual demand. It's the author's belief that wavelet based systems are very suitable for dynamic spectrum allocation due to great flexibility they offer in the assignment of subcarriers and subcarriers' bandwidths.

Thirdly, in the last years OFDM–MIMO (Multiple-Input Multiple-Output) combination has been successfully used to enhance the throughput and range of wireless networks by neither requiring more bandwidth nor more power. The motivation to use MIMO in OFDM is because of relatively reduced multi-channel equalization when compared to single carrier systems. Fundamentally, OFDM and WPMCM share many similarities as both are orthogonal multi-carrier techniques and therefore I think that there is a similar potential in WPMCM-MIMO combination which should be further investigated.
Finally, for more representative results it is necessary to evaluate WPMCM systems in different real channel environments, taking into consideration fading, multipath, etc.

5.3 My Perspective

The wireless revolution has already begun and the insatiable appetite for more speed and broadband application will continue so for the foreseeable future. At the same time the most part of usable spectrum is already sliced into tiny pieces and allocated to various applications, ranging from mobile phones, TV and radio to wireless light switches and garage door openers. This conflict of limited spectrum resources and increasing demand for wireless services is most important design challenge which telecommunication engineers are facing today. Therefore, many efforts are made to optimize use of the spectrum by developing an intelligent communication system that can estimate the channel and adaptively reconfigure resources. Such system configuration however imposes various constraints on the modulation technique used, which cannot be completely satisfied with techniques used at this moment.
I believe that WPMCM is uniquely qualified to address this challenge with its distinctive features as:

- Freedom in preference of multicarrier attributes.
- Flexibility in the assignment of subcarriers.
- Flexibility in the assignment of subcarriers' bandwidths.
- Low side lobes.
- Bandwidth efficiency.

These advantages together with simple implementation make WPMCM a perfect candidate for the future generation wireless communication systems.

List of Publications

[1] D.Karamehmedović, M.K.Lakshmanan, H.Nikookar, "Performance of Wavelet Packet Modulation (WPM) and OFDM in the Presence of Carrier Frequency Offset and Phase Noise" , in Proc. European Wireless Technology Conference (EuWiT), October 2008

[2] D.Karamehmedović, M.K.Lakshmanan, H.Nikookar, "Performance Degradation Study of Wavelet Packet based Multicarrier Modulation Under Time Synchronization Errors", in Proc. International Wireless Personal Multimedia Communications Symposium (WPMC), September 2008

[3] D.Karamehmedović, M.K.Lakshmanan, H.Nikookar, "Phase Noise Effects on the Performance of Wavelet Packet Multi-Carrier Modulation", Wireless Communication Society, Vehicular Technology, Information Theory and Aerospace & Electric System Technology (Wireless VITAE), May 2009

[4] D.Karamehmedović, M.K.Lakshmanan, H.Nikookar, "Performance of WPMCM and OFDM in the Presence of Carrier Frequency Offset and Phase Noise", submitted to Journal of Communications (JCM 2008)

[5] D.Karamehmedović, M.K.Lakshmanan, H.Nikookar, "Optimal Wavelet Packet Design for Multicarrier Modulation with Time Synchronization Error", submitted to IEEE Global Communications Conference (Globecom 2009)

Bibliography

[1] S.Haykin, “Cognitive Radio: Brain-Empowered Wireless Communications”, IEEE JSAC, Vol.23, No.2, pp.201-220, February 2005

[2] J.Mitola, G.Q.Maguire, “Cognitive Radio: Making Software Radios More Personal”, IEEE Personal Communications, Vol.6, No.4, pp.13-18, August 1999

[3] A.Lindsay, “Wavelet Packet Modulation for Orthogonally Transmultiplexed Communications”, IEEE Transaction on Communications, Vol.45, pp.1336-1339, May 1997

[4] G.Wornell, “Emerging Applications of Multirate Signal Processing and Wavelets in Digital Communications”, Proc. of IEEE, Vol.84, pp.586-603, April 1996

[5] M.K.Lakshmanan, H.Nikookar, “A Review of Wavelets for Digital Wireless Communication”, Springer Journal on Wireless Personal Communication, Vol.37, No.3-4, pp.387-420, May 2006

[6] B.G.Negash, H.Nikookar, “Wavelet-based Multicarrier Transmission Over Multipath Wireless Channels”, IEE Electronic Letters, Vol.36, No.21, pp.1787-1788, October 2000

[7] M.K.Lakshmanan, H.Nikookar, “Wavelet Packet based Strategy to Mitigate Wideband Interference on Impulse Radio”, IEEE (PIMRC ‘2007) Personal, Indoor and Mobile Radio Communications, pp.1-5, September 2007

[8] D.Karamehmedović, M.K.Lakshmanan, H.Nikookar, “Performance of Wavelet Packet Modulation (WPM) and OFDM in the Presence of Carrier Frequency Offset and Phase Noise” , in Proc. European Wireless Technology Conference (EuWiT ‘08), October 2008

[9] D.Karamehmedović, M.K.Lakshmanan, H.Nikookar, “Performance Degradation Study of Wavelet Packet based Multicarrier Modulation Under Time Synchronization Errors”, in Proc. International Wireless Personal Multimedia Communications Symposium (WPMC ’08), September 2008

[10] I.Daubechies, “Ten Lectures on Wavelets”, Philadelphia: SIAM, 1992

[11] G.Strang, T.Nquyen, “Wavelets and Filter Banks”, Wellesley-Cambridge Press, 1996

[12] M.Vetterli, I.Kovačević, “Wavelets and Subband Coding”, Englewood Cliffs, New Jersey: Pentice Hall PTR, 1995

[13] G.Jovanović-Dolecek, “Multirate Systems: Design & Applications”, Hershey PA: IDEA Group Publishing, 2002

[14] P.P.Vaidyanathan, “A Theory for Multiresolution Signal Decomposition: The Wavelet Representation”, IEEE Trans. Pattern Anal. Machine Intell., Vol.11, pp.674-693, July 1989

[15] C.S.Burns, R.A.Gopinath, H.Guo, “Introduction to Wavelets and Wavlet Transform, a Primer”, Upper Saddle River, New Jersey: Prentice Hall, 1998

[16] A.Cohen, J.Kovačević, "Wavelets: The Mathematical Background", in Proc. IEEE, Vol.84, No.4, pp.514-522, April 1996

[17] E. Hernandez, G. Weiss, "A First Course on Wavelets", CRC Press, 1996

[18] G.Kaiser, "A Friendly Guide to Wavelets", Boston: Bitkhäuser, 1994

[19] A.Akansu, et al., "Wavelet and Subband Transforms: Fundamentals and Communication Applications Frequency", IEEE Communications Magazine, Vol.35, pp.104-115, December 1997

[20] S.G.Mallat, "A Theory for Multiresolution Signal Decomposition: The Wavelet Representation", IEEE Transaction on Pattern Recognition and Machine Intelligence, Vol.11, pp.674-693, July 1989

[21] S.G.Mallat, "Multiresolution approximation and wavelet orthonormal bases of L2", Transactions of the American Mathematical Society, Vol.315, pp.69-87, 1989

[22] M.Weeks, "Digital Signal Processing using MATLAB and Wavelets", Hingham: Infinity Science Press LLC, 2007

[23] A.Lindsday, "Wavelet Packet Modulation for Orthogonally Transmultiplexed Communications", IEEE Transactions on Signal Processing, Vol.45, pp.1336-1339, May 1997

[24] A.Khoirul, A.U.Priantoro, M.Saito, T.Hara, M.Okada, H.Yamamoto, "On the PAPR Reduction for Wavelet Based Transmultiplexer", International Symposium on Communications and Information Technologies, pp.812-815, October 2004

[25] M.Gautier, J.Lienard, "Performances of Complex Wavelet Packet based Multicarrier Transmission through Double Dispersive Channel", IEEE Nordic Signal Processing Symposium, June 2006

[26] M.Gautier, C.Lereau, M.Arndt, J.Lienard, "PAPR Analysis for Wavelet Packet Modulation", IEEE International Symposium on Communications (ISCCSP '08), March 2008

[27] S.B.Slimane, "Peak-to-Average Power Ratio Reduction of OFDM Signals using Pulse Shaping", IEEE Global Telecommunications Conference, Vol.41, pp.1412-1416, December 2006

[28] T.Pollet, M.van Bladel, M.Moeneclaey, "BER Sensitivity of OFDM Systems to Carrier Frequency Offset and Wiener Phase Noise", IEEE Transaction on Communications, Vol.43, pp.191-193, April 1995

[29] A.G.Armada, "Understanding the Effect of Phase Noise in OFDM", IEEE Transaction on Broadcasting, Vol.47, No.2, pp.153-159, June 2001

[30] H.Nikookar, R.Prasad, "On the Sensitivity of Multicarrier Transmission over Multipath Channels to Phase Noise and Frequency Offset", in Proc. 7th IEEE International Symposium Personal, Indoor Mobile Radio Communication (PIMRC '96), Vol.1, pp.68-72, October 1996

[31] T.C.W.Schenk, R.W.van der Hofstad, E.R.Fledderus, "Distribution of the ICI Term in Phase Noise Impaired OFDM Systems", IEEE Transaction on Wireless Communications, Vol.6,No.4, pp.1488-1500, April 2007

[32] H.Steendam, M.Moeneclaeym "Sensitivity of Orthogonal Frequency Division Multiplexed Systems to Carrier and Clock Synchronization Errors", Elsevier Signal Processing, pp.1217-1229, November 1997

[33] L.Tomba, "On the Effect of Wiener Phase Noise in OFDM Systems", IEEE Transaction on Communications, Vol.46, No.5, May 1998

[34] K.Sathananthan, C.Tellambura, "Probability of Error Calculation of OFDM System with Frequency Offset", IEEE Transaction on Communications, Vol.49, No.11, pp.1884-1888, November 2001

[35] H.Nikookar, B.G.Negash, "Frequency Offset Sensitivity Reduction of Multicarrier Transmission by Waveshaping", in Proc. IEEE International Conference on Personal Wireless Communications (ICPWC '2000), pp.444-448, December 2000

[36] J.Armstrong, "Analysis of New and Existing Methods of Reducing Intercarrier Interference Due to Frequency Offset in OFDM", IEEE Transaction on Communications, Vol.47, No.3, pp.365-369, March 1999

[37] P.H.Moose, "A Technique for Orthogonal Frequency Division Multiplexing Frequency Offset Correction", IEEE Transaction on Communications, Vol.42, No.10, pp.2908-2914, October 1994

[38] A.G.Armada, M.Calvo, "Phase Noise and Sub-Carrier Spacing Effects on the Performance of an OFDM Communication System", IEEE Communication Letters, Vol.2, No.1, pp.11-13, January 1998

[39] Y.C.Lion, K.C.Chen, "Estimation of Wiener Phase Noise by the Autocorrelation of the ICI Weighting Function in OFDM System", in Proc. 16th IEEE International Symposium on Personal, Indoor and Mobile Radio Communications (PIMRC '05), pp.725-729, 2005

[40] P.Robertson, S.Kaiser, "Analysis of the Effects of the Phase Noise in Orthogonal-Frequency Division Multiplexed (OFDM) Systems", in Proc. IEEE International Conference on Communications (ICC '95), Vol.3, pp.1652-1657, June 1995

[41] V.S.Abhayawardhana, I.J.Wassell, 'Common Phase Error Correction with Feedback for OFDM in Wireless Communication", in Proc. IEEE Globecom, Vol.1, pp.651-655, November 2002

[42] C.R.N.Athaudage, "BER Sensitivity of OFDM Systems to Time Synchronization Error", in Proc. IEEE International Conference on Communication Systems (ICCS 2002), Vol.1, pp.42-46, November 2002

[43] Y.Mostofi, D.C.Cox, "Mathematical Analysis of the Imapct of Timing Synchronization Errors on the Performance of an OFDM System", IEEE Transaction on Communications, Vol.54, No.2, February 2002

[44] D.Liu, Y.Tang, D.Sang, S.Li, "Impact of the Timing Error on BER Performance of TDD Pre-equalized OFDM System", in Proc. IEEE International Conference on Personal Wireless Communications (ICPWC '2000), Vol.1, pp.714-718, September 2004

[45] D.Lee, K.Cheun, "Coarse Symbol Synchronization Algorithms for OFDM Systems in Multipath Channels", IEEE Communication Letters, Vol.6, No.10, pp.446-448, October 2002

[46] M.Sandell, J.J.Beekm P.O.Brjesson, "Timing and Frequency Synchronization in OFDM Systems using the Cyclic Prefix", International Symposium on Synchronization, pp.16-19, 1995

[47] M.Tanda, "Blind symbol-timing and frequency-offset estimation in OFDM systems with real data symbols", IEEE Transactions on Communications, Vol.52, No.10, pp.1609-1612, October 2004.

[48] A.J.Coulson, "Maximum likelihood synchronization for OFDM using a pilot symbol: algorithms", IEEE Journal on Selected Areas in Communications, Vol.19, No.12, pp. 2486-2494, December 2001.

[49] B. Yang, K.B.Letaief, R.S.Cheng , Z.Cao,"Timing recovery for OFDM transmission", IEEE Journal on Selected Areas in Communications, Vol.18, No.11, pp.2278-2291, November 2000.

[50] A.Demir, A.Mehrotra, J.Roychowdhury, "Phase Noise in Oscillators: a Unifying Theory and Numerical Methods for Characterization", IEEE Transactions on Circuits and Systems, pp.655-674, May 2000

[51] R.Corvaja, S.Pupolin, "Phase Noise Limits in OFDM Systems", in Proc. International Wireless Personal Multimedia Communications Symposium (WPMC '03), pp.19-22, October 2003

[52] A.Karmakar, A.Kumar, R.K.Patney, "Design of an Optimal Two-Channel Orthogonal Filterbank Using Semidefinite Programming", IEEE Signal Processing Letters, Vol.14, No.10, pp.692-694, October 2007

[53] J.Wu, K.M.Wong, "Wavelet Packet Division Multiplexing and Wavelet Packed Design Under Timing Error Effects", IEEE Transaction on Signal Processing, Vol.45, No.12, pp.2877-2890, December 1997

[54] J.K.Zhang, T.N.Davidson, K.M.Wong, "Efficient Design of Orthonormal Wavlet Bases for Signal Representation", IEEE Transactions on Signal Processing, Vol.52, No.7, July 2007

[55] E.L.Lawler and D.E.Wood, "Branch-And-Bound Methods: A Survey", JSTOR Operations Research, Vol.14, No.4, pp.699-719, Augustus 1966

[56] E.Alizadeh, "Interior Point Methods in Semidefinite Programming with Applications to Combinatorial Optimization", SIAM Journal of Optimization, Vol.5, pp.13-51, 1995

[57] Y.Ye, "Interior Point Algorithms: Theory and Analysis", New York, Wiley, 1997

[58] S.Boyd, L.El Ghaoui, E.Feron, V.Balkrishnan, "Linear Matrix Inequalities in System and Control Theory", SIAM Study in Applied Mathematics, Vol.15, June 1994

[59] S.Boyd, L.Vandenberghe, “Convex Optimization”, Cambridge University Press, 2004

[60] L.Vandenberghe, S.Boyd, “Semidefinite Programming”, SIAM review, Vol.38, No.1, pp.49-95. March 1998

[61] H.Wolkowicz, R.Saigal, L.Vandenberghe, “Handbook of Semidefinite Programming, Kluwer Academic Publisher, 2000

[62] R.Hettich, K.O.Kortanek, “Semidefinite Programming: Theory, Methods and Applications, SIAM Review, Vol.35, No.3, pp.380-429, September 1993

[63] S.P.Wu, S.Boyd, L.Vandenberghe, “FIR Filter Design via Semidefinite Programming and Spectral Factorization”, in Proceeding IEEE Concerence on Decision and Control, pp.271-279, 1996

[64] B.Alkire, L.Vandenberghe, “Convex Optimization Problems Involving Finite Autocorrelation Sequences”, Mathematical Programming, Series A93, pp.331-359, 2002

[65] T.N.Davidson, L.Zhi-Quan, K.M.Wong, “Orthogonal Pulse Shape Design via Semidefinite Programming”, IEEE International Conference on Acoustics, Speech and Signal Processing (ICASSP ’99), Vol.5, pp.2651-2654, March 1999

[66] T.N.Davidson, L.Zhi-Quan, J.F.Sturm, “Linear Matrix Inequality Formulation of Spectral Mask Constraints With Applications to FIR Filter Design”, IEEE Transaction on Communications, Vol.50, No.11, pp.2702-2715, November 1999

[67] J.F.Sturm, “Using SeDuMi 1.02, a MATLAB toolbox for optimization over symmetric cones”, Optimization Methods and Software, Vol. 11–12, pp. 625–653, 1999
[Available Online] http://sedumi.mcmaster.ca/

[68] J.Löfberg, “A Toolbox for Modeling and Optimization in MATLAB”, Proceedings of the CACSD Conference, 2004
[Available Online] http://control.ee.ethz.ch/~joloef/wiki/pmwiki.php

Appendix A: Normalization Theorem

Integrating the scaling function from $-M$ to M with respect to t gives:

$$\begin{aligned}\int_{-M}^{M}\varphi(t)dt &= \sqrt{2}\sum_{n}h(n)\int_{-M}^{M}\varphi(2t-n)dt \\ &= \frac{1}{\sqrt{2}}\sum_{n}h(n)\int_{-2M-n}^{2M-n}\varphi(t')dt'\end{aligned} \tag{A.1}$$

Where

$$\left|\int_{-2M-n}^{2M-n}\varphi(t')dt'\right| \le \|\varphi\|_1, \quad \forall\ n\in\mathbb{Z} \tag{A.2}$$

Since equation (A.2) is valid the theorem of the Lebesgue can be applied to the sum on the right hand side of equation (A.1). Let M go to infinity in (A.1):

$$b = \frac{1}{\sqrt{2}}\sum_{n}h(n)b \ \rightarrow\ \sum_{n}h(n) = \sqrt{2} \tag{A.3}$$

From equation (A.3) follows the normalization theorem.

Appendix B: Orthonormality Theorem

The shifted scaling functions form an orthonormal basis of V_0 if:

$$\langle \varphi(t), \varphi(t-n) \rangle = \delta(n) \quad \forall\ n \in \mathbb{Z} \tag{B.1}$$

Using refinement equation (2.13) and condition (B.1) we get:

$$\begin{aligned}
\delta(n) &= \int_{-\infty}^{\infty} \varphi(t)\varphi(t-n)dt \\
&= 2\int_{-\infty}^{\infty} \sum_{k=0}^{L-1} h(k)\varphi(2t-k) \sum_{l=0}^{L-1} h(l)\varphi(2(t-n)-l)dt \\
&= 2\sum_{k=0}^{L-1} h(k) \sum_{l=0}^{L-1} h(l) \int_{-\infty}^{\infty} \varphi(\tau)\varphi(\tau+k-2n-l)d\tau/2 \\
&= \sum_{k=0}^{L-1} h(k) \sum_{l=0}^{L-1} h(l)\delta(-k+2n+l) \\
&= \sum_{k=0}^{L-1} h(k)h(k-2n)
\end{aligned} \tag{B.2}$$

From equation (B.2) follows the orthonormality theorem.

Appendix C: Partitioning of Energy

The sum of squares of the time series elements x is given by:

$$\|x\|^2 = \sum_{t=0}^{N-1} x(t)^2 \tag{C.1}$$

Energy is preserved at any level $1 \le l \le J$ of the transform as given by (C.2), where ζ denotes WPT coefficients.

$$\|x\|^2 = \sum_{p=0}^{2^l-1} \left\|\zeta_l^p\right\|^2 \tag{C.2}$$

Proof

Let us first define equivalent sequence filter υ, built from the combination of filters $h(m)$, $g(m)$ and downsampling as:

$$\upsilon_{l,p,n} = \sum_{i=0}^{L-1} \upsilon_{p,i}\upsilon_{l-1,\lfloor p/2 \rfloor, n-2^{l-1}i} \tag{C.3a}$$

where

$$\begin{aligned} \upsilon_{1,0,n} &= h(n) \\ \upsilon_{1,1,n} &= g(n) \end{aligned} \tag{C.3b}$$

The discrete Fourier transform (DFT) of x is given by:

$$X(k) = \sum_{t=0}^{N-1} x(t) e^{-j2\pi\frac{k}{N}t} \tag{C.4}$$

Similarly follows the DFT of the filter υ:

$$\Upsilon_{l,p,k} = \prod_{m=0}^{l-1} M_{l,p,m,2^m k \bmod N} \tag{C.5a}$$

where

$$
\begin{aligned}
M_{0,2^m i \bmod N} &\equiv H_{2^m i \bmod N} \\
M_{1,2^m i \bmod N} &\equiv G_{2^m i \bmod N} \\
\tilde{H}_i &= \sum_{n=0}^{N-1} h(n) e^{-j2\pi \frac{n}{N} k} \\
\tilde{G}_i &= \sum_{n=0}^{N-1} g(n) e^{-j2\pi \frac{n}{N} k}
\end{aligned}
\tag{C.5b}
$$

Parseval's theorem states that the sum of squares of a sequence with length N is equal to the sum of the moduli squared of its DFT divided by N. Now the WPT coefficients are given by the convolution of time domain filter sequence with elements x, which in frequency domain can be expressed as:

$$
\begin{aligned}
\sum_{p=0}^{2^l-1} \left\| \zeta_l^p \right\|^2 &= \sum_{p=0}^{2^l-1} \frac{1}{N} \sum_{k=0}^{N-1} \left| X(k) \right|^2 \left| \Upsilon_{l,p,k} \right|^2 \\
&= \frac{1}{N} \sum_{k=0}^{N-1} \left| X(k) \right|^2 \sum_{n=0}^{2^l-1} \left| \Upsilon_{l,p,k} \right|^2 \\
&= \frac{1}{N} \sum_{k=0}^{N-1} \left| X(k) \right|^2 \sum_{n=0}^{2^l-1} \left| \prod_{m=0}^{l-1} M_{l,p,m,2^m k \bmod N} \right|^2 \\
&= \frac{1}{N} \sum_{k=0}^{N-1} \left| X(k) \right|^2 \prod_{m=0}^{l-1} \left[\left| \tilde{H}_{2^m k \bmod N} \right|^2 + \left| \tilde{G}_{2^m k \bmod N} \right|^2 \right]
\end{aligned}
\tag{C.6}
$$

The wavelet and scaling filter are chosen in such way that their frequency responses are mirror images of each other with respect to frequency of ½ π. Therefore, we get for the normalized wavelets:

$$
\left| \tilde{H}(\omega) \right|^2 + \left| \tilde{G}(\omega) \right|^2 = 1 \tag{C.7}
$$

The equation (C.6) can hence be written as:

$$
\sum_{n=0}^{2^l-1} \left\| \zeta_l^p \right\|^2 = \frac{1}{N} \sum_{k=0}^{N-1} \left| X(k) \right|^2 \prod_{m=0}^{l-1} I(m) = \sum_{t=0}^{N-1} x(t)^2 = \left\| x \right\|^2 \tag{C.8}
$$

Appendix D: Spectral Factorization

The Kolmogorov spectral factorization method is based on construction of the minimum phase spectral factor $SF_{mp}(z)$ from the autocorrelation function. The power series expansion of $SF_{mp}(z)$ is given by:

$$\log SF_{mp}(z) = \sum_{n=0}^{\infty} d_n z^{-n} \quad for\ |z| \geq 1\ \ and\ \ d_n \in \mathbb{R} \tag{D.1}$$

We can decompose $\log SF_{mp}$ to real and imaginary part:

$$\log SF_{mp}(z) = \mu(z) + j\eta(z) \tag{D.2}$$

The $\mu(\omega)$ and $\eta(\omega)$ are Hilbert transform pairs, for $z = e^{j\omega}$ we have:

$$\begin{aligned} \mu(\omega) &= \log\left|SF_{mp}(e^{j\omega})\right| \\ &= \frac{1}{2}\log R_h(\omega) \\ &= \sum_{n=0}^{\infty} d_n \cos n\omega, \qquad \eta(\omega) = -\sum_{n=0}^{\infty} d_n \sin \omega n \end{aligned} \tag{D.3}$$

In (4.26) $R(\omega)$ denotes the Fourier transform of autocorrelation sequence. We can find the coefficients d_n by:

$$d_n = \frac{1}{2\pi}\int_0^{2\pi} \frac{1}{2}\log R_h(\omega) e^{-jn\omega} d\omega \tag{D.4}$$

Appendix E: Sum of Squares of Cross-Correlation

The sum of squares of cross-correlation magnitude is related to the autocorrelation sequences of low pass filter *H* and high pass filter *G* according to the following equation:

$$\begin{aligned}\sum_{n=0}^{L-1}\left|r_{hg}(n)\right|^2 &= \sum_{n=0}^{L-1} r_h(n)\left((-1)^n r_h(n)\right)\\ &= r_h(n)\cdot r_g(n)\end{aligned} \tag{E.1}$$

Proof

$$\begin{aligned}\sum_n\left|r_{hg}(n)\right|^2 &= \sum_n\left(\sum_p h(p+n)g(p)\right)^2\\ &= \sum_n\sum_m\sum_p h(p+n)g(p)h(m+n)g(m)\\ &= \sum_m\sum_p g(p)g(m)\sum_n^L h(p+n)h(m+n)\\ &= \sum_m\sum_p g(p)g(m)\sum_{n=m-p} h(m)h(2m-p)\\ &= \sum_m\sum_p r_h(m-p)g(p)g(m)\\ &= \sum_p\sum_{n=m-p} r_h(n)g(p)g(n+p)\\ &= \sum_n r_h(n)r_g(n)\\ &= r_h(n)\cdot r_g(n)\end{aligned} \tag{E.2}$$